Enzymatic Transamination: (*R*)-Selective ω-Aminotransferases for the Production of Enantiomerically Pure Amines

Inaugural-Dissertation

zur Erlangung des Doktorgrades
der Mathematisch-Naturwissenschaftlichen Fakultät
der Heinrich-Heine-Universität Düsseldorf

vorgelegt von

Linda Herring
aus Düsseldorf

Essen, Juni 2017

aus dem Institut für
der Heinrich-Heine-Universität Düsseldorf

Gedruckt mit der Genehmigung der
Mathematisch-Naturwissenschaftlichen Fakultät der
Heinrich-Heine-Universität Düsseldorf

Referent: Prof. Dr. Karl-Erich Jaeger

Korreferent: Prof. Dr. Jörg Pietruszka

Tag der mündlichen Prüfung: 05.07.2017

"Science and everyday life cannot
and should not be separated."

– Rosalind Franklin

Acknowledgements

I would like to thank Dr. Thorsten Eggert and Dr. Michael Puls for giving me the opportunity to work on my thesis at evocatal GmbH.

I would like to express my very great appreciation to Prof. Dr. Karl-Erich Jaeger for his supervision at Heinrich-Heine-University and his helpful inspiration and Prof. Dr. Dr. Jörg Pietruszka for beeing the second examiner of my thesis.

My special thanks go to Dr. Christian Leggewie and especially Dr. Andrea Weckbecker for their scientific support and advice during my laboratory work and finally during writing my thesis.

I also would extend my special thanks to Dr. Renu Batra-Safferling, Dr. Joachim Granzin and the team at beamline ID23-1 at the European Synchrotron Radiation Facility in Grenoble for doing the crystallographic experiments and analysis.

I am particularly grateful for the kind working atmosphere at evocatal GmbH. Thank you very much for your helping hands and advice. Especially, I would like to thank you for your sympathy and the normal everyday working life you gave me during my very bad times.

Dani and Sabine, thank your for giving me the first orientation in the lab and the cloning techniques. Ralf, thank you for “I love chromatography” and your help with chemical problems. Thank you Anja, for the knitted hat and so much more. And Verena, thank you very much for beeing the best bench neighbour and friend, also beyond work.

And last but not least, möchte ich den wichtigstens Menschen in meinem Leben für ihre Liebe, Unterstützung und vor allem Geduld danken. Meiner Familie und dem kleinen aber feinen Freundeskreis, für die sehr vielen schönen Momente aber auch den Rückhalt in schweren Zeiten.

Mama und Papa, auch wenn ihr es immer für selbstverständlich haltet, danke, dass ihr so tolle Eltern seid. Danke Tanja, dass du nicht nur meine Schwester, sondern auch meine Freundin bist.

Besonderer Dank gilt meinem Mann Philipp, ohne dessen Unterstützung und Beharrlichkeit ich diese Arbeit vermutlich nie fertig gestellt hätte.

Contents

List of Tables

List of Figures

List of Abbreviations

µF	microfarad
AAO	amino acid oxidase
AAT	amino acid aminotransferase
Arg, R	arginine
BCAT	branched-chain aminotransferase
BLAST	basic local alignment search tool
bp	base pair(s)
°C	degree Celsius
CAGR	compound annual growth rate
CDW	cell dry weight
DNA	deoxyribonucleic acid
dNTP	deoxyribonucleotide
DTT	dithiothreitol
EDTA	ethylenediaminetetraacetic acid
e.g.	for example
FDA	Food and Drug Administration
g, mg	gramme, milligramme
GC	gas chromatography
GDH	glucose dehydrogenase
Glu, E	glutamic acid
GSH	glutathione
GSSG	glutathione disulfide

h	hour
His-tag	polyhistidine-tag
HPLC	high pressure liquid chromatography
HRP	horse radish peroxidase
HTP	high throughput
IPTG	isopropyl β-D-1-thiogalactopyranoside
kDa	kilodalton
Kp_i	potassium phosphate
kV	kilovolt
L, mL, µL	litre, millilitre, microlitre
LB	lysogeny broth
LDH	lactose dehydrogenase
LTP	low throughput
Lys, K	lysine
M, mM, µM, nM	molar, millimolar, micromalar, nanomolar
Met, M	methionine
min	minute
mol, mmol, µmol, nmol	mole, millimole, micromole, nanomole
MTBE	methyl *tert*-butyl ether
NAD^+	nicotinamide adenine dinucleotide, oxidized form
NADH	nicotinamide adenine dinucleotide, reduced form
Ni-NTA	nickel nitrilotriacetic acid
nm	nanometre
PCR	polymerase chain reaction
Phe, F	phenylalanine
PLP	pyridoxal-5'-phosphate
PMP	pyridoxamine phosphate

rpm	rounds per minute
SDS-PAGE	sodium dodecyl sulfate polyacrylamide gel electrophoresis
SOC	super optimal broth with catabolite repression
TA	transaminase
TB	terrific broth
TAE	triethanolamine
Tris	tris(hydroxymethyl)aminomethane
Tyr, Y	tyrosine
U	units, 1U=1 µmol/min
UV	ultraviolet light
V	volt

I. Zusammenfassung

Das Hauptziel dieser Arbeit war die Identifizierung neuer (*R*)-selektiver ω-Transaminasen. Ein weiterer Schwerpunkt war die Charakterisierung der neuen Kandidaten bezüglich ihrer Substratspektren allgemein und insbesondere ihre Aktivität mit sperrigen Substraten. Diese Studien sollten die Fähigkeit dieser Enzyme zur Produktion verschiedener chiraler Amine darstellen und einen Einblick in ihr zwei-bindiges aktives Zentrum geben.

Für die Identifizierung der neuen (*R*)-selektiven ω-Transaminasen wurden zwei Runden eines *in silico* Screenings durchgeführt. Die Sequenzen der (*R*)-selektiven Transaminasen aus *Mesorhizobium loti* MAFF303099 und *Arthrobacter* sp. KNK168 wurden als Suchsequenzen in Protein-Alignments (BLAST = Basic Local Alignment Search Tool) gegen die NCBI-Datenbank eingesetzt. Insgesamt wurden 13 Proteine für die Expression in *E. coli* ausgewählt (davon eines aus Metagenom-Sequenzen). Vier dieser Proteine zeigten Transaminaseaktivität, und auch das Protein aus Metagenom-Sequenzen konnte nach der Rückfaltung aus *Inclusion Bodies* als Transaminase identifiziert werden. Die Expressionsstudien der Transaminasen zeigten nach Zugabe des Cofaktors Pyridoxal-5'-phosphat (PLP) zum Kulturmedium höhere Aktivitäten.

Um die Kandidatenliste weiter einzugrenzen, wurden die identifizierten Enzyme mit literaturbekannten ω-Transaminasen verglichen. Die meisten der in der Literatur beschriebenen ω-Transaminasen besitzen Phenylalanin (Phe) an der Position 95 des von Höhne *et al.*[1] postulierten Sequenzmotivs und scheinen aktiver zu sein als ω-Transaminasen mit Tyrosin (Tyr) an dieser Position. Aufgrund dieses Unterschieds, und da sie sich als vielversprechende Kandidaten herausstellten, wurden zwei ω-Transaminasen mit Phe (R-FPTA) beziehungsweise Tyr (R-TRTA) an der Position 95 weiter untersucht.

Für das Screening der ω-Transaminase-Aktivität wurden gaschromatographische und spektrophotometrische Tests genutzt. Um einen Vergleich der initialen Aminierungs- und Desaminierungsaktivitäten zu ermöglichen wurde neben der Handhabung auch die Zusammensetzung der vorhandenen Tests optimiert.

Neben den unterschiedlichen Aminosäuren an der Schlüsselposition 113 (= Position 95 im Sequenzmotiv), zeigten die ausgewählten ω-Transaminasen R-TRTA und R-FPTA Unterschiede in ihren biochemischen Eigenschaften. Mit pH-Optima bei pH 9 und

pH 7,5 lagen beide in dem für Transaminasen typischen Bereich. Von beiden hatte R-TRTA eine höhere Temperaturstabilität. R-FPTA wies bereits nach der Inkubation bei 30 °C eine signifikant geringere Aktivität auf und war nach der Inkubation bei 41,2 °C nahezu inaktiv. R-TRTA zeigte dagegen nach der Inkubation bei 41,2 °C immer noch 50 % der ursprünglichen Aktivität. Die höhere Temperaturstabilität von R-TRTA geht auf Kosten einer geringeren Aktivität. Die katalytischen Parameter von R-FPTA (V_{max}=797.92±8.13 mU/mg und K_m=0.28±0.05 mM) entsprechen im Vergleich zu R-TRTA (V_{max}=241.80±4.70 mU/mg, K_m=4.43±0.12 mM) einer deutlich höheren Aktivität mit 1-Phenylethylamin **1a**. R-TRTA zeigte die höchsten Aktivitäten mit sperrigen Substraten. Darüber hinaus wies dieses Enzym im Vergleich zu R-FPTA größere Unterschiede in der Aktivität auf, was auf ein breiteres Substratspekrum von R-TRTA hinweist. R-FPTA zeigte ein ausgewogeneres Substratspektrum als R-TRTA mit einer Präferenz für aliphatische und daher flexiblere Substrate. Durch die Aufklärung der Kristallstruktur von R-TRTA wurden zudem genauere Einblicke in das aktive Zentrum dieser ω-Transaminase gewonnen.

An der Position 113 wurde zwischen der großen und kleinen Bindetasche eine ortsspezifische Mutagenese mittels eines degenerierten NNK-Codons durchgeführt. Aus dem darauffolgenden Screening wurden zwei Varianten jeder ω-Transaminase ausgewählt. Da angenommen wurde, dass ω-Transaminasen mit Phe an der Position 113 (R-FPTA) aktiver sind als ω-Transaminasen mit Tyr (R-TRTA) an dieser Position, wurden Varianten von R-FPTA und R-TRTA mit der jeweils anderen Aminosäure ausgewählt.

Es wurden die Varianten R-TRTA_C-His Y113F, R-TRTA_C-His Y113R, R-FPTA_C-His F113Y und R-FPTA_C-His F113M E115K untersucht. Neben dem Einfluss auf das Substratspektrum durch Änderungen in der Größe der Bindungstasche und der Polarität hatten die Mutationen Einfluss auf die pH-Optima. Die Änderungen in R-TRTA führten zu niedrigerem pH-Optimum und einer geringeren Akzeptanz großer Substrate. In R-FPTA induzierten die Änderungen eine Verschiebung des pH-Optimums zu höheren pH-Werten und verursachten eine höhere Präferenz für große Substrate. Es wird angenommen, dass der Austausch der Aminosäuren an Position 113 die Wechselwirkung der Aminosäuren auslöst, die für die Substratbindung verantwortlich sind, beeinflusst.

Die ursprüngliche Annahme, dass (R)-selektive ω-Transaminasen mit Phe an der Position 113 aktiver sind als ω-Transaminasen mit Tyr an dieser Position, wurde mit R-TRTA und R-FPTA bestätigt. Es wurde ebenfalls gezeigt, dass die Hydroxylgruppe von Tyr für bestimmte Substrate wichtig zu sein scheint, insbesondere für 4-Phenyl-2-butanon **2c**. Die Möglichkeit, Wasserstoffbrückenbindungen ausgehend von der Position 113 zum Substrat auszubilden, könnte wichtiger für die Substratselektivität sein als die Größe

der Aminosäure, was mit R-TRTA_C-His Y113R gezeigt wurde. In dem speziellen Fall vom Substrat 2-Tetralon **2f** wurde die Enantioselektivität mit R-TRTA_C-His Y113F von 65 % *ee* auf 95 % *ee* verbessert.

In dieser Arbeit konnte gezeigt werden, dass die neuen (*R*)-selektiven ω-Transaminasen R-TRTA und R-FPTA potente und anpassbare Biokatalysatoren sind. Dabei ergänzen sich die Eigenschaften beider ω-Transaminasen bezüglich Aktivität und Stabilität. Die Einführung von Punktmutationen zeigte, dass diese Enzyme für bestimmte pH-Optima optimiert werden können und dass das Substratspektrum durch geringfügige Änderungen innerhalb der Bindungsstaschen beeinflusst werden kann. Daher sind sie für vielfältige Reaktionen geeignet und können so die steigende Nachfrage an Aminierungskatalysatoren erfüllen.

I. Summary

ω-Transaminases open the access to a broad variety of chiral amines. The main purpose of this work was the identification of new (*R*)-selective ω-transaminases. Another key aspect was the characterisation of the new candidates concerning their substrate spectra and their activity with bulky substrates. These studies should demonstrate the ability of these enzymes to produce different chiral amines and give an insight into their two-binding active site.

For the identification of novel (*R*)-selective ω-transaminases, two rounds of an *in silico* screening were done. The sequences of the (*R*)-selective transaminases from *Mesorhizobium loti* MAFF303099 and *Arthrobacter* sp. KNK168 were used as query sequences in protein alignments (BLAST = Basic Local Alignment Search Tool) against the NCBI database. Altogether, thirteen proteins (whereof one was from metagenome sequences) were chosen for expression in *E. coli*. Four proteins showed transaminase activity and also the protein from metagenome sequences could be identified as a transaminase after refolding from inclusion bodies. The expression studies with the transaminases showed an increased activity upon addition of the cofactor pyridoxal-5'-phosphate (PLP) to the culture medium.

To reduce the list of candidates, the identified enzymes were compared to literature known ω-transaminases. Most ω-transaminases described in literature have phenylalanine at position 95 of the sequence motif postulated by Höhne *et al.*[1] and appear to be more active than ω-transaminases with tyrosine at this position. Being the most promising candidates, the two ω-transaminases with Phe (R-FPTA) and Tyr (R-TRTA) at position 95 were studied in detail.

For screening of the ω-transaminase activity, gas chromatographic and spectrophotometric assays were used. To enable a comparison of the initial amination and deamination activities, the handling and composition of the existing assays were optimized.

Besides different amino acids at the key position 113 (= position 95 in the sequence motif), the ω-transaminases R-TRTA and R-FPTA showed differences in their biochemical characteristics. With pH optima at pH 9 and pH 7.5 both lay in the typical pH range of transaminases. Of these two, R-TRTA had higher temperature stability. The activ-

ity of R-FPTA was already significantly reduced after incubation at 30 °C and nearly completely lost after incubation at 41.2 °C, whereas R-TRTA showed still 50 % activity after incubation at 41.2 °C. The higher temperature stability of R-TRTA is at expense of a lower activity. The catalytic parameters of R-FPTA (V_{max}=797.92±8.13 mU/mg and K_m=0.28±0.05 mM) resembled a much higher activity with 1-phenylethylamine **1a** compared to R-TRTA (V_{max}=241.80±4.70 mU/mg, K_m=4.43±0.12 mM). R-TRTA had its highest activities with bulky substrates. Furthermore, it showed a broader activity range compared to R-FPTA, which indicated a higher variation of the substrate spectrum of R-TRTA. R-FPTA showed a more balanced substrate spectrum than R-TRTA with a preference for the aliphatic and therefore more flexible substrates. Additionally, more detailed insights into the active site of R-TRTA were gained by solving the crystal structure of this ω-transaminase.

Site-directed mutagenesis was performed at position 113 between the large and small bindig pocket, using a degenerated NNK codon. From the following screening two variants were chosen for each ω-transaminase. Since it was presumed that ω-transaminases with phenylalanine (Phe) at position 113 (R-FPTA) are more active than ω-transaminases with tyrosine (Tyr, R-TRTA) at this position, variants of R-FPTA and R-TRTA where Phe was replaced by Tyr and vice versa, were part of the chosen variants.

The variants R-TRTA_C-His Y113F, R-TRTA_C-His Y113R, R-FPTA_C-His F113Y and R-FPTA_C-His F113M E115K were characterized. Besides the influence on the substrate spectrum by changes in the size of the binding pocket and polarity of the amino acids, the mutations had also an influence on the pH optima. The changes of R-TRTA lead to a lower pH optimum and a lower acceptance of large substrates. In R-FPTA, the changes induced a shift of the pH optimum to higher pH values and caused a higher preference for larger substrates. It is presumed that the change of the amino acid at position 113 alters the interaction of the amino acids which are responsible for the substrate binding.

The initial presumption that (*R*)-selective ω-transaminases with Phe at position 113 are more active compared to ω-transaminases with Tyr at this position was confirmed by R-TRTA and R-FPTA. It was also shown that the hydroxyl group of Tyr seems to be important for certain substrates, in particular 4-phenyl-2-butanone **2c**. The possibility to build hydrogen bonds between the position 113 and the substrate could be more important for substrate selectivity than the overall size of the amino acid, which was shown for R-TRTA_C-His Y113R. In the particular case of the substrate 2-tetralone **2f**, the enantioselectivity was improved from 65 % *ee* to 95 % *ee* with the R-TRTA_C-His Y113F variant.

Altogether, the new (*R*)-selective ω-transaminases R-TRTA and R-FPTA are potent and tunable biocatalysts. Whereas R-FPTA is more active, R-TRTA is more stable. The mutagenesis of both ω-transaminases on a small scale showed that these enzymes can be optimized for certain pH optima and the substrate spectrum can be influenced by minor alteration in their binding pockets. Therefore, they are suitable for versatile reactions and accommodate the increasing demand of amination catalysts.

II. Introduction

1. From fermentation to industrial biotechnology

Nowadays, products from fermentation and industrial biotechnolgy are part of the everyday life. Some of these products derive from ancient times, others originate from current research. When our ancestors settled and started farming in the Fertile Crescent in the Near East, microorganisms became their invisible assistants. Beer, wine and dairy products complemented their menue.[2,3] But also in China and America fermented beverages were produced.[3,4] Many of these products were probably generated by chance and it took centuries to understand the necessary processes. In the late 17th century, Leeuwenhoek made *wee animacules* visible[5] and gave the signal for microbiology as a science. The discoveries of Pasteur,[6] Koch, Fischer and Buchner[7] explained microbiological and enzymatic processes. The growing industries and the requirements within two world wars were a driving force to industrial fermentation processes of solvents and the production of penicillin.[8] The resolution of the DNA structure in 1953 by Watson, Crick and Franklin laid the foundation for molecular biology.[9–11] The new DNA technologies, developed during the 1970s and 1980s, enabled the manipulation of genetic material and lead to a continuous increase of importance of the industrial biotechnology. Today, the achievements of our ancestors and of modern biotechnology are an integral part of everyday life.

2. Biocatalysis

While industrial fermentation processes gained importance during the two world wars, crude oil has become the main resource base for chemical industry since World War II.[12] Nowadays, cost-effective chemical processes have to follow strict safety requirements and life cycle responsibilities for chemical products are becoming more and more important.[13] The increasing need of chemical products and a growing environmental impact, caused by fossil exploitation and pollution, demand for sustainable processes. Biocatalysis has the capability to improve the sustainability of chemical processes.

Even though biocatalysis seems to be an up to date technology, it has to compete with the existing cost-effective chemical processes.[14] The developments in recombinant DNA technology during the last four decades enable a fast access to huge biodiversity at low cost and reduce the screening effort of mutant libraries.[15,16] Tailor-made biocatalysts therefore become cheaper.[13]

A bottleneck of biocatalytic processes are often low product concentrations and a complex downstream processing.[13,14] But with optimized systems, biocatalysis provides environmentally friendly processes and enables the shift towards the use of renewable raw materials. Biocatalytic processes can for example be optimized via the biocatalyst (enzyme/cell selection, optimization for the substrate) or the process (reaction conditions suitable for catalyst, kind of application). Further optimization aspects are given in Fig. 2.1.

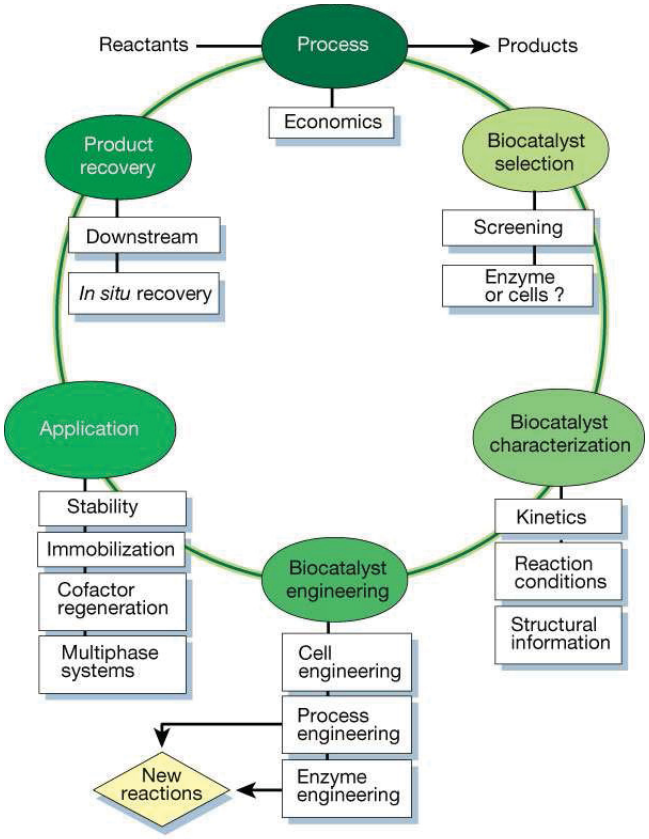

Fig. 2.1. *Development of biocatalytic processes.*
Reprinted by permission from Macmillan Publishers Ltd © 2001.[17]

2.1. Enzyme Engineering

One possibility to optimize a biocatalytic process is enzyme engineering. Thus, the enzyme can be optimized for e.g. the substrate, temperature or pH optimum, thermal stability or enantioselectivity.[18] For the optimization of an enzyme itself, the genetic manipulation of the corresponding DNA is necessary. To accelerate the natural process of evolution, several molecular biological methods are available. These methods are classified into directed evolution (random mutagenesis) and rational design (site-directed mutagenesis).

The directed evolution mimicks the process of natural evolution. One method of directed evolution is error prone PCR. Since it is a random mutagenesis it is often used for enzymes without detailed structural information. Random mutagenesis inserts only small changes. Therefore, several rounds of mutagenesis are necessary and large mutant libraries are created.[19–22]

If detailed structural and functional information about the enzyme are available, rational design can be used to create enzymes with the desired properties. With site-directed mutagenesis mutations can be inserted at selected positions and the library size is reduced significantly.[23] This is important, since the screening of engineered enzymes is limited by a lack of suitable high-throughput screening methods.[24]

Both methods, directed evolution and rational design can also be combined in semi-rational design approaches.

2.2. Benefits from Biocatalysis

The main advantages of biocatalysis are their high versatility, substrate selectivity, regio- and stereoselectivity.[14] Especially the pharmaceutical industry benefits from biocatalysis. Difficult syntheses with multiple protection and deprotection steps are circumvented and metal catalysts are replaced by non-metal biocatalysts.[25] The mild reaction conditions and high optical purity qualify biocatalysts for the production of chiral pharmaceutical reagents. In the past pharmaceuticals were often administered as racemic mixtures, whereof only one enantiomer had the desired effect. Since the other enantiomer is inactive or even responsible for side effects, enantiomerically pure pharmaceuticals are important.[26] With the publication of formal guidelines on the development of chiral drugs by the FDA in 1992, the sales of chiral drugs as single-enantiomer started to grow.[27] From 2011 to 2016 the chiral technology market was expected to increase at a CAGR (compound annual growth rate) of 6.5 % to $7.2 billion.[28]

Biocatalytic approaches therefore offer optimized processes concerning sustainability

and product purity for the chemical industry. An excellent example for the implementation of a biocatalyst within an industrial process is the production of Sitagliptin by an engineered (*R*)-selective ω-transaminase.[13,29–31]

3. Transaminases

The first enzymatic transamination reaction was discovered in the mid-1930s by Braunstein and co-workers in mammalian tissue.[32] About twenty years later, Rudman and Meister obtained transaminase activities from *Escherichia coli* extracts.[32] Despite this early discovery, transaminases only slowly gained scientific attraction. The first biocatalytic process for the synthesis of chiral amines using transaminases was developed by Celgene in the late 1980s.[33] Along with the "chiral shift" in 1992, academia became more interested in transaminases in the 1990s. In the last fifteen years these enzymes received major research interest in the biocatalytic field.[18,34,35]

Optically active amines are one of the most important substance classes which are used for building blocks or auxiliaries in the pharmaceutical, agrochemical and chemical industries.[36,37] For instance, about 40–50 % of pharmaceuticals contain a chiral amine moiety.[38] Transaminases sparked such an interest, because they can be used as a tool for the production of chiral amines (for examples see Fig. 2.2).

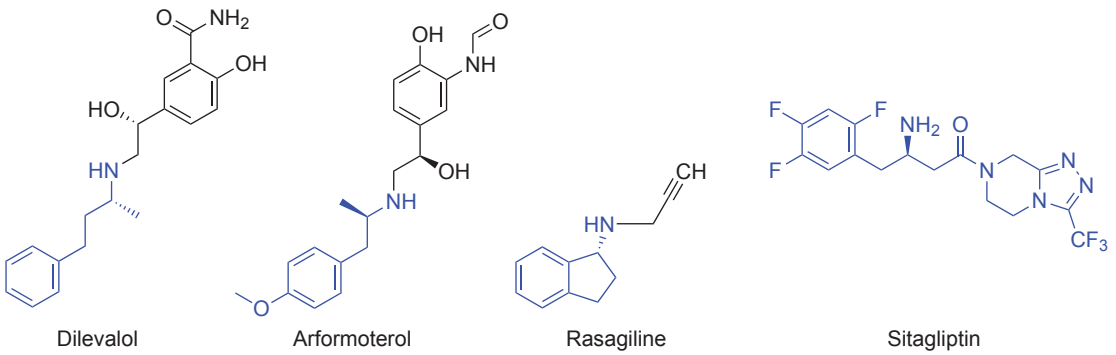

Fig. 2.2. *(*R*)-amine containing pharmaceuticals. The parts of the molecules which can be aminated by transaminases are highlighted in blue.*[37,39–43] *The depicted drug names describe the (*R*)- and (*R,R*)-enantiomers, respectively.*

In nature, transaminases or aminotransferases take part in the amino acids metabolism and are of frequent occurrence in other pathways as well, for example for the production of antibiotic compounds.[44,45] Transaminases catalyse the reversible transfer of an amino group to an *oxo*-function (see Fig. 2.3).

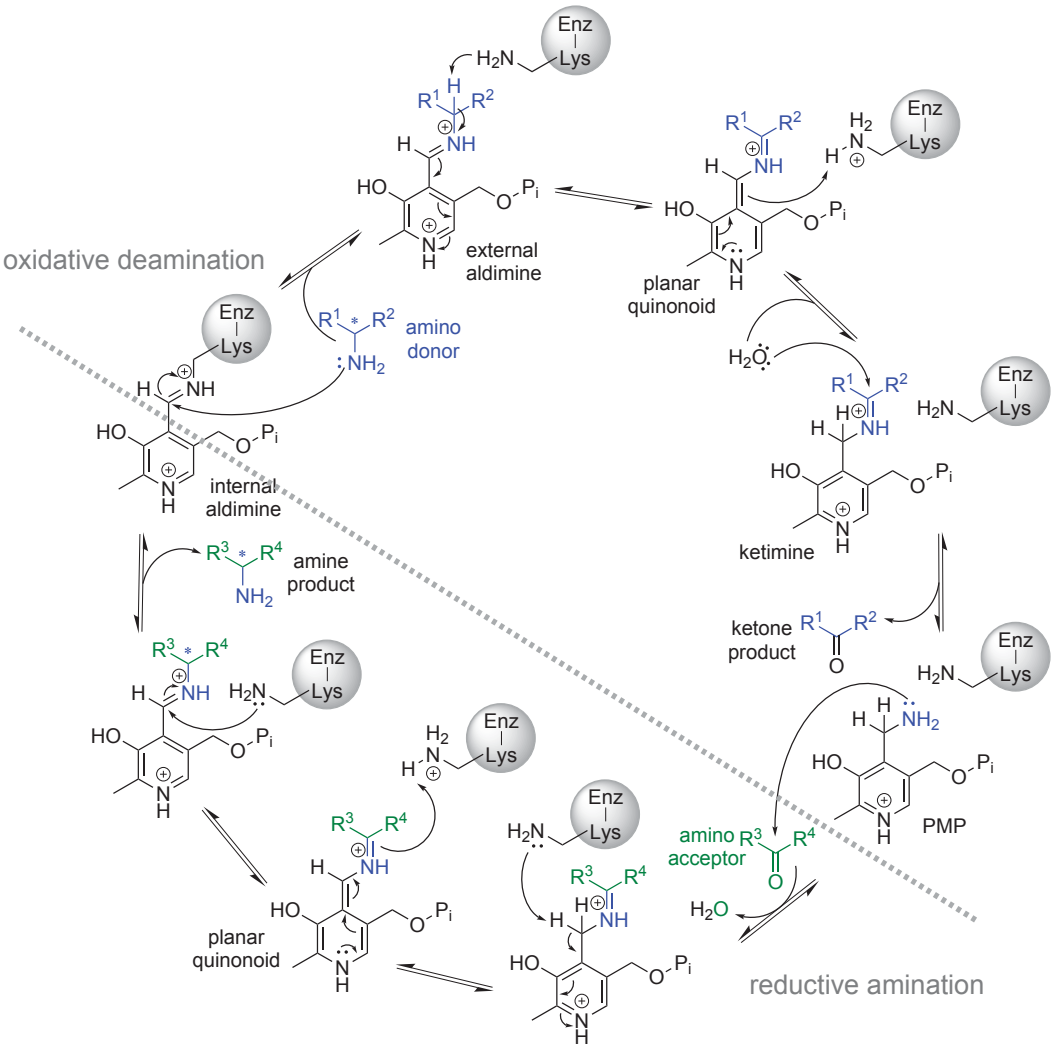

Fig. 2.3. *Transamination via the cofactor pyridoxal-5'-phosphate (PLP).*[35,46–48] *PLP is covalently bound via a Schiff base to a lysine (Lys) residue inside the active site of the enzyme (Enz-Lys). The transamination reaction consists of two half reactions: the oxidative deamination (above) and the reductive amination (below). The amino donor is highlighted in blue, the amino acceptor is highlighted in green. For more details see text.*

The cofactor pyridoxal-5'-phosphate (PLP) is covalently bound via a Schiff base to a lysine (Lys) residue inside the active site (internal aldimine). The transamination reaction proceeds in two half reactions: the oxidative deamination and the reductive amination. During the first half reaction, the internal aldimine is attacked by the amino donor nitrogen and the external aldimine is formed. The active site Lys now reacts as a Lewis base and abstracts a proton from the external aldimine resulting in a planar quinonoid. By hydrolysis of the ketimine the ketone product is released, while PLP is

converted to pyridoxamine phosphate (PMP). The amino group of PMP is transferred to an aldehyde or ketone, acting as an amino acceptor in the reductive amination. The internal aldimine is regenerated again and in case of a ketone as amino acceptor, a chiral amine is produced. The whole transamination mechanism is described as a ping pong bi-bi mechanism.[35,46–48]

With pyridoxal-5'-phosphate (PLP) as cofactor, transaminases belong to the large superfamily of vitamin B_6 dependent enzymes.[45,49] These PLP dependent enzymes can be classified by their fold type. α-Transaminases and ω-transaminases belong to the fold type I, whereas the D-amino acid aminotransferases (D-AAT) and branched-chain aminotransferases (BCAT) belong to the fold type IV.[45,50] Based upon their multiple sequence alignments in Pfam database,[51] transaminases can be divided into five subgroups: α-TAs (EC 2.6.1.2) belong to subgroups I and II, ω-transaminases (EC 2.6.2.18) to subgroup III and D-AAT (EC 2.6.1.21) and BCAT (EC 2.6.1.42) to subgroup IV.[52] Thus, the classification of Metha *et al.* was expanded by an additional subgroup.[49]

3.1. ω-Transaminases

Enzymes which transfer terminal amino groups attached to a primary carbon atom belong to the subgroup of ω-transaminases: (acetyl-)ornithine-transaminases, lysine ϵ-transaminase, β-alanine-transaminase and γ-aminobutyrate-transaminase.[53,54] In contrast to α-transaminases, ω-transaminases do not need a carboxylic acid function in α-position to the ketone or amine moiety of the molecule.[34] When Shin and Kim discovered an ω-transaminase, which did not use β-alanine as amino donor, they named this enzyme amine:pyruvate transaminase.[53,55,56] This ω-transaminase could convert (*S*)-1-phenylethylamine **1a**.[57] To confine the group of ω-transaminases which are able to convert substrates lacking any carboxylic acid function such as amines and ketones, Höhne *et al.* called this type of ω-transaminases amine transaminases (amine-TA, as opposed to amino acid transaminase).[1,54] In this work, the term ω-transaminase refers to amine transaminase.

Because of their possibility to synthesize various amines, ω-transaminases complement the biochemical tools for the enzymatic synthesis of optically active amines besides hydrolases and oxidoreductases.[36,37] The transamination is a reversible reaction. In Fig. 2.4, the kinetic resolution a) and asymmetric synthesis b) with the widely used standard substrate 1-phenylethylamine **1a** are shown. In contrast to α-transaminases which use α-ketoglutarate, ω-transaminases accept pyruvate as an universal amino acceptor.[54]

Challenges for the production of chiral amines arise from the equilibrium of the ω-transaminase reaction, as well as from substrate and/or product inhibition. The

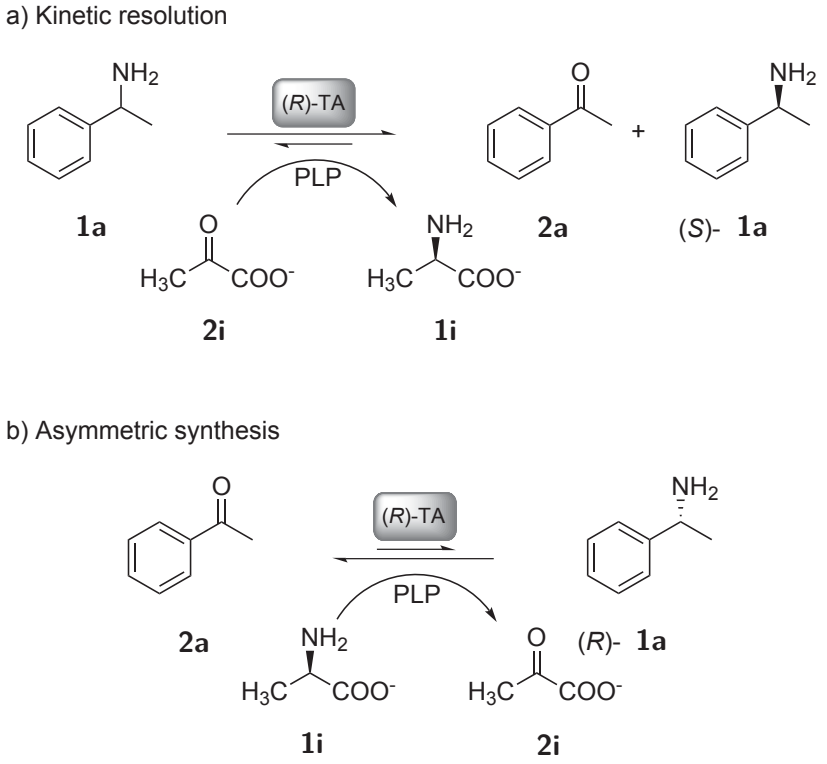

Fig. 2.4. *Standard ω-transaminase reactions with an* (R)*-selective ω-transaminase (*(R)*-TA). a) Kinetic resolution, starting from* rac*-1-phenylethylamine* ***1a*** *results in acetophenone* ***2a*** *and* (S)*-1-phenylethylamine* (S)-***1a***. *Pyruvate is used as amino acceptor and reacts to* D*-alanine . The possible yield is 50 %* (S)-***1a*** *and the equilibrium lies on the product side.*
b) Asymmetric synthesis with the corresponding ketone ***2a*** *offers a theoretical yield of 100 %* (R)-***1a***. *The amino donor* ***1i*** *is deaminated to* ***2i***. *Since the equilibrium lies on the educt side, an excess of amino donor has to be applied to drive the equilibrium to the product side.*

equilibrium constant of the deamination reaction with pyruvate as amino acceptor is above 1, meaning the formation of alanine is favoured.[35,36] For asymmetric synthesis of chiral amines, the equilibrium has to be shifted to the product side and inhibitors have to be removed. Several methods have been developed to increase the amine production (see Fig. 2.5).[58] For example, an excess of amino donor is applied or inibitory (co)products (ketone or α-keto acid) are removed from the reaction via technical, physical or enzymatic approaches.[59–61] A recycling of the amino donor via coupled enzymatic reactions is also possible.[62] But, as the thermodynamic equilibrium of the reaction is determined by the amino donor,[63] there is no universal approach to shift the equilibrium to the amine product.

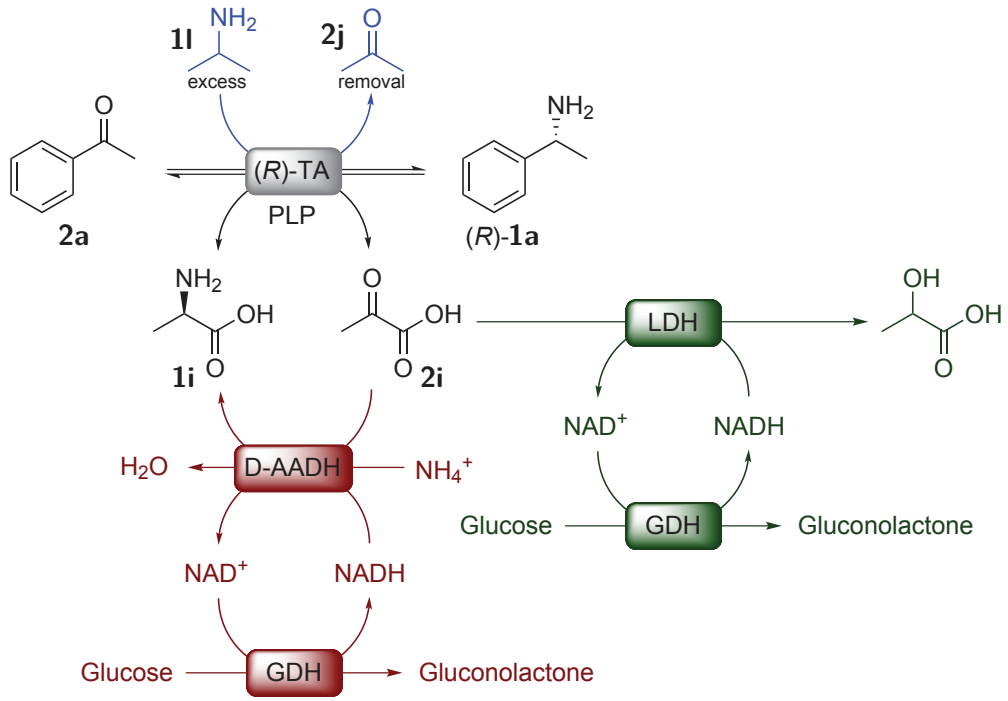

Fig. 2.5. *Ways to shift the equilibrium of the transaminase reaction. With isopropylamine* ***1l*** *as amino donor, the co-product aceton* ***2j*** *can be easily removed from the reaction (blue). The enzymatic reactions with lactose dehydrogenase (LDH, green) and* D*-amino acid dehydrogenase (D-AADH, red) remove or recycle pyruvate* ***2i****. The coupled glucose dehydrogenase (GDH) is used for the co-factor recycling of* NAD^+*.*

Before high throughput (HTP) screening methods were developed for ω-transaminases, low throughput (LTP) chromatographic methods were used to determine the substrate specificity and enatioselectivity of these enzymes.[64] The first HTP assay was developed by Hwang *et al.* and is based upon $CuSO_4$ which forms blue complexes with α-amino acids.[65] Other methods which are independent from additional staining or added enzyme are a conductometric method and the widely used acetophenone assay which were both developed by Schätzle *et al.*[66,67]

The acetophenone assay is simply the deamination reaction of 1-phenylethylamine **1a** and uses the absorption of acetophenone which can be measured photometrically. The coupled enzymatic reactions to shift the equilibrium which were mentioned above, can also be used for HTP screenings of transaminase activity. By coupling glucose dehydrogenase (GDH) to the transaminase reaction (see Fig. 2.5), the formation of gluconolactone leads to a pH reduction. This pH shift can be measured with a pH sensitive dye.[62]

An assay to measure the deamination activity and enantioselectivity of ω-transaminases with additional enzymes uses amino acid oxidase (D- or L-AAO), horse radish peroxidase (HRP) and a redox dye (pyrogallol red).[68] In contrast to the acetophenone assay, this assay is independent from the used transaminase substrate. Both assays are described in more detail in chapter III, section 6.3 and section 6.4.

ω-Transaminases are a powerful tool for the production of enantiomerically pure amines, resulting in a high demand for both, (*S*)- and (*R*)-selective ω-transaminases. Remarkably, the ω-transaminases found in natural sources were mainly (*S*)-selective.[34] Up to 2010, only one (*R*)-selective ω-transaminase was known, the (*R*)-selective ω-transaminase from *Arthrobacter* sp.[1,34,69,70] The apparently rare occurrence of (*R*)-selective ω-transaminases in nature induced an increased interest in finding these enzymes. Since classical screening methods of natural samples and strain collections were less successful, modern approaches were chosen for finding new (*R*)-selective ω-transaminases.[71] For the identification of new (*R*)-selective ω-transaminases, Höhne *et al.* developed an *in silico* strategy for a sequence-based prediction of substrate specificity and enantiopreferrence.[1] The prediction of the key amino acids led to sequence motifs for the fold class IV PLP-dependent enzymes (see Tab. 2.1) and 17 new (*R*)-selective ω-transaminases.

Tab. 2.1. *Sequence motifs for the fold class IV PLP-dependent transaminases.*[1]

Position	**31**	**36**	**38**	**40**	**95ff**	**105ff**
D-AAT	F	Y	V	K(R/X)	xzYzQ	RxH
BCAT	Y	F	G	R(K)	YzR	zGz
(*R*)-amine-TA	H/R	Y	V/T	S(T/A/H/P)	F(Y)VE(ANQ)	—

z: V, I, L or M; x: any amino acid

For the synthesis of chiral amines, ω-transaminases offer new opportunities besides chemical paths. But the substrate acceptance of the ω-transaminases is limited. In addition to the challenging equilibrium of the ω-transaminase reaction, the binding pocket of the enzyme predefines the structure of the accepted substrates. On the basis of the substrate structure–reactivity relationship, an active site model of an ω-transaminase was developed. Since the reactivity towards substrates with a large aryl group was the highest, the active site model suggested a large and a small binding site within the studied enzyme.[72] The model of the active site with a large and small binding pocket was later verified by several three dimensional structures of (*S*)- and (*R*)-selective ω-transaminases.[46,73–76]

Fig. 2.6. *The small (green) and large (blue) binding pockets of* (S)*-selective and* (R)*-selective ω-transaminases.*

The two-binding site appearance of the ω-transaminases limits the variety of substrate candidates. For the production of complex chiral amines, e.g. bulky-bulky amines with two large groups, the active site of a ω-transaminase has to be altered. Savile *et al.* enlarged the small binding pocket of the (*R*)-selective ω-transaminase from *Arthrobacter* sp. by directed evolution for the production of the bulky-bulky compound Sitagliptin.[29,77] This successful approach illustrated that the alteration of the ω-transaminases' active site is extensive but possible.

4. Aim of this study

Since ω-transaminases are a potential tool for the production of chiral amines, there is a high demand for such enzymes. As already mentioned, chiral amines are an important substance class for active pharmaceutical ingredients. Whereas many (*S*)-selective ω-transaminases have been described, there is a lack of their (*R*)-selective counterpart. Therefore, the aim of this study is the identification of novel (*R*)-selective ω-transaminases. Potential new candidates are to be characterized especially concerning their substrate spectra and their activity towards bulky substrates, because the two-binding site appearance of the ω-transaminases limits the production of large complex chiral amines (for example Sitagliptin).

The substances were selected to examine different types of substrates (see Fig. 2.7, for corresponding ketones see A, Fig. A.22). 1-Phenylethylamine **1a** is widely used as a standard ω-transaminase substrate. The chlorinated variant **1b** with the electron withdrawing chlorine substituent and 1-methyl-3-propylamine **1c** with an elongated side chain complement this benzyl type. Furthermore, **1c** is a precursor of the antihypertensive drug dilevalol.[39,40] As bulky substrates the bicyclic substances 1-(2-naphthyl)ethylamine **1d**, 1-aminoindane **1e** and 2-aminotetralin **1f** were chosen. Counting from the phenyl group, the amino groups of this substrates are at different distances.

The substances **1e** and **1f** have psychoactive properties[78] or are used as precursors, for example **1e** is a precursor of Rasagiline, a drug for the treatment of Parkinson's disease.[41–43]

Additionally, the substrates 2-aminopentane **1g** and 2-aminononane **1h** were chosen as aliphatic substrates with chain lengths of five and nine carbon atoms.

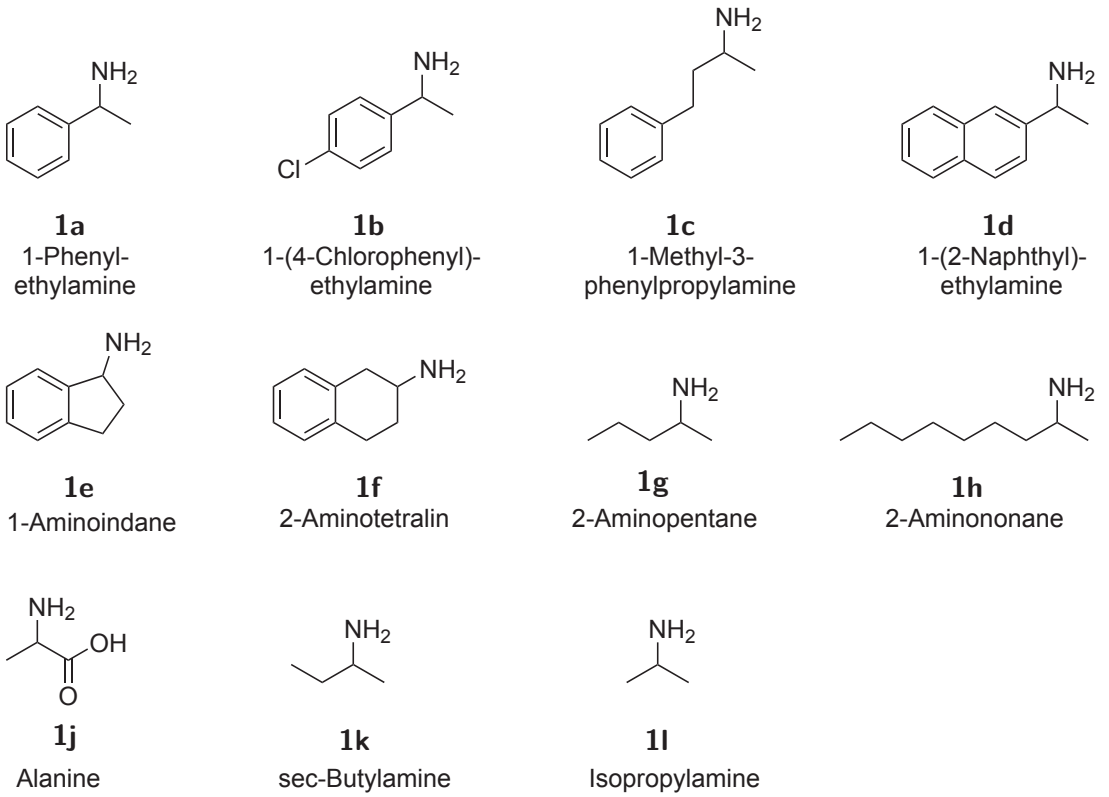

Fig. 2.7. *Chosen substrates for the characterization of* (R)*-selective ω-transaminases shown as amines. The corresponding ketones are numbered from* ***2a*** *to* ***2j****. See also Fig. A.22.*

III. Material and Methods

1. Chemicals and Enzymes

All chemicals used in this work were purchased in a purity not less than *p. a.* quality grade from Alfa Aesar (Karslruhe, Germany), AppliChem GmbH (Darmstadt, Germany), BASF SE (Ludwigshafen, Germany), Becton, Dickinson and Company (Franklin Lakes, USA), Carl Roth GmbH+Co KG (Karlsruhe, Germany), Evonik Degussa (Marl, Germany), GE Healthcare Europe GmbH (Freiburg, Germany), Merck KGaA (Darmstadt, Germany), Molekula (Dorset, UK), New England Biolabs GmbH (Frankfurt am Main, Germany), PEQLAB Biotechnology GmbH (Erlangen, Germany), Qiagen GmbH (Hilden, Germany), Serva (Heidelberg, Germany), Sigma-Aldrich Chemie GmbH (Steinheim, Germany), TCI Europe (Zwijndrech, Belgium) and Thermo Fisher Scientific GmbH (Dreieich, Germany).

All enzymes used in this work were purchased from Alpha Diagnostic Intl. Inc (San Antonio, USA), AppliChem GmbH (Darmstadt, Germany), New England Biolabs GmbH (Frankfurt am Main, Germany), Roche Diagnostics GmbH (Mannheim, Germany), Serva (Heidelberg, Germany) and Sigma-Aldrich Chemie GmbH (Steinheim, Germany).

2. Media and Solutions

Media and solutions were sterilized by autoclaving them for 20 minutes at 121 °C . Heat sensitive components like pyridoxal 5'-phosphate (PLP) and antibiotics were sterile filtrated through a CME (cellulose mixed ester) membrane filter with a pore size of 0.22 µm (Carl Roth GmbH+Co KG, Karlsruhe, Germany). When possible, antibiotics were diluted in auto-sterile 70 % ethanol.

2.1. Culture Media

2.1.1. Lysogeny Broth (LB) Medium

The components of the Lysogeny Broth (LB) medium[79,80] (Tab. 3.1) were diluted in bidistilled water and autoclaved. For LB agar plates, LB medium was supplemented with 1.5 % (w/v) agar before autoclaving.

Tab. 3.1. *Components of LB medium.*

Components	**Concentration [g/L]**
Tryptone	10.00
NaCl	10.00
Yeast extract	5.00

2.1.2. Terrific Broth (TB) Medium

For 1 L TB medium, the components (Tab. 3.2) were dissolved to a final volume of 880 mL in bidistilled water. 10 x TB salts and glucose were dissolved seperately to a final volume of 1 L in bidistilled water. The solutions were autoclaved and after cooling, the TB medium was complemented with 100 mL of 10 x TB salts and 20 mL of 50 % (w/v) glucose.

Tab. 3.2. *Components of TB medium.*

Components	**Concentration [g/L]**
Tryptone	12.00
Glycerol	5.00
Yeast extract	24.00
10x TB salts	
KH_2PO_4	23.12
K_2HPO_4	125.41
Glucose	500.00

2.1.3. M9 Minimal Medium

The components of M9 minimal medium[81,82] (Tab. 3.3) were diluted in bidistilled water and autoclaved. The trace elements for US* trace elements solution were dissolved in

1 M HCl and autoclaved. M9 medium was supplemented with 2 mL/L sterile 1 M $MgSO_4$ solution, 1 mL/L US* trace elements solution (Tab. 3.4) and 5 g/L sterile glucose.

Tab. 3.3. *Components of M9 minimal medium.*

Components	**Concentration [g/L]**
Na_2HPO_4	6.8
KH_2PO_4	3.0
NH_4Cl	1.0
NaCl	0.5
add: $MgSO_4$, US* trace element solution, glucose	

Tab. 3.4. *Components of US* trace element solution (1 000 fold).*

Components in 1 M HCl	**Concentration [g/L]**
$MnCl_2 \cdot 4\ H_2O$	1.50
$ZnSO_4 \cdot 7\ H_2O$	1.87
H_3BO_3	0.30
$Na_2MoO_4 \cdot 2\ H_2O$	0.25
$CuCl_2 \cdot 2\ H_2O$	0.15
$Na_2EDTA \cdot 2\ H_2O$	0.84
$CaCl_2 \cdot H_2O$	4.12
$FeSO_4 \cdot 7\ H_2O$	4.87

2.2. Media for the Transformation of *E. coli*

2.2.1. TMF Buffer

Heat competent *E. coli* cells were prepared in TMF buffer. The ingredients of the TMF buffer (see Tab. 3.5) were dissolved in bidistilled water and autoclaved.

Tab. 3.5. *Components of TMF buffer.*

Components	**Concentration [mM]**
$CaCl_2$	100.00
RbCl	50.00
$MnCl_2$	40.00

2.2.2. Super Optimal Broth with Catabolite Repression (SOC) Medium

The components of super optimal broth with catabolite repression medium (SOC medium,[83] see Tab. 3.6) were complemented with solutions of 1 M $MgCl_2$ and 1 M $MgSO_4$, to gain a final concentration of 10 mM each. The components were dissolved in bidistilled water and autoclaved. Afterwards, the medium was supplemented with 20 % (w/v) sterile glucose to a final concentration of 0.4 % (w/v) glucose. The SOC medium was stored at 4 °C.

Tab. 3.6. *Components of SOC medium.*

Components	**Concentration [g/L]**
Tryptone	20.00
NaCl	0.50
Yeast extract	5.00
add: $MgCl_2$, $MgSO_4$, glucose	

2.3. Buffers

2.3.1. Potassium Phosphate (Kp_i) Buffer

KH_2PO_4 and K_2HPO_4 were diluted in bidistilled water to a final concentration of 0.2 M each. The desired pH was adjusted by mixing the two components. Finally, the buffer was diluted to the desired concentration with bidistilled water.

2.3.2. Tris HCl Buffer

2-Amino-2-hydroxymethyl-propane-1,3-diol (tris(hydroxymethyl)aminomethane, Tris) was diluted in bidistilled water to a final concentration of 500 mM. The desired pH was adjusted with HCl. Afterwards, the buffer was diluted with bidistilled water to the desired concentration.

2.3.3. Citrate-Phosphate Buffer

A solution of 200 mM citric acid was adjusted to the desired pH with a solution of 400 mM Na_2HPO_4.

2.3.4. TEA Buffer

Triethanolamine (tris(2-hydroxyethyl)amine, TEA) HCl was diluted in bidistilled water to a final concentration of 200 mM and adjusted to the final pH with NaOH.

2.3.5. Glycine-NaOH Buffer

A solution of 400 mM Glycine and 800 mM NaCl in bidistilled water was prepared. 10 mL of this solution were adjusted to the desired pH with 800 mM NaOH and the volume was adjusted with bidistilled water to a final volume of 20 mL.

2.4. Bacterial Strains and Plasmids

E. coli BL21(DE3) was used for the heterologous expression of transaminase genes. Plasmids generated by site-directed mutagenesis (see section 4.4.2) were directly introduced into *E. coli* BL21(DE3).

The *E. coli* strain XL1-Blue was used for cloning purposes and storage of the plasmids, containing the transaminase genes.

Tab. 3.7. *Bacterial strains and their characteristics used in this work.*

Strain	Characteristics	Reference(s)
Escherichia coli		
BL21(DE3)	F$^-$ *omp*T *dcm lon hsd*S$_B$(r$_B{}^-$ m$_B{}^-$) *gal* λ(DE3)	Studier *et al.* (1986)[84]
XL1-Blue	*rec*A1 *end*A1 *gyr*A96 *thi*-1 *hsd*R17 *sup*E44 *rel*A1 *lac* [F´ *pro*AB *lac*I^{q}ZΔM15 Tn10 (Tet^r)]	Stratagene

The synthesis of the transaminase genes was performed by GeneArt® (part of Life Technologies GmbH, Darmstadt, Germany). The genes were codon optimized for *E. coli* and were delivered subcloned. For expression experiments, the genes were cloned via the restriction sites *Nde*I and *Xho*I into the favoured expression vector.

Tab. 3.8. *Plasmids and their characteristics used in this work.*

Plasmid	**Characteristics**	**Reference(s)**
pET-19b	Vector for heterologous gene expression (pBR322 origin, amp^R, T7*lac*, N-terminal His-tag, enterokinase cleavage site)	Novagen
pET-19b_R-FPTA_N-His	pET-19b with *r-fpta* gene and N-terminal His-tag	this work
pET-19b_R-TRTA_N-His	pET-19b with *r-trta* gene and N-terminal His-tag	this work
pET-21a(+)	Vector for heterologous gene expression (pBR322 origin, f1 origin, amp^R, T7*lac*, C-terminal His-tag, N-terminal T7-tag)	Novagen
pET-21a(+)_R-AFTA	pET-21a(+) with *r-afta* gene	this work
pET-21a(+)_ATA-117	pET-21a(+) with *ata-117* gene	this work
pET-21a(+)_ATA-117-110	pET-21a(+) with *ata-117-110* gene	this work
pET-21a(+)_R-CGTA1	pET-21a(+) with *r-cgta1* gene	this work
pET-21a(+)_R-CGTA2	pET-21a(+) with *r-cgta2* gene	this work
pET-21a(+)_R-CMTA	pET-21a(+) with *r-cmta* gene	this work
pET-21a(+)_R-CPTA	pET-21a(+) with *r-cpta* gene	this work
pET-21a(+)_R-FPTA	pET-21a(+) with *r-fpta* gene	this work
pET-21a(+)_R-FPTA_C-His	pET-21a(+)_R-FPTA with C-terminal His-tag	this work

Plasmid	**Characteristics**	**Reference(s)**
pET-21a(+)_R-FPTA_C-His_F113Y	pET-21a(+)_R-FPTA_C-His with Phe113→Tyr113 exchange	this work
pET-21a(+)_R-FPTA_C-His_F113M_E115K	pET-21a(+)_R-FPTA_C-His with Phe113→Tyr113 and Glu115→Lys115 exchange	this work
pET-21a(+)_R-GCTA	pET-21a(+) with *r-gcta* gene	this work
pET-21a(+)_R-MKTA	pET-21a(+) with *r-mkta* gene	this work
pET-21a(+)_R-PMTA	pET-21a(+) with *r-pmta* gene	this work
pET-21a(+)_R-TATA	pET-21a(+) with *r-tata* gene	this work
pET-21a(+)_R-TOTA	pET-21a(+) with *r-tota* gene	this work
pET-21a(+)_R-TRTA	pET-21a(+) with *r-trta* gene	this work
pET-21a(+)_R-TRTA_C-His	pET-21a(+)_R-TRTA with C-terminal His-tag	this work
pET-21a(+)_R-TRTA_C-His_Y113R	pET-21a(+)_R-TRTA_C-His with Tyr113→Arg113 exchange	this work
pET-21a(+)_R-TRTA_C-His_Y113F	pET-21a(+)_R-TRTA_C-His with Tyr113→Phe113 exchange	this work
pET-21a(+)_R-TVTA	pET-21a(+) with *r-tvta* gene	this work

2.5. Oligonucleotides

The oligonucleotides used in this work are shown in Tab. 3.9.

Tab. 3.9. *Oligonucleotides used in this work.*

Primer	**Sequence (5'→3')**	**Feature**
R-FPTA NdeI	GGA ATT CCA TAT GAG CAC CAT GGA TAA AAT C	*Nde*I
R-FPTA XhoI His	CCG CTC GAG CAG TTT CAG TTT CTG ATA ATC AAT TTT	*Xho*I, no Stop
R-FPTA QC fw	GAT GCC NNK GTT GAA CTG ATT GTT ACC CGT GGT CTG AAA CCG GTT CGT GAA G	F113X (TTT→NNK)
R-FPTA QC rv	CAG TTC AAC MNN GGC ATC TTT AAT ACC GCT TTT TGC CAG CAT ATC AAA CAG GGT CAT AC	F113X (AAA→MNN)
R-TRTA NdeI	GGA ATT CCA TAT GAG CTG GAT GAA TAG CCT GTT TG	*Nde*I
R-TRTA XhoI His	CCG CTC GAG CTG GCT ATA TTC AAC TGC GGT G	*Xho*I, no Stop
R-TRTA QC F113 fw	GAT TTT GTT GAA CTG ATT GTT ACC CGT GGT CTG AAA GGT GTT CGT GGT AG	Y113F (TAT→TTT)
R-TRTA QC F113 rv	CAG TTC AAC AAA GGC ATC ACG CAT ACC GCT TTT GGC AAC CAT ATC AAA CAG	Y113F (ATA→AAA)
R-TRTA QC fw	GAT NNK GTT GAA CTG ATT GTT ACC CGT GGT CTG AAA GGT GTT CGT GGT AG	Y113X (TAT→NNK)
R-TRTA QC rv	CAG TTC AAC MNN GGC ATC ACG CAT ACC GCT TTT GGC AAC CAT ATC AAA CAG	Y113X (ATA→MNN)

3. Microbiological Methods

3.1. Cultivation and Storage of *E. coli* Strains

The cultivation of *E. coli* was performed in LB medium at 37 °C. Precultures or cultures for DNA isolation up to a volume of 5 mL were incubated in a test tube overnight. For cultures with a higher volume, Erlenmeyer flasks with baffles were used. The media volume did not exceed 20 % of the flask volume. Cultures were incubated in a shaking device at 180 rpm. Overnight cultures were incubated for at least 16 h. Plasmid containing strains with ampicillin resistance marker genes were cultiviated in 100 µg/mL ampicillin containing medium. All cultures were inoculated with single cell colonies from LB agar plates.

For the storage of bacterial strains, overnight cultures from test tubes were supplemented with 21.5 % sterile gylcerol (v/v) and overnight cultures from microtiter plates were supplemented with 10 % sterile glycerol (v/v), respectively. These cryo cultures were stored at –80 °C.

3.2. Gene Expression in Recombinant *E. coli* Strains

Expression cultures were inoculated from precultures to an optical density of OD_{580}=0.05. Cultivations were performed using baffled Erlenmeyer flasks with LB medium, unless stated otherwise, in addition with the appropriate antibiotic and in case of transaminases with 0.1 mM pyridoxine. The volume of medium did not exceed 20 % of the flask volume. Expression cultures were grown to an OD_{580}=0.5–0.7 at 37 °C and 180 rpm. Unless otherwise noted, the gene expression was induced by adding 0.3 mM IPTG. The incubation of the cultures was continued at 18–30 °C for 4–16 h.

For the screening of transaminase mutants, clones were cultivated in microtiter plates (96 wells, 2.2 mL volume; Sarstedt AG & Co, Nümbrecht) in 1 mL TB medium, supplemented with 100 µg/mL ampicillin and 0.1 mM pyridoxine. The wells were inoculated with single cell colonies from agar plates and the microtiter plates were incubated overnight at 600 rpm (TiMix 5 control, Edmund Bühler GmbH, Hechingen, Germany). The gene expression was induced by adding 0.3 mM IPTG and the incubation was continued at 30 °C and 600 rpm in case of *E. coli* pET-21a(+) *r-trta_c-his* and at 25 °C and 400 rpm in case of *E. coli* pET-21a(+) *r-fpta_c-his*.

Transaminase variants were produced in a total volume of 500 mL TB medium for further characterization. The medium was complemented with 100 µg/mL ampicillin and 0.1 mM pyridoxine. Since Erlenmeyer flasks without baffles were used, the media

volume was 10 % of the flask volume. The cultures were inoculated with singles cell colonies and incubated for 15 h at 37 °C and 180 rpm. By adding 0.3 mM IPTG, the gene expression was induced. The temperature was lowered to 25 °C and the cultures were incubated for another 7 h.

All cultures up to a volume of 100 mL were harvested by centrifugation for 10–20 min at 4 °C and 4 000 rpm (centrifuge 5810 R, Eppendorf AG, Hamburg, Germany). Larger cultures were harvested by centrifugation for 20 min at 4 °C and 8 000 rpm (centrifuge J2-21M/E, Beckman Coulter GmbH, Krefeld, Germany). The supernatants were discarded and cell pellets were used directly or stored for later use at –20 °C.

3.3. High Cell Density Fed-Batch Fermentation for the Production of Transaminases

The high cell density fermentation for the production of transaminases was performed in fed-batch modus in a 7.5 L fermenter (Labfors 3, Infors AG, Bottmingen, Switzerland) according to the company-internal protocol in a minimal medium. After 24 h of fermentation, the biomass was harvested by centrifugation (centrifuge J2-21M/E, Beckman Coulter GmbH, Krefeld, Germany).

4. Molecular Biology Methods

4.1. Preparation of Plasmid DNA

Plasmid DNA was isolated from *E. coli* precultures using the GeneJet Plasmid Miniprep Kit (Thermo Fisher Scientific GmbH, Dreieich, Germany).

DNA concentration was determined by agarose gel electrophoresis or measured at 260 nm in a spectrophotometer (NanoDrop ND-2000, PEQLAB Biotechnology GmbH, Erlangen, Germany).

4.2. Restriction, Dephosphorylation and Ligation of DNA *in vitro*

In general, cloning techniques described by Sambrook *et al.*[85] were used. Restriction enzymes from NEB (New England Biolabs, Schwalbach, Germany) were used for cutting DNA strands. For dephosphorylation and ligation purposes, shrimp alkaline phosphatase and T4 ligase from Roche (Roche Diagnostics Deutschland GmbH, Mannheim, Germany) were used. All enzymes were applicated following the manufacturer's guidelines.

4.3. Preparation of Competent Cells and Transformation of *E. coli*

For the preparation of chemical competent cells, 100 mL of LB medium were complemented with 10 mM $MgCl_2$ and 10 mM $MgSO_4$ and inoculated with 1 mL from a 4 mL overnight preculture. The culture was incubated in a 500 mL Erlenmeyer flask without baffles at 180 rpm and 37 °C, up to an optical density of OD_{600}=0.5–0.7. The culture was split up on 50 mL tubes and the cells were harvested by centrifugation (4 °C, 4 000 rpm, 20 min; centrifuge 5810 R, Eppendorf AG, Hamburg, Germany). The supernatant was discarded and the cell pellets were carefully resuspended in 25 mL ice cold TMF buffer (see Tab. 3.5). The cells were incubated for 1 h on ice, harvested and resuspended in 5 mL ice cold TMF buffer and 1.5 mL ice cold glycerol (86 % (v/v)). Aliquots of 100 µL were prepared and directly used for heat shock transformation or stored at –80 °C.

To prepare electrocompetent cells, cells were grown and harvested as described above, but in LB medium without supplements. Each cell pellet was carefully resuspended in 50 mL ice cold sterile bidistilled water and centrifuged (4 °C, 4 000 rpm, 20 min; centrifuge 5810 R, Eppendorf AG, Hamburg, Germany) again. The supernatant was discarded and the cells were resuspended in 25 mL ice cold sterile bidistilled water and centrifuged again. Then, the cell pellets were resuspended in 1.25 mL ice cold sterile glycerol (10 % (v/v)), centrifuged once again and were finally resuspended in 400 µL ice cold sterile glycerol (10 % (v/v)). The cells were divided into aliquots of 40 µL and directly put at –80 °C.

Transformation of chemical competent cells was done via heat shock. Plasmid DNA solution (depending on DNA concentration in plasmid DNA solution) was added to an aliquot of competent cells and incubated on ice for 30 min. For the heat shock, the cells were placed for 30–90 sec at 42 °C and afterwards directly on ice for 5 min. To regenerate the cells, 300 µL LB medium or 950 µL SOC medium (see Tab. 3.6) were added to the cells. The cells were incubated for 1 h at 37 °C and 180 rpm and were plated on LB agar plates containing the appropriate antibiotic. The plates were incubated overnight at 37 °C (heating chamber ED115, BINDER GmbH, Tuttlingen, Germany). Whenever high transformations efficiencies were necessary, only 30 sec incubation time at 42 °C and SOC medium were chosen.

For transformation of the electrocompetent cells, an ice cold 1 mm electroporation cuvette was filled with one aliquot of electrocompetent cells and desalted plasmid DNA solution (1–3 µL plasmid DNA solution depending on DNA concentration). The electro shock (1.6 kV, 250 Ω, 25 µF) was applied to the cells and 950 µL pre-warmed SOC medium were added subequently. The cell suspension was transferred to a tube and incubated for 1 h at 37 °C and 180 rpm to regenerate. Afterwards, the cells were plated on selective LB

agar plates and were incubated at 37 °C overnight (heating chamber ED115, BINDER GmbH, Tuttlingen, Germany).

4.4. Polymerase Chain Reaction (PCR)

The polymerase chain reaction (PCR) was used to amplify the transaminase genes[86] and enable the fusion His-Tags and the implementation of mutations, respectively.

4.4.1. DNA Amplification for the Fusion of His-Tags

The PCR for the fusion of His-tags to transaminase genes was performed in a total volume of 50 µL, containing 50–100 ng plasmid DNA as template and the corresponding DNA primers in a concentration of 10 µM as well as 0.2 mM deoxynucleotides (dNTPs). The reaction batch was complemented with 1 U Phusion® High-Fidelity polymerase (New England Biolabs, Schwalbach, Germany) in the corresponding buffer, provided by the manufacturer.

The PCR was performed in the PCR instrument Mastercycler® ep gradient (Eppendorf AG, Hamburg, Germany), starting with an initial denaturating step at 98 °C for 2 min. The cycle of denaturation, annealing and elongation (98 °C: 30 sec, 58 °C: 30 sec, 72 °C: 30 sec) was repeated 25 times. The final elongation step was performed for 10 min at 72 °C and the PCR was finished at 4 °C. All PCR products were purified via agarose gelelectrophoresis (see section 4.6).

4.4.2. Site-Directed Mutagenesis

For the implementation of point mutations into the transaminase genes on double stranded plasmid DNA, long DNA primers carrying the desired mutation,[87] were used (see Tab. 3.9). By using the degenerated `NNK` codon, the wild-type codon was replaced by triplets coding for all twenty amino acid with focus on small amino acids.

In Fig. 3.1, the process of the site-directed mutagenesis is illustrated. Whole plasmids are amplified. The oligonucleotides which are used as primers for the PCR contain the desired mutation. Since the amplified plasmid DNA with the mutation is not methylated, only the methylated template DNA is digested by using the restriction enzyme DpnI. Ideally, the complete template DNA is digested and cells are only transformed with the plasmid DNA carrying the mutation. Inside the cell, nicked DNA ends are closed and during replication these plasmids are also methylated.

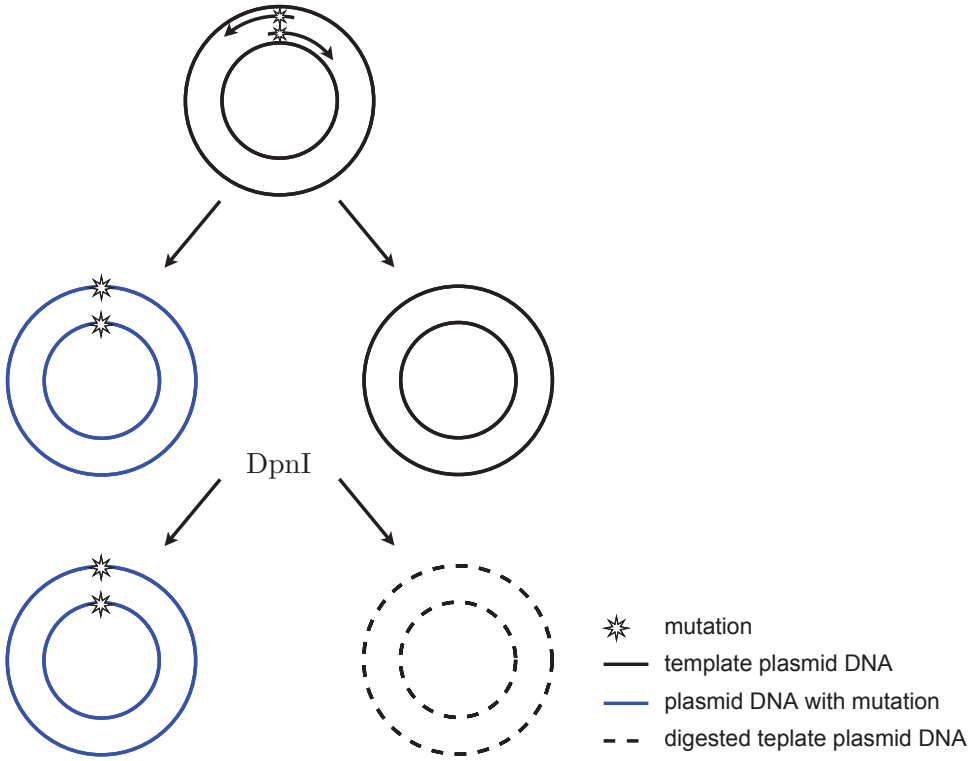

Fig. 3.1. *Site-directed mutagenesis. The mutation lies on the oligonucleotides used as primer. The whole plasmid is replicated and only the methylated template DNA is digested by the endonuclease DpnI.*

The reaction mix contained reduced concentrations of plasmid DNA as template (1–2 ng) and DNA primer (10 µM each), 0.2 mM dNTPs, 3 % DMSO and 2 U Phusion® High-Fidelity polymerase (New England Biolabs, Schwalbach, Germany) in the corresponding buffer. Following an initial denaturating step (98 °C, 3 min), the cycle of denaturation, annealing and elongation (98 °C: 1 min, 62 °C/66 °C/72 °C: 25 sec, 72 °C: 30 sec/kb) was repeated 26 times. The reaction was run at three different annealing temperatures. After the final elongation step (72 °C: 10 min), the PCR was finished at 4 °C. The PCR products were purified (omni-pure-OLS®, OLS OMNI Life Science GmbH & Co. KG, Bremen, Germany) and the methylated parental plasmid DNA was digested with the restriction enzyme *Dpn*I. *E. coli* BL21(DE3) cells were transformed (see section 4.3) with the mutation carrying plasmids and used for the screening of transaminases.

4.5. DNA Sequencing

The DNA sequencing reactions were performed at GATC Biotech AG (Konstanz, Germany) by the method of Sanger.[88]

4.6. Agarose Gel Electrophoresis

DNA fragments were analysed and purified by agarose gel electrophoresis based on the method described by Sambrook.[85] 0.5x TBE buffer or 1x TAE buffer were used as electrophoresis buffer. Agarose gels were prepared by diluting 1.2 % agarose in buffer. For the staining of DNA, the agarose dilution was supplemented with EtBr (ethidium bromid) and in case of DNA purification after PCR with peqGreen (PeqLab), respectively. "1 kB DNA ladder" (Thermo Fisher Scientific, Waltham, USA and New England Biolabs; Ipswich, USA) was used as a size standard.

Results of gel electrophoresis were documented using a gel imaging system (G:BOX, Syngene; Frederick, USA). For the extraction of DNA from agarose gels, desired DNA fragments were cut from the agarose gel and the DNA was isolated via the omni-pure-OLS® kit (OLS OMNI Life Science GmbH & Co. KG, Bremen, Germany).

5. Biochemical Methods

5.1. Preparation of Cell Extracts and Lyophilisates

Cells from expression cultures were resuspended to 25 % in 100 mM Tris HCl buffer, pH 7.2. The cells were disrupted by two passages of ultrasonication on ice for 1.5 min and 5 cycles at 15–40 % (Bandelin Sonopuls UW 2070; Sonotrode MS 72, BANDELIN electronic GmbH & Co. KG, Berlin, Germany). Insoluble cell fragments and cell extracts were separated by centrifugation for 20 min at 4 °C and 15 000 rpm (centrifuge MIKRO 200 R, Hettich Lab Technology, Tuttlingen, Germany). The soluble fractions were used for further analyses.

Cells from microtiter plate cultures were treated with lysozyme to digest the cell walls and DNase to prevent viscosity because of the release of DNA from the cells. Cell pellets were resuspended in a solution of 500 µL 100 mM Kp_i buffer pH 8, containing 0.25 mg/mL lysozyme, 1 µg/mL DNase (≈ 3.23 U/mL), 0.5 mM $MgCl_2$ and 0.05 mM PLP and incubated overnight at 4 °C. Afterwards, cell fragments and the cell extract were separated by centrifugation for 10 min at 4 °C and 15 000 rpm (centrifuge 5810 R, Eppendorf AG, Hamburg, Germany).

The biomass obtained from high cell density fermentations and from larger shaking flask cultures were disrupted in two passages through a homogenizer (APV-1000, SPX Flow Technology, Crawley, UK). Cell pellets were prepared as described above and the resuspension solution was supplemented with 1 mM $MgCl_2$ and 3 U/mL DNase. The homogenization was performed with a pressure of 800–900 bar and meanwhile the sus-

pension was held on ice. Smaller samples from shaking flask cultures were centrifuged directly for 20 min at 4 °C and 11 000 rpm (centrifuge Multifuge X3R, Thermo Fisher Scientific GmbH, Dreieich, Germany). The supernatants were filled in pre-cooled lyophilisation bowls and frozen at –20 °C.

Samples from high cell density fermentations were processed as described in the company-internal protocol. The resulting supernatants were frozen in lyophilisation bowls at –20 °C.

The frozen supernatants were freeze dried for 1–2 days in a lyophilizer (Alpha 1-4 LSC, Martin Christ Gefriertrocknungsanlagen GmbH, Osterode am Harz, Germany). Lyophilisates were directly put into storage vessels and stored at –20 °C.

5.2. His-Tag Purification

Purification of transaminases to determine the functionality of the attached His-tag was performed using Ni-NTA spin columns, following the manufacturer's protocol (Qiagen GmbH, Hilden, Germany). Cells from 50 mL expression culture were resuspended in lysis buffer and disrupted by ultrasonication as already mentioned. For better elution, a second elution buffer with 350 mM imidazole was used additionally.

For crystallisation purposes, purification of a large amount of protein was performed in a batch mode as described in the "HisPur® Ni-NTA Superflow Agarose" (Thermo Fisher Scientific GmbH, Dreieich, Germany) instructions, with 4 mL Ni-NTA Superflow resin (Qiagen GmbH, Hilden, Germany) in a 15 mL reaction tube. Buffers for equlibration, washing and elution were prepared as described for Qiagen's Ni-NTA spin coloums. Because of the larger amount of protein needed, enzyme was purified from lyophilisate instead of cell extracts. For binding the His-tagged protein to the resin, the reaction tube was incubated for 90 min on a rotary mixer at 22 rpm at room temperature.

The fractions showing transaminase activity were rebuffered to remove the detergents. To prevent a denaturation of the enzyme, the buffer was first changed to lysis buffer with a low concentration of imidazol and finally to 100 mM Tris HCl buffer, pH 7.2. For rebuffering, Vivaspin 20 (Sartorius AG, Göttingen, Germany) centrifugal concentrators with a molecular weight cut-off of 10 kDa were used.

5.3. Refolding from Inclusion Bodies

To increase the amount of solouble enzymes the proteins from inclusion bodies were denatured and refolded again. The procedure and the used buffers were established on basis of the manuals from the "QuickFold® Protein Refolding Kit" (Athena Environmental

Sciences, Inc., Baltimore, USA) and the "Pro-Matrix® Protein Refolding Kit" (Thermo Fisher Scientific GmbH, Dreieich, Germany).

Cells from transaminase expression cultures were disrupted by ultrasonication as described already and centrifuged for 30 min at 4 °C and 20 000×g (centrifuge 50804R, Eppendorf AG, Hamburg, Germany). The pellet was washed twice in 5 mL washing buffer (4 M urea, 0.5 M NaCl, 1 mM EDTA (ethylenediaminetetraacetic acid) and 1 mg/mL sodium deoxycholate in 50 mM TrisCl, pH 8) with centrifugation steps (15 min at 4 °C and 20 000×g) in between. The washed pellet was resuspended in 2 mL/g denaturation buffer (8 M guanidine HCl and 10 mM DTT (dithiothreitol) in 10 mM Tris HCl, pH 8) and incubated at 4 °C overnight. The solution was centrifuged (30 min, 4 °C, 20 000×g) and DTT was removed using a PD10 column (GE Healthcare Europe GmbH, Freiburg, Germany), equilibrated with buffer without DTT. 50 µL of this protein solution were added to 950 µL of nine different refolding buffers, consisting of 18 mM NaCl, 0.8 mM KCl, 0.1 mM pyridoxal 5'-phosphate and different concentrations of DTT, guanidine, L-arginine, GSH (glutathione) and GSSG (glutathione disulfide) in 50 mM Tris HCl, pH 8.2. The refolding samples were incubated at 4 °C for 18 h. Subsequently, transaminase activity (acetophenone assay, see section 6.3) of the refolding probes was determined and denaturated protein (white precipitation) was documented.

For the analysis on SDS-PAGE, the washed and rebuffered inclusion bodies were precipitated with ice cold ethanol to remove the detergents. Refolding samples were precipitated with trichloroacetic acid. The precipitated inclusion bodies and proteins were then resuspended in SDS gel loading buffer and denaturated for 10 Min at 95 °C. Calculated from the dilution of the samples, 20 µg of protein were loaded on the gels.

6. Analytical Methods

6.1. Determination of Protein Concentrations

Protein concentrations were determined via the Bradford assay[89] in microtiter plates (Greiner-Bio-One GmbH, Frickenhausen, Germany) at 595 nm (SpectraMax 250, Molecular Devices, Sunnyvale, USA). As Bradford reagent, ready-to-use "Roti®-Quant" solution (Carl Roth GmbH+Co KG, Karlsruhe, Germany) was used. Defined concentrations of bovine serum albumine (BSA) were used to generate a standard curve. The samples were measured in duplicate.

6.2. SDS Polyacrylamide Gel Electrophoresis (PAGE)

Sodium dodecyl sulfate polyacrylamide gel electrophoresis (SDS-PAGE) was performed to analyse the expression of target proteins. Discontinuous gels were prepared as described by Laemmli[90] in a "Mini-PROTEAN® Tetra" (Bio-Rad Laboratories GmbH, Munich, Germany) handcast system. The separation gels contained 12 % acrylamide or 15 % acrylamide for the separation of His-tagged proteins, respectively. The stocking gels contained 5 % acrylamide. Prior to separation, protein samples were supplemented with protein gel loading buffer ("Roti®-Load 1", Carl Roth GmbH+Co KG, Karlsruhe, Germany) and denaturated for 10 Min at 95 °C. Generally, gels were loaded with 20 µg protein. As size standards "Unstained Protein Marker, Broad Range (2–212 kDa)" (New England Biolabs, Schwalbach, Germany) or "PageRuler™ Prestained Protein Ladder (10–170 kDa)" (Thermo Fisher Scientific GmbH, Dreieich, Germany) were used.

Electrophoresis was run in "Mini-PROTEAN® Tetra" (Bio-Rad Laboratories GmbH, Munich, Germany) chambers, filled with electrophoresis buffer (25 mM Tris, 129 mM glycine, 0.1 % SDS) at 120–140 V. The gels were stained in a solution of 25 % (v/v) 2-propanol and 10 % (v/v) acetic acid with 0.05 % (w/v) Coomassie Brilliant Blue R-250.

6.3. Acetophenone Assay

Transaminase activities were determined towards the substrate 1-phenylethylamine **1a** The formation of the product acetophenone **2a** was measured spectrophotometrically (see Fig. 3.2) in UV microtiterplates (Greiner-Bio-One GmbH, Frickenhausen, Germany) based on the method of Schätzle *et al.*[67]

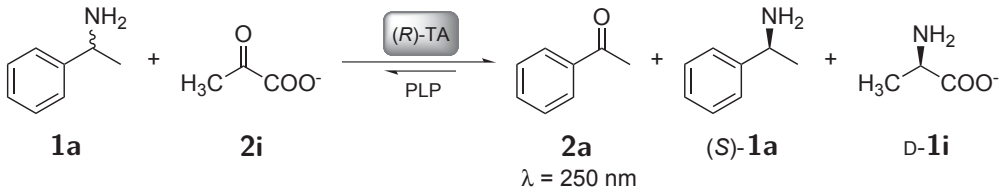

Fig. 3.2. *Acetophenone assay.*

The reaction was started by adding substrate solution (final concentrations in a total volume of 200 µL: 5 mM 1-phenylethylamine **1a**, 5 mM pyruvate **2i** and 5 µM PLP in 100 mM Kpi, pH 8) to cell extracts or resuspended lyphilisates in an appropriate dilution. During the incubation at 30 °C in a microplate reader (SpectraMax 250, Molecular Devices, Sunnyvale, USA), the change of absorbance was monitored over 20 min at

250 nm. The volume actvities were determined following the equation 6.1:

$$U/ml = \frac{\frac{\Delta E}{\Delta t} \cdot V}{\epsilon \cdot d \cdot v} \cdot f \tag{6.1}$$

$\frac{\Delta E}{\Delta t}$	=	change of absorbance per min at 250 nm
V	=	total volume
ϵ	=	molar absorption coefficient of acetophenone $\left[11.046 \frac{\text{L}}{\text{mmol·cm}}\right]$
d	=	optical path length
v	=	sample volume
f	=	dilution of the sample

The molar absorption coefficient of **2a** was determined by measuring the absorbance of different concentrations of **2a** in H_2O at 250 nm. Plotting the measured absorbance against the concentration of **2a** gave a linear slope with gradient corresponding to the molar absorption coefficient of 11.046 $\frac{\text{L}}{\text{mmol·cm}}$.

For the determination of the pH optima of transaminases, the Kp_i buffer was substituted by different buffers, according to the desired pH value:

- pH 5–7: citrate-phosphate buffer
- pH 6–8: Kp_i buffer
- pH 7–8.5: TEA buffer
- pH 7.5–9: Tris HCl buffer
- pH 8.5–11: glycine-NaOH buffer

The activities were measured in duplicate. From results for identic pH values, the mean value was determined.

Temperature stability was measured with enzyme solutions (100 µL), which were incubated for 10 min at different temperatures from 0–50 °C in a PCR cycler (TProfessional, Biometra GmbH, Göttingen, Germany) and cooled on ice afterwards. The reference sample was held on ice the whole time. The activities were then measured with the acetophenone assay.

6.3.1. Determination of Kinetic Parameters

The catalytic parameters for the ω-transaminases were determined with the acetophenone assay. The activities were measured with a constant concentration of 5 mM **2i** and concentrations of **1a** in a range from 0.3 mM to20 mM. The initial velocities were plotted against the substrate concentrations and the curves were fitted with the bi-substrate Hill-Equation[91,92] 6.2 and the Michaelis-Menten equation[93] 6.3.

Since the transamination reaction is a two substrate reaction, the bi-substrate Hill equation was used for the fitting. Additionally, values up to the maximum (beginning of substrate inhibition) were fitted with the Michaelis-Menten equation. The catalytic parameters of the ω-transaminases were determined with these equations.

$$V = \frac{P_{max}}{[1 + (\frac{K_a}{[S]})^{H_a}][1 + (\frac{[S]}{K_i})^{H_i}]} \tag{6.2}$$

$$V = \frac{V_{max}[S]}{K_m + [S]} \tag{6.3}$$

where:

V	=	initial velocity	H_a	=	activation Hill coefficient
P_{max}	=	maximal velocity	H_i	=	inhibitory Hill coefficient
$[S]$	=	substrate concentration	V_{max}	=	maximal velocity
K_a	=	half-maximal activating [S]	K_m	=	Michaelis-Menten constant
K_i	=	half-maximal inhibitory [S]			

6.4. D-Amino Acid Oxidase (D-AAO) Assay

Since the acetophenone assay is limited on **1a** as substrate, the coupled D-amino axid oxidase (D-AAO) assay (see Fig. 3.3) was adapted from Hopwood *et al.*[68] for the screening of other transaminase substrates (see Fig. 2.7). The colour reagent used here, *o*-dianisidine (2,2'-dimethoxy-4,4'-benzidine) is oxidized by horse radish peroxidase to a bisazobiphenyl product,[94] resulting in a red colour.

The assay was run in microtiter plates (Greiner-Bio-One GmbH, Frickenhausen, Germany) in a total volume of 100 µL per well. The substrate mixtures in 100 mM Kp_i pH 8, containing 5 mM pyruvate **2i**, 5 mM of each amine **1a**–**1h** and 5 µL PLP were complemented with the enzymes D-AAO (1.6 U/mL) and HRP (25 µg/mL) and the colour reagent *o*-dianisidine (0.1 mg/mL). According to the transaminase activity, several of

the measurements were also performed with half of the amount of D-AAO, HRP and *o*-dianisidine. The reaction was started by adding 20 µL of transaminase cell extracts in an adequate dilution.

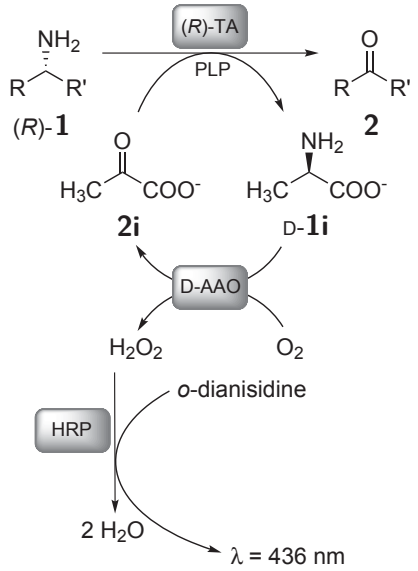

Fig. 3.3. *D-AAO assay. The deamination of the amine by the transaminase is followed by the back reaction of* D*-alanine to pyruvate, catalysed by D-AAO (*D*-amino acid oxidase). D-AAO thereby reduces oxygen to hydrogen peroxide. The hydrogen peroxide is further reduced to water by HRP (horseradish peroxidase). o-Dianisidine serves as electron acceptor and is oxidized by HRP to the reddish bisazobiphenyl product.*

During the incubation at 30 °C in a microplate reader (SpectraMax 250, Molecular Devices, Sunnyvale, USA), the colour reaction was monitored over 20 min at 436 nm. The volume actvities were determined following the equation 6.4:

$$U/ml = \frac{\frac{\Delta E}{\Delta t} \cdot V}{\epsilon \cdot d \cdot v} \cdot f \tag{6.4}$$

$\frac{\Delta E}{\Delta t}$	=	change of absorbance per min at 436 nm
V	=	total volume
ϵ	=	molar absorption coefficient of *o*-dianisidine $\left[8.1 \frac{\mathrm{L}}{\mathrm{mmol \cdot cm}}\right]$
d	=	optical path length
v	=	sample volume
f	=	dilution of the sample

6.5. Gas Chromatography

The amination and deamination reactions were determined by gas chromatography (GC) (Focus GC gas chromatograph with a TriPlus autosampler, Thermo Fisher Scientific GmbH, Dreieich, Germany) on a CP-CHIRASIL-DEX CB chiral column (25 m × 0.25 mm ID, Agilent Technologies, Inc., Santa Clara, USA) with an FID (flame ionization detector). The mobile phases were Helium and Hydrogen, respectively.

The reactants were extracted from the basic aqueous reaction medium by solvent extraction with ethyl acetate or methyl *tert*-butyl esther (MTBE). For this purpose, 100 µL sample were supplemented with 10 µL 5 % NaOH (the reaction in samples from the biotransformation assay (see section 7) was stopped by adding 10 µL 5 % NaOH) and 100 µL solvent was added. By vortexing the mixture the reactants were transferred into the solvent. The samples were then centrifuged briefly to separat the organic phase from the aqueous phase and the organic phase was transferred to GC vials. By adding 5 µL of acetic acid anhydride and 10 µL of pyridine or 5 µL of acetic acid anhydride containing 5 mg/mL DMAP (4-dimethylaminopyridine) to the GC vials, amines were turned to their corresponding amides. The derivatization of amines to amides was necessary to improve the separation of the enantiomers. As references, the pure compounds or their racemic mixtures were used.

Below, the temperature programs to separate the ketones and amides are given. The retention times for ketones t_K, (*S*)-enantiomer t_S and (*R*)-enantiomer t_R are given as well.

Mobile phase: He

2a/1a-acetamide A) Constant flow, 3 mL/min. 3 min at 80 °C, heating at 10 °C/min to 170 °C and keeping at 170 °C for 3 min. t_K=6.82 min, t_S=11.69 min, t_R=11.81 min.
B) Constant pressure, 75 kPa. 1 min at 150 °C, heating at 5 °C/min to 170 °C and keeping at 170 °C for 5 min. t_K=3.5 min, t_S=8.57 min, t_R=8.87 min.

2b/1b-acetamide Constant pressure, 75 kPa. 1 min at 150 °C, heating at 5 °C/min to 170 °C and keeping at 170 °C for 15 min. t_K=5.16 min, t_S=18.43 min, t_R=19.37 min.

2c/1c-acetamide A) Constant pressure, 100 kPa. 15 min at 160 °C, heating at 50 °C/min to 200 °C and keeping at 200 °C for 1.6 min. t_K=3.52 min, t_S=15.53 min, t_R=15.73 min.
B) Constant pressure, 100 kPa. 17 min at 160 °C, heating at 50 °C/min to 200 °C and keeping at 200 °C for 1.6 min. t_K=3.65 min, t_S=15.73 min, t_R=16.38 min.

2d/1d-acetamide Constant flow, 2.5 mL/min. 50 min at 160 °C. t_K=7.35 min, t_S=43.17 min, t_R=45.32 min.

2e/1e-acetamide Constant flow, 2.5 mL/min. 5 min at 155 °C, heating at 5 °C/min to 180 °C and keeping at 180 °C for 2 min. t_K=2.64 min, t_S=8.90 min, t_R=9.24 min.
2f/1f-acetamide Constant flow, 2.5 mL/min. 27 min at 155 °C. t_K=4.17 min, t_S=22.83 min, t_R=24.31 min.
2g/1g-acetamide Constant flow, 3 mL/min. 3 min at 60 °C, heating at 10 °C/min to 170 °C and keeping at 170 °C for 3 min. t_K=2.18 min, t_S=9.23 min, t_R=9.60 min.
2h/1h-acetamide Constant flow, 3 mL/min. 3 min at 100 °C, heating at 7 °C/min to 180 °C, heating at 20 °C/min to 200 °C and keeping at 200 °C for 3 min. t_K=4.63 min, t_S=11.17 min, t_R=11.45 min.

Mobile Phase: H_2
2a/1a-acetamide Constant flow, 1.5 mL/min. Starting at 110 °C, heating at 10 °C/min to 140 °C, heating at 5 °C/min to 165 °C and heating at 120 °C/min to finally 225 °C. t_K=2.72 min, t_S=7.28 min, t_R=7.48 min.
2b/1b-acetamide Constant flow, 1.5 mL/min. Starting at 145 °C, heating at 5 °C/min to 185 °C and heating at 120 °C/min to finally 225 °C. t_K=2.56 min, t_S=7.58 min, t_R=7.80 min.
2c/1c-acetamide Constant flow, 1.5 mL/min. Starting at 130 °C, heating at 20 °C/min to 150 °C, heating at 3 °C/min to 180 °C and heating at 120 °C/min to finally 225 °C. t_K=2.39 min, t_S=7.99 min, t_R=8.23 min.
2d/1d-acetamide Constant flow, 1.5 mL/min. Starting at 140 °C, heating at 20 °C/min to 170 °C, heating at 4 °C/min to 210 °C and heating at 120 °C/min to finally 225 °C. t_K=4.41 min, t_S=10.13 min, t_R=10.50 min.
2e/1e-acetamide Constant flow, 1.5 mL/min. Starting at 150 °C, heating at 10 °C/min to 185 °C, heating at 5 °C/min to 210 °C and heating at 120 °C/min to finally 225 °C. t_K=2.27 min, t_S=4.80 min, t_R=4.93 min.
2f/1f-acetamide Constant flow, 1.5 mL/min. Starting at 145 °C, heating at 5 °C/min to 195 °C and heating at 120 °C/min to finally 225 °C. t_K=5.08 min, t_S=9.35 min, t_R=9.48 min.
2g/1g-acetamide Constant flow, 1.5 mL/min. 2 min at 55 °C, heating at 5 °C/min to 65 °C and heating at 20 °C/min to finally 225 °C. t_K =2.49 min, t_S=7.61 min, t_R=7.77 min.
2h/1h-acetamide Constant flow, 1.5 mL/min. Starting at 105 °C, heating at 7 °C/min to 130 °C, heating at 10 °C/min to 200 °C, keeping for 1 min at 200 °C and heating at 120 °C/min to finally 225 °C. t_K=2.86 min, t_S=7.34 min, t_R=7.48 min.

7. Biotransformation of Amines and Ketones with Transaminases

To determine the conversion of amine to ketone catalysed by transaminases and vice versa as well as the enantiomeric selectivity, biotransformation assays were performed. Biotransformations with new enzymes (see Tab. 3.1 amination and deamination A)) were performed in a total volume of 250 µL at 30 °C and 300 rpm in a ThermoMixer® (Eppendorf AG, Hamburg, Germany). Samples were taken at several time points and the reaction was stopped by adding 10 µL of 5 % NaOH. Subsequently, the samples were prepared for gas chromatography (see section 6.5). The enantiomeric excess was determined by chiral gas chromatography.

Tab. 3.1. *Components of biotransformation assays.*

Reaction	**Components**
Amination	A) 10 mM Kp_i pH 7, 500 mM D-alanine, 1 mM PLP, 5 mM ketone
	B) 10 mM Kp_i pH 7, 250 mM *sec*-butylamine, 1 mM PLP, 5 mM ketone
Deamination	A) 25 mM Tris HCl pH 7.5, 5 mM pyruvate, 5 mM amine
	B) 31.25 mM Tris HCl pH 7.5, 6.3 mM pyruvate, 6.2 mM amine

Substrate spectra of transaminases were recorded with a more precise method (see Tab. 3.1 amination and deamination B)). For each time point samples were prepared in a total volume of 100 µL and the reaction was stopped directly in the reaction vessel by adding 10 µL of 5 % NaOH. Incubation and further processing of the samples were performed as described above.

8. Software and Databases

"Clone Manager 9 Professional Edition" (Scientific and Educational Software, Cary, USA) was used for drawing vector and plasmid maps. Also analysis of oligonucleotides was done with "Clone Manager". Sequence alignments were either done with "Clone Manager" or "BioEdit".[95] Database searching for new enzymes was done with the the "Basic Local Alignment Search Tool–BLAST" (http://blast.ncbi.nlm.nih.gov/Blast.cgi). Protein structures were visualized with UCSF Chimera (Resource for Biocomputing, Visualization, and Informatics at the University of California, San Francisco, USA).[96] The

program “SoftMax Pro v5.3” (Molecular Devices, Sunnyvale, USA) was used for recording and analysis of kinetic measurements. The analysis of chromatograms from gas chromatographic measurements was done with “Chrom-Card Gas Chromatography Data System” (Thermo Fisher Scientific GmbH, Dreieich, Germany). For fermenter regulations, “IRIS 5.02” (Infors AG, Bottmingen, Switzerland) software was used.

IV. Results

1. Identification of Novel (*R*)-Selective ω-Transaminases

Several ω-transaminases have been described during the last decade, providing only one enzyme with (*R*)-selective transaminase activity.[34,69,70] So far, this is the only ω-transaminase with (*R*)-selectivity that was found by screening soil samples or strain collections. Höhne *et al*. described a new *in silico* strategy as an instrument to identify new ω-transaminases.[1] In this work, a more basic approach was performed by comparing the sequence of the first known (*R*)-selective ω-transaminase with the protein sequences in the BLAST database to find novel (*R*)-selective ω-transaminases. Moreover, metagenome sequences were scanned for new (*R*)-selective ω-transaminases.

1.1. First Round: *In Silico* Screening for new (*R*)-Selective ω-Transaminases

From previous *in silico* screenings, the sequence of an (*R*)-selective branched-chain aminotransferase from *Mesorhizobium loti* MAFF303099 was known. The sequence of this (*R*)-selective branched-chain aminotransferase and the sequence of the first known ω-transaminase from *Arthrobacter* sp. KNK168 were used as query sequences in a protein BLAST against the NCBI (National Center for Biotechnology Information) database. From the results, four protein sequences were chosen:

- class IV aminotransferase R-CMTA from *Cordyceps militaris*
- D-alanine aminotransferase R-TRTA from *Trichoderma reesei*
- branched-chain amino acid aminotransferases R-MKTA from *Methanopyrus kandleri*
- branched-chain amino acid aminotransferases R-TOTA from *Thermosediminibacter oceani*

Additionally, the sequence of the

- putative (*R*)-selective ω-transaminase R-CPTA from *Candidatus Pelagibacter ubique*

was found in metagenome sequences. The new enzymes and the query enzymes had sequence identities of 32–55 % (see Tab. 4.1).

Tab. 4.1. *Amino acids sequence identities and Expect (E) values (BLAST version 2.231+) of new* (R)*-selective ω-transaminases from the first* in silico *screening.*

	***Arthrobacter* sp. KNK168**		***Mesorhizobium loti* MAFF303099**	
ω-Transaminase	**E-value**	**Identity**	**E-value**	**Identity**
R-CMTA	2e–84	44 %	5e–78	45 %
R-CPTA	4e–65	37 %	5e–124	55 %
R-MKTA	7e–48	36 %	1e–49	32 %
R-TOTA	4e–42	33 %	1e–50	33 %
R-TRTA	3e–84	45 %	1e–70	39 %

1.1.1. Heterologous Expression of Putative Transaminase Genes and Verification of ω-Transaminase Activity

Based on the protein sequences of R-CMTA, R-MKTA, R-TOTA and R-TRTA, DNA sequences optimized for an expression in *E. coli* were created. For cloning the transaminase genes into the expression vector pET-21a(+) the restriction site for *Nde*I was added to the 5' end. To the 3' end of the sequences restriction site for *Xho*I and a stop codon were added. These codon optimized genes were synthesized by GeneArt® (part of Life Technologies GmbH, Darmstadt, Germany) and provided on GeneArt® plasmids. For the expression in *E. coli*, the transaminase genes were cloned via the restriction sites *Nde*I and *Xho*I into the pET-21a(+) vector (plasmid maps see Appendix, section 1).

Heterologous expression of the transaminase genes in *E. coli* BL21(DE3) was tested in 100 mL LB medium. The gene expression was induced with 0.3 mM IPTG and afterwards the expression cultures were incubated for 4 h at 30 °C and 25 °C, respectively. The production of the putative transaminases was visualized with SDS-PAGE. The gels illustrate transaminase production (see Fig. 4.1). Lanes 1–4 show samples from cell extracts and lanes 5–8 samples from the insoluble cell fractions after cell disruption.

All transaminases were produced in *E. coli* BL21(DE). Gene expression at 30 °C lead to an overproduction of R-TRTA and R-TOTA in the soluble and insoluble fraction.

R-MKTA was overexpressed in soluble form, whereas R-CMTA was only present in the insoluble fraction. To optimize the expression of the proteins in soluble form, the expression temperature was lowered to 25 °C in a second approach. The production of the transaminases was reduced (especially in insoluble form) by lowering the temperature to 25 °C. At lower temperature, R-TOTA is mainly produced in soluble form. The overexpression of R-CMTA in soluble from could not be improved by lowering the temperature.

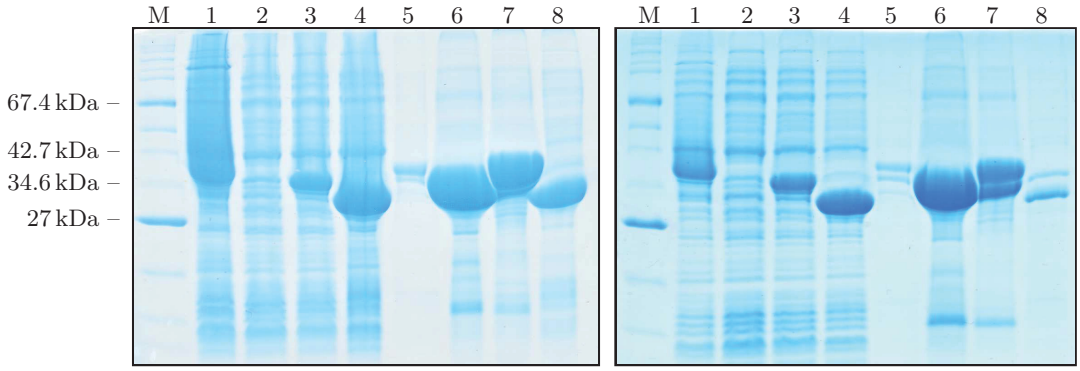

(a) 30 °C **(b)** 25 °C

Fig. 4.1. *SDS-PAGE from samples of the first expression of the novel transaminases in* E. coli *BL21(DE). The cultivation was done in LB medium and the gene expression was induced with 0.3 mM IPTG. The incubation was continued at (a) 30 °C and (b) 25 °C. Lanes 1, 5: R-MKTA (33 kDa). Lanes 2, 6: R-CMTA (37 kDa). Lanes 3, 7: R-TRTA (36 kDa). Lanes 4, 8: R-TOTA (33 kDa). Lanes 1–4: Samples from cell extracts. Lanes 5–8: Samples from insoluble fractions after cell disruption. M: Unstained Protein Marker, Broad Range (New England Biolabs).*

The ω-transaminase activity was investigated by the biotransformation of the ω-transaminase standard substrates acetophenone **2a** and phenylethylamine **1a**, respectively (see chapter III, section 7: amination and deamination A)). Since these measurements were initial tests, only single samples were taken. R-TRTA showed distinct activity against both, ketone **2a** and amine **1a** (see Fig. 4.2). Due to the proven overproduction of R-MKTA and R-TOTA in soluble form, transaminase activity in cell extracts with R-MKTA and R-TOTA was also expected. Nevertheless, transaminase activity was not observed for R-MKTA and R-TOTA with the substrates **2a** and **1a**. R-CMTA also showed no ω-transaminase activity but as seen on the SDS gels, no production of R-CMTA was visible in samples from cell extracts.

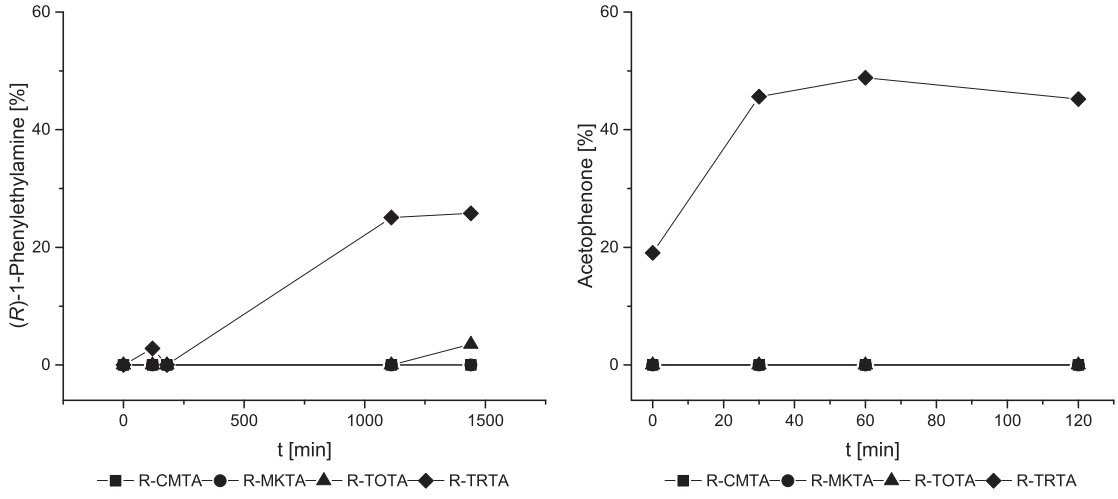

(a) Amination **(b)** Deamination

Fig. 4.2. *Biotransformation of* ***2a*** *and* ***1a*** *with novel ω-transaminases. R-TRTA shows distinct activity against the substrates (a) acetophenone* ***2a*** *and (b) phenylethylamine* ***1a****.*

In addition to the conversion of the transaminase substrates, the concentration of the enantiomers of **1a** was determined. Fig. 4.3 shows the amination of **2a** with R-TRTA. After 24 h, approximately 26 % of **2a** were converted to the corresponding (*R*)-amine with an enantiomeric excess of 75 % *ee*. Therefore, the enzyme R-TRTA is an (*R*)-selective ω-transaminase. In further biotransformation assays (with *sec*-butylamine **1k** as amino donor), an enantiomeric excess of 99.99 % for the (*R*)-amine was reached (see Appendix, Fig. A.23).

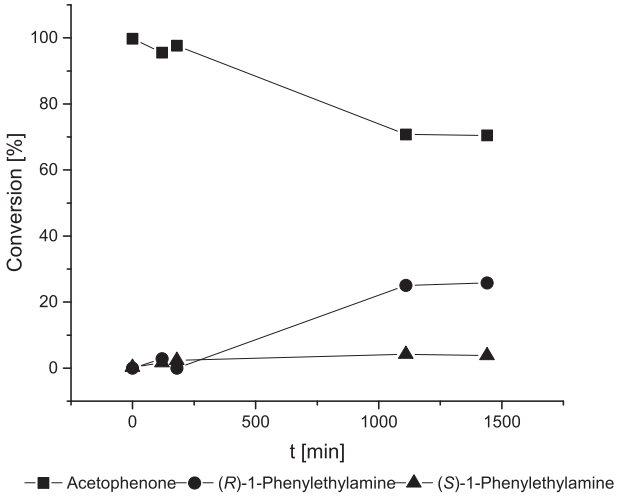

Fig. 4.3. *Amination of* ***2a*** *with R-TRTA. After 24 h approx. 26 % of* ***2a*** *is aminated to* (R)-***1a****.*

1.1.2. Effect of Pyridoxine on Transaminase Activity

Transaminases use pyridoxal 5'-phosphate (PLP) as a cofactor which is already produced by the cell itself. Presumably, the overproduction of transaminases leads to a higher demand for PLP. Since cofactors have a significant effect on protein folding,[97] a lack of the cofactor could lead to an inactive enzyme due to improper folding. Hence, the influence of the PLP precursor pyridoxine on transaminase expression and activity was investigated.

E. coli BL21(DE3) pET-21a(+)_R-CMTA and pET-21a(+)_R-TRTA were cultivated in 100 mL M9 medium with and without 0.1 mM pyridoxine. *E. coli* BL21(DE3) without transaminase plasmid served as a control. The gene expression was induced with 0.05 mM IPTG and the cultures were incubated for another 4 h at 25 °C and 180 rpm. Cell extracts were produced by ultrasonication and used for the biotransformation of **2a** and **1a** (see chapter III, section 7). Fig. 4.4 shows the decrease of (*R*)-**1a** during the deamination of *rac*-**1a** followed by chiral GC. As Fig. 4.4 shows, both R-CMTA and R-TRTA convert (*R*)-**1a**, so its percentage declines.

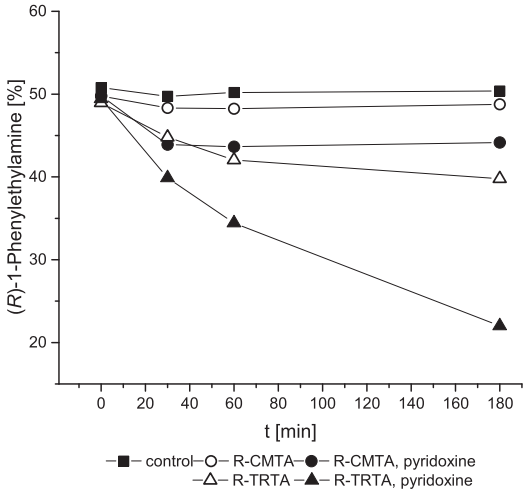

Fig. 4.4. *Effect of cultivation with supplementary pyridoxine on ω-transaminase activity.*

Comparing the transaminases with and without addition of pyridoxine to the culture medium, pyridoxine enhances the transaminase activity. Since the SDS-PAGE analysis (see chapter Appendix, Fig. A.24) showed no differences in the amount of the produced transaminase with and without pyridoxine, the same amount of enzymes seems to be more active. The activity of R-TRTA from cultures with supplemental pyridoxine is increased about fourfold and the activity of R-CMTA is increased about fivefold.

Even if R-CMTA showed no transaminase activity in the initial experiment (see section 1.1.1), the altered expression conditions and the addition of pyridoxine lead to an active enzyme and the (*R*)-selectivity of the transaminase R-CMTA was proven.

In subsequent cultivations for transaminase expression the addition of pyridoxine during cultivation therefore became standard, beginning with the putative transaminase from metagenome sequences.

1.1.3. Heterologous Expression and Activity of Putative Transaminase from Metagenome Sequences

The gene sequence of the putative transaminase from metagenome sequences R-CPTA was optimized and synthesized as already described above. The cultivation of *E. coli* BL21(DE) pET-21a(+)_R-CPTA was performed in 100 mL LB medium, supplemented with 0.1 mM pyridoxine. The gene expression was induced with 0.3 mM and 0.1 mM IPTG, respectively. By adding the inductor, the temperature was shifted to 25 °C and the cultures were incubated for additional 4 h. The SDS gels in Fig. 4.5 show the samples from expression cultures after cell disruption by ultrasonication.The cultivation at 25 °C as well as at 30 °C led to an overproduction of R-CPTA in the insoluble fraction only. Corresponding to the lack of R-CPTA in cell extracts, transaminase activity could not be measured.

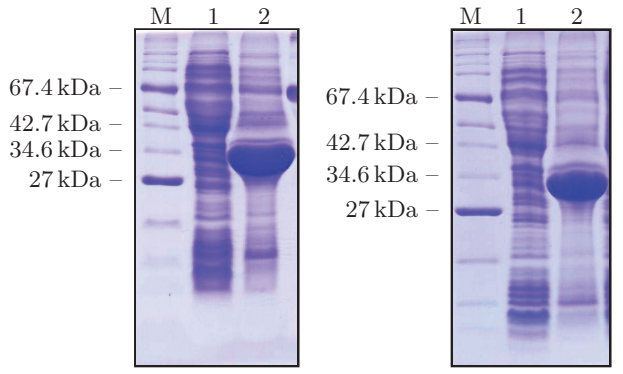

(a) 0.1 mM IPTG **(b)** 0.3 mM IPTG

Fig. 4.5. *SDS-PAGE from samples of the first expressions of the transaminase R-CPTA from metagenome sequences. The cultivation was carried out in LB medium with 0.1 mM pyridoxine. The induction of the gene expression was done with (a) 0.1 mM IPTG and (b) 0.3 mM IPTG and further incubation at 25 °C.*
1: Samples from cell extracts. 2: Samples from insoluble fractions after cell disruption. M: Unstained Protein Marker, Broad Range (New England Biolabs).

1.1.4. Refolding from Inclusion Bodies

Since the majorities of R-CMTA and R-CPTA were produced in insoluble and therefore not active form, a refolding approach was performed to prove the transaminase activity of

these enzymes. The transaminase activity of R-CMTA was already demonstrated, thus the refolding of R-CMTA served as a proof of principle. Inclusion bodies were isolated from the insoluble fractions after cell disruption. Proteins from inclusion bodies were first denaturated with guanidine HCl and DTT and then refolded under nine different redox conditions (see chapter III, section 5.3).

Tab. 4.2. *Refolding conditions of R-CMTA and R-CPTA from inclusion bodies. Dithiothreitol (DTT), glutathione disulfide (GSSG) and glutathione (GSG) were used as redox agents for refolding. The highest activities were set as 100 %.*

	GndCl	**L-Arg**	**Redox Condition**	**Protein Precipitation**		**Relative Activity**	
				R-CMTA	R-CPTA	R-CMTA	R-CPTA
1	0.4 M	0.0 M	5.0 mM DTT	yes++	yes++	16 %	9 %
2	0.4 M	0.4 M	2.0 mM GSH 0.2 mM GSSG	yes+	yes	0 %	32 %
3	0.4 M	0.8 M	2.0 mM GSH 0.4 mM GSSG	no	yes	12 %	65 %
4	0.9 M	0.0 M	2.0 mM GSH 0.2 mM GSSG	yes+	yes	6 %	14 %
5	0.9 M	0.4 M	2.0 mM GSH 0.4 mM GSSG	yes	yes	3 %	87 %
6	0.9 M	0.8 M	5.0 mM DTT	no	no	100 %	41 %
7	1.4 M	0.0 M	2.0 mM GSH 0.4 mM GSSG	yes	yes	34 %	74 %
8	1.4 M	0.4 M	5.0 mM DTT	no	no	75 %	100 %
9	1.4 M	0.8 M	8.0 mM GSH 0.2 mM GSSG	no	no	20 %	94 %

+ strong,++ very strong

After the refolding process, the samples showed different amounts of precipitation. The precipitate was removed by centrifugation and the activity of the refolded transaminases was determined via the acetophenone assay. Because the high concentration of detergents influenced the protein analytics, only relative activities are given.

R-CMTA showed the highest activity after refolding in buffer 6. After refolding in buffer 8 a relative activity of 75 % was measured and after refolding in buffer 7, 34 % activity

were achieved. Except for buffer 2, all refolding buffers lead to a partial restoration of the enzyme activity after the denaturation of the probably wrongly folded transaminase (see Tab. 4.2).

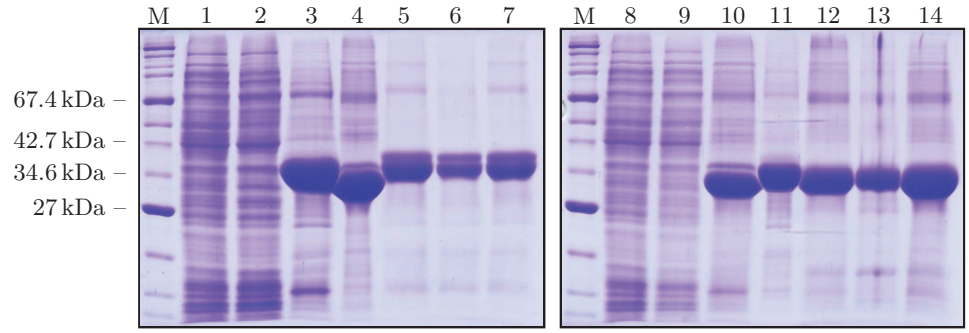

(a) R-CMTA **(b)** R-CPTA

Fig. 4.6. *SDS-PAGE from samples of the refolding of (a) R-CMTA and (b) R-CPTA. Lanes 1, 8: Cell extract from* E. coli *BL21(DE3). Lanes 2, 9: Soluble fraction. Lanes 3, 10: Insoluble fraction. Lanes 4, 11: Purified inclusion bodies. Lane 5: Sample 6. Lane 6: Sample 8. Lane 7: Sample 7. Lane 12: Sample 8. Lane 13: Sample 9. Lane 14: Sample 5. M: Unstained Protein Marker, Broad Range (New England Biolabs).*

To visualize the refolding approach, samples from the washing and refolding steps with the highest activities were analyzed on SDS gels. As the gels show, the inclusion bodies were almost fully recovered (see Fig. 4.6).

In conclusion, the transaminases could be recovered from inclusion bodies by this refolding approach.

1.2. Second Round: Sequence Alignment with new (*R*)-Selective ω-Transaminases

For finding further (*R*)-selective ω-transaminase, the sequences of R-TRTA and R-CMTA were used as query sequences in another BLAST against the NCBI database. Eight more sequences of putative (*R*)-selective ω-transaminases were chosen from the results:

- branched-chain amino acid aminotransferases R-AFTA from *Aspergillus flavus*
- branched-chain amino acid aminotransferases R-GCTA from *Grosmannia clavigera*
- branched-chain amino acid aminotransferases R-PMTA from *Penicillium marneffei*
- hypothetical protein R-FPTA from *Fusarium pseudograminearum*

- hypothetical protein R-TATA from *Trichoderma virens*
- hypothetical protein R-TVTA from *Trichoderma atroviride*
- putative class IV aminotransferases R-CGTA1 from *Colletotrichum gloeosporioides*
- putative class IV aminotransferases R-CGTA2from *Colletotrichum gloeosporioides*

The commercially used transaminases

- ATA-117
- ATA-117-110 (Sitagliptin producing variant of ATA-117[29])

were chosen as benchmark enzymes.

The chosen sequences matched to the query sequences of R-TRTA and R-CMTA to 35–83 % (see Tab. 4.3).

Tab. 4.3. *Amino acid sequence identities and Expect (E) values (BLAST version 2.231+) of new (*R*)-selective ω-transaminases from the second in silico screening.*

	R-TRTA		**R-CMTA**	
ω-Transaminase	**E-value**	**Identity**	**E-value**	**Identity**
ATA-117	9e–86	44 %	4e–88	45 %
ATA-117-110	1e–81	42 %	5e–85	44 %
R-AFTA	1e–70	59 %	1e–80	68 %
R-CGTA1	9e–170	65 %	0.0	75 %
R-CGTA2	1e–148	60 %	4e–166	67 %
R-FPTA	1e–167	64 %	6e–179	70 %
R-GCTA	3e–55	35 %	9e–56	39 %
R-PMTA	1e–78	60 %	2e–87	66 %
R-TATA	0.0	79 %	2e–164	62 %
R-TVTA	0.0	83 %	3e–169	65 %

1.2.1. Heterologous Expression of Putative Transaminase Genes and Verification of ω-Transaminase Activity

The new transaminase genes were prepared and cloned as described in section 1.1.1. The first expression of the transaminase genes was performed in *E. coli* BL21(DE3) in 20 mL LB medium, supplemented with 0.1 mM pyridoxine. The gene expression was induced with 0.3 mM IPTG and the cultures were incubated for 4 h at 30 °C. Cell extracts were

prepared by ultrasonication of the cells. For the determination of the ω-transaminase activity in cell extracts, the acetophenone assay was used.

The analysis of the fractions after cell disruption on SDS gels (see Fig. 4.7) showed a production of all transaminases in *E. coli* BL21(DE3) mainly in the insoluble fractions. The sizes of the overproduced proteins correspond to the former calculated sizes of 17–37 kDa. Thereby, the minor size of 17 kDa of R-AFTA is outstanding. The transaminases ATA-117 and ATA-117-110 (lanes 1–4) were clearly overproduced in soluble form. A slight overproduction in the soluble fraction is visible from R-TATA (lanes 17–18) and R-TVTA (lanes 19–20).

Despite the overexpression of ATA-117, ATA-117-110, R-TATA and R-TVTA in soluble form, only ATA-117 and R-TVTA showed activity against the substrate **1a** in the acetophenone assay. Even R-FPTA (lanes 11–12), which was not visibly overexpressed in soluble form, showed transaminase activity. Because of the minor production of R-FPTA and R-TVTA in soluble form, further expression conditions were investigated. The inductor concentration was varied from no IPTG up to 1 mM IPTG and the temperature during expression was lowered to 25 °C. The best conditions were a temperature shift to 30 °C and inductor concentrations of 0.6 mM IPTG for R-TVTA and no IPTG for R-FPTA.

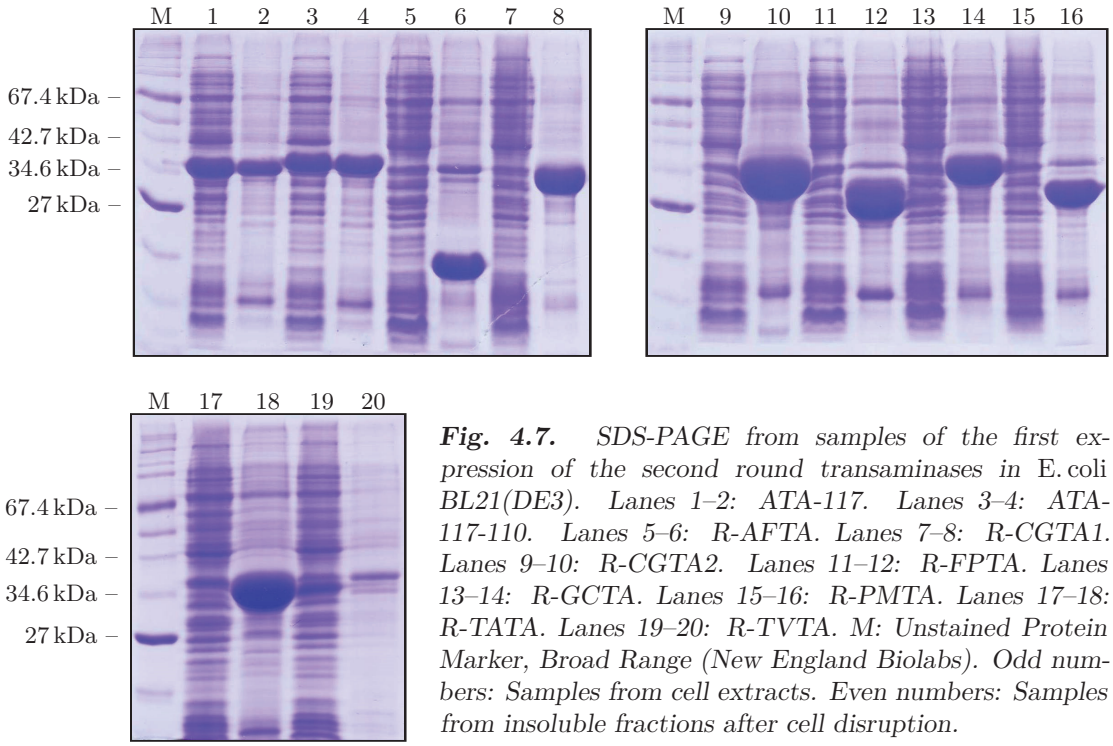

Fig. 4.7. *SDS-PAGE from samples of the first expression of the second round transaminases in* E. coli *BL21(DE3). Lanes 1–2: ATA-117. Lanes 3–4: ATA-117-110. Lanes 5–6: R-AFTA. Lanes 7–8: R-CGTA1. Lanes 9–10: R-CGTA2. Lanes 11–12: R-FPTA. Lanes 13–14: R-GCTA. Lanes 15–16: R-PMTA. Lanes 17–18: R-TATA. Lanes 19–20: R-TVTA. M: Unstained Protein Marker, Broad Range (New England Biolabs). Odd numbers: Samples from cell extracts. Even numbers: Samples from insoluble fractions after cell disruption.*

The activity of the benchmark ATA-117 was 642 mU/$mg_{protein}$, whereas the variant ATA-117-110 showed no activity against the substrate **1a**. From the first expression, R-FPTA had an activity of 168 mU/$mg_{protein}$ and R-TVTA an activity of 158 mU/$mg_{protein}$. By adjustment of the expression conditions, the activity of R-FPTA was raised to 868 mU/$mg_{protein}$. The activity of R-TVTA was 246 mU/$mg_{protein}$ with optimized expression conditions (see Fig. 4.8).

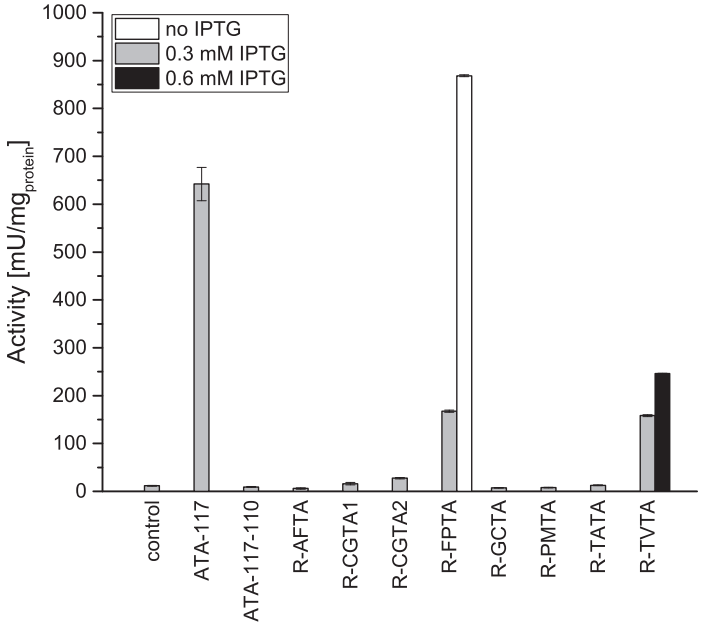

Fig. 4.8. *Activities of second round transaminases after first expression in* E. coli *BL21(DE3). R-FPTA and R-TVTA showed distinct activity against the substrate* ***1a*** *in the acetophenone assay.*

As seen on the SDS gels (Fig. 4.9), the production of R-FPTA and R-TVTA in soluble form is optimized by adjusting the expression conditions. By the addition of IPTG to the expression cultures, R-FPTA is mainly produced in its insoluble form. Increasing the temperature from 25 °C to 30 °C even leads to a higher formation of the enzyme in the insoluble fraction. The production of soluble and active R-FPTA is reached by the omittance of IPTG. R-TVTA is best produced in soluble form with an inductor concentration of 0.6 mM IPTG. Increasing the IPTG concentration did not lead to an increased protein production.

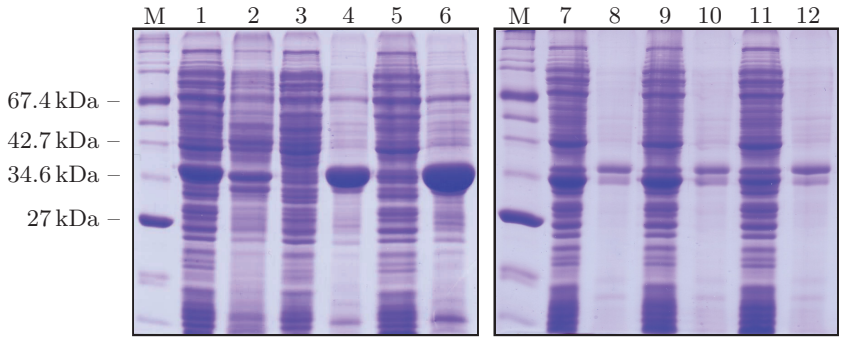

(a) R-FPTA **(b)** R-TVTA

Fig. 4.9. *SDS-PAGE of samples from expressions of (a) R-FPTA and (b) R-TVTA in E. coli BL21(DE3) with adjusted expression conditions. Lanes 1–2: no IPTG, 30 °C. Lanes 3–4: 0.3 mM IPTG, 25 °C. Lanes 5–6: 0.1 mM IPTG, 30 °C. Lanes 7–8: 0.6 mM IPTG, 30 °C. Lanes 9–10: 1 mM IPTG, 30 °C. Lanes 11–12: 1 mM IPTG, 25 °C. M: Unstained Protein Marker, Broad Range (New England Biolabs). Odd numbers: Samples from cell extracts. Even numbers: Samples from insoluble fractions after cell disruption.*

1.2.2. Optimization of R-FPTA Expression

Further expression experiments of R-FPTA showed differences in overproduction yields and transaminase activities. Expressions with the optimized conditions, especially without IPTG and the temperature shift to 30 °C, were not reproducibile in transaminase overproduction and activity. Because of this variation, the expression conditions were investigated in detail. Inductor concentrations from 0.01–1 mM IPTG were tested at 37 °C, 30 °C and 25 °C. The incubation time during gene expression was extended from 4 h to 22 h.

After cultivation at 30 °C and 37 °C, only minimal transaminase activities were measured in cell extracts. Compared to ATA-117, R-FPTA reached higher activities when cultivated at 25 °C with a minimum of 0.05 mM IPTG. In cell extracts from cultures which were induced with IPTG concentrations between 0.01 mM–0.3 mM, the transaminase activity increased with the concentration of IPTG. Higher IPTG concentrations than 0.3 mM lead to fluctuating activities. With approx. 900 $mU/mg_{protein}$, the transaminase activity after cultivation at 25 °C with 0.01 mM IPTG was nine times higher than the transaminase activity measured after cultivation at 37 °C with 0.01 mM IPTG(Fig. 4.10(a)).

Since the highest activities of R-FPTA were reached by cultivation at 25 °C, the reproducibility of the transaminase activity after cultivation at 25 °C with IPTG concentrations of 0.3 mM and 0.8 mM IPTG was investigated. With both cultivation condi-

tions, transaminase activities of around 800 mU/$mg_{protein}$ were reached. Adding 0.1 mM pyridoxine to the cultures lead to an almost twofold increase of transaminase activity (Fig. 4.10(b)). An increase of the IPTG concentration from 0.3 mM to 0.8 mM was not paired with significant enhancement of the transaminase activity or production (Fig. 4.10(c)). Therefore, 25 °C and 0.3 mM IPTG were chosen as the optimal conditions for the production of R-FPTA.

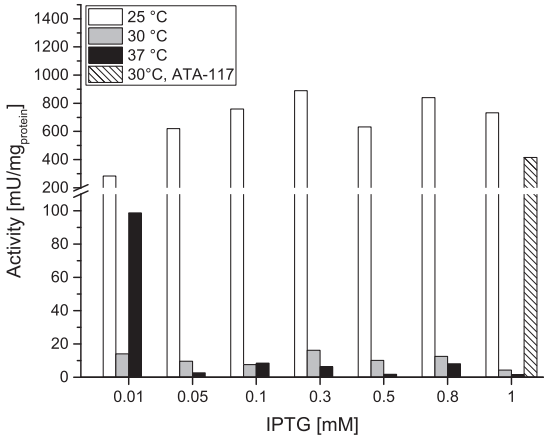

(a) Screening of expression conditions

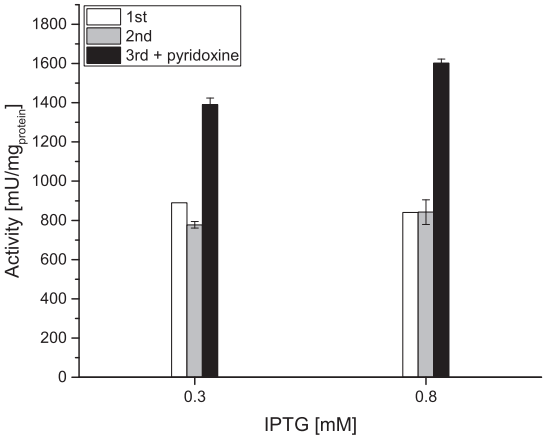

(b) Reproducibility of best conditions

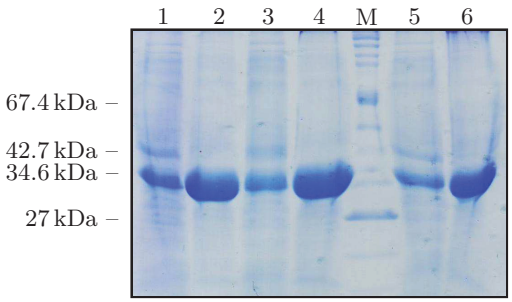

(c) SDS-PAGE

Fig. 4.10. *(a) Screening of conditions for the production of R-FPTA in* E. coli *BL21(DE3). IPTG concentrations between 0.01–1 mM at 25 °C, 30 °C and 37 °C were tested. (b) Reproduction of best cultivation conditions and addition of 0.1 mM pyridoxine. (c) SDS-PAGE from samples of the expression of R-FPTA with different IPTG concentrations at 25 °C. Lanes 1–2: 0.8 mM IPTG. Lanes 3–4: 0.3 mM IPTG. Lanes 5–6: 0.1 mM IPTG. M: Unstained Protein Marker, Broad Range (New England Biolabs) Odd numbers: Samples from cell extracts. Even numbers: Samples from insoluble fractions after cell disruption.*

1.3. Addition of His-Tags

As promising candidates, R-TRTA and R-FPTA were chosen for further experiments. For crystallization purposes, both ω-transaminases were first fused with His-tags. To do so, the transaminase genes were cloned into appropriate pET vectors. *R-trta* and *r-fpta*

were amplified without stop codon for the C-terminal His-tag and cloned via *Nde*I and *Xho*I into the vector pET-21a(+). For the N-terminal His-tag, the transaminase genes were cloned into the vector pET-19b without prior modification. To verify the addition of the His-tags, the expressions of the modfied transaminase genes were performed in *E. coli* BL21(DE3).

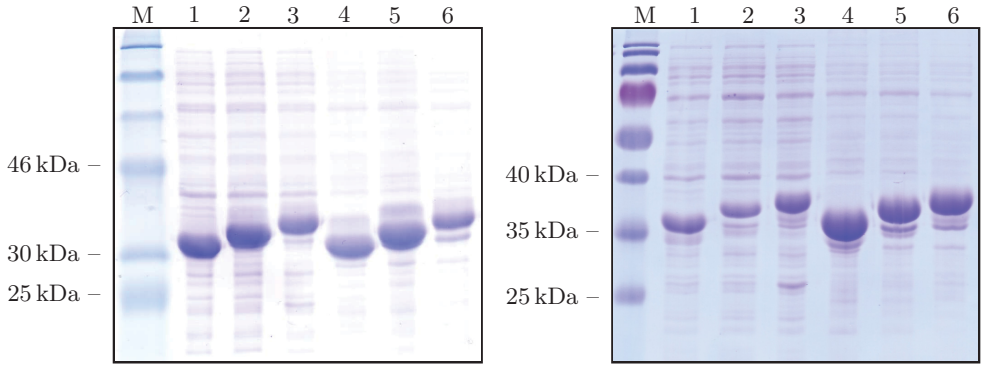

(a) R-TRTA **(b)** R-FPTA

Fig. 4.11. *SDS-PAGE with 15 % acrylamid gels from samples of the expressions of R-TRTA and R-FPTA with His-tags. (a) R-TRTA and (b) R-FPTA. Lanes 1, 4: no His-tag (R-TRTA 35.5 kDa, R-FPTA 36.9 kDa). Lanes 2, 5: C-terminal His-tag (R-TRTA_C-His 36.9 kDa, R-FPTA_C-His 38 kDa). Lanes 3, 6: N-terminal His-tag (R-TRTA_N-His 38.6 kDa, R-FPTA_N-His 39.7 kDa). Lanes 1–3: Samples from cell extracts. Lanes 4–6: Samples from insoluble fractions after cell disruption. M: Prestained Protein Marker ((a) New England Biolabs, (b) Thermo Scientific).*

First expressions (see optimized conditions for R-FPTA, section 1.2.2) of the tagged transaminase genes compared to the genes without His-Tag modifications, showed an increase in size of R-TRTA and R-FPTA, as expected (see Fig. 4.11). Since R-TRTA and R-FPTA were produced with both, C-terminal and N-terminal His-tag, the activities and the proper functioning for the purification with Ni-NTA spin columns were investigated. Compared to the pure R-TRTA, the tags had minor influence on the transaminase activity. On the contrary, the C-terminal His-tag decreased the activity of R-FPTA by 40 % (see Tab. 4.4).

Tab. 4.4. *Mean activities of the ω-transaminases R-TRTA and R-FPTA with His-tags.*

His-Tag	**R-TRTA** [$\mathbf{mU/mg_{protein}}$]	**R-FPTA** [$\mathbf{mU/mg_{protein}}$]
none	265.84±2.71	1765.56±19.66
C-His	301.42±3.91	1057.64±39.73
N-His	248.82±5.12	1902.94± 8.97

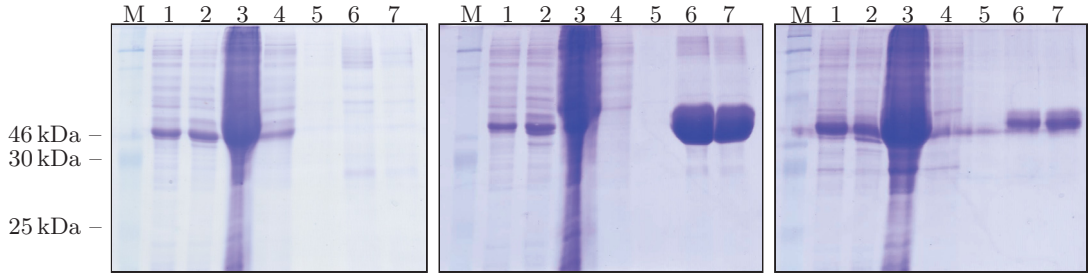

(a) no His-tag **(b)** C-terminal His-tag **(c)** N-terminal His-tag

Fig. 4.12. *SDS PAGE of Ni-NTA purification fractions of R-TRTA with (a) no His-tag, (b) C-terminal His-tag and (c) N-terminal His-tag. M: Prestained Protein Marker (New England Biolabs). Lane 1: Samples from cell extracts. Lane 2: Samples from insoluble fractions after cell disruption. Lane 3: Flow through. Lane 4: First washing. Lane 5: Second washing. Lane 6: First elution. Lane 7: Second elution.*

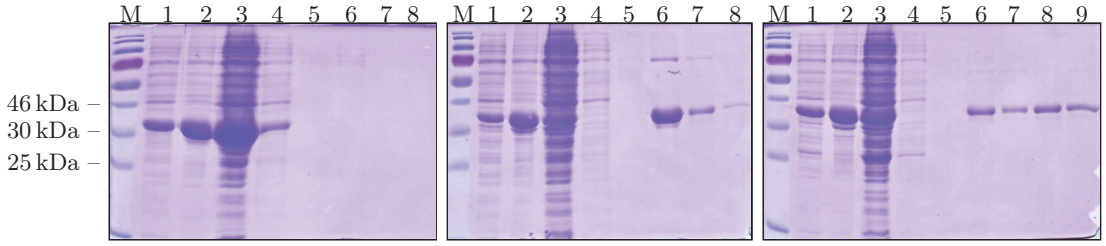

(a) no His-tag **(b)** C-terminal His-tag **(c)** N-terminal His-tag

Fig. 4.13. *SDS PAGE of Ni-NTA purification fractions of R-FPTA with (a) no His-tag, (b) C-terminal His-tag and (c) N-terminal His-tag. M: Prestained Protein Marker (Thermo Scientific). Lane 1: Samples from cell extracts. Lane 2: Samples from insoluble fractions after cell disruption. Lane 3: Flow through. Lane 4: First washing. Lane 5: Second washing. Lane 6: First elution. Lane 7: Second elution. Lane 8: Third elution. Lane 9: Fourth elution.*

Testing the functionality of the His-tags and further analysis of the purification fractions showed that the C-terminal His-tag performed better for both transaminases R-TRTA and R-FPTA. As the wild-type enzymes had no His-tag and therefore did not bind to the Ni-NTA column, R-TRTA and R-FPTA were already eluted during the first washing step (Fig. 4.12 (a) and Fig. 4.13 (a)). With the N-terminal His-tag attached, part of the enzyme was eluted from the column during the first washing step but the other part was hardly eluted from the column, even by increasing the concentration of the elution buffer. Especially R-FPTA_N-His stayed attached (Fig. 4.12 (c) and Fig. 4.13 (c)). R-TRTA_C-His and R-FPTA_C-His bound strong enough to the column that they were not eluted by washing the column. With the elution buffers, R-TRTA_C-His and R-FPTA_C-His could be eluted in high concentrations and purity (see Fig. 4.12

(b) and Fig. 4.13 (b)). Therefore, despite the decreased activity of R-FPTA_C-His, the transaminases with C-terminal His-tag were chosen.

2. Customization of Transaminase Analytics

A fast and sensitive assay for the determination of ω-transaminase activity is the acetophenone assay.[67] Using the acetophenone assay in microtiter plates allows its application for high throughput screening. However, the acetophenone assay can only be used for the measurement of the deamination activity against the standard ω-transaminase substrate **1a**. Alternative methods have to be used to determine the activity against other ketone and amine substrates as well as the enantioselectivity of the ω-transaminases.

2.1. Determination of Conversion and Enantiomeric Excess: Gas Chromatographic Screening Assay

While spectrophotometric measurements provide continuous kinetic data, single samples have to be taken for chromatographic measurements. Moreover, the enzymatic reaction has to be stopped and the samples have to be prepared for gas chromatography. Sampling and stopping the reaction have to be accurate to ensure an exact measurement of the enzyme activity and to allow the comparison of different enzymes and substrates. But, in contrast to spectrophotometric measurements, chiral GC comprises the possibility to determine the conversion of different ω-transaminase substrates and the enantiomeric excess of amines at the same time.

To optimize the GC assay for screening purposes, the sample handling was adjusted. Instead of preparing one bulk reaction vessel from which the samples were taken, samples for every measurement were put in an extra vessel. By stopping the reaction and preparing the sample directly in the sample vial, less pipetting steps had to be done. Sampling was therefore faster and more accurate.

The ω-transaminase activity is determined by measuring the initial velocity of the reaction, which corresponds to the gradient of the linear area of the saturation plot (see Fig. 4.14(a)). For this purpose, the concentration of the enzyme was adjusted so as to gain linear plots over the whole reaction time. Fig. 4.14(b) shows the typical plots for the deamination reaction with the optimized GC assay.

The assay was done in triplicate to verify the reliability of the handling and the measurements. The resulting linear plots were almost congruent with only minimal deviations. However, the time zero samples showed already a conversion of 10 %. The reaction in these samples was stopped by adding first MTBE and then NaOH. By changing the

order to first add NaOH and then MTBE, the reaction was stopped immediately. The measurements for the saturation plot were done with the changed order. Like Fig. 4.14(a) shows, no conversion was measured in the time zero samples.

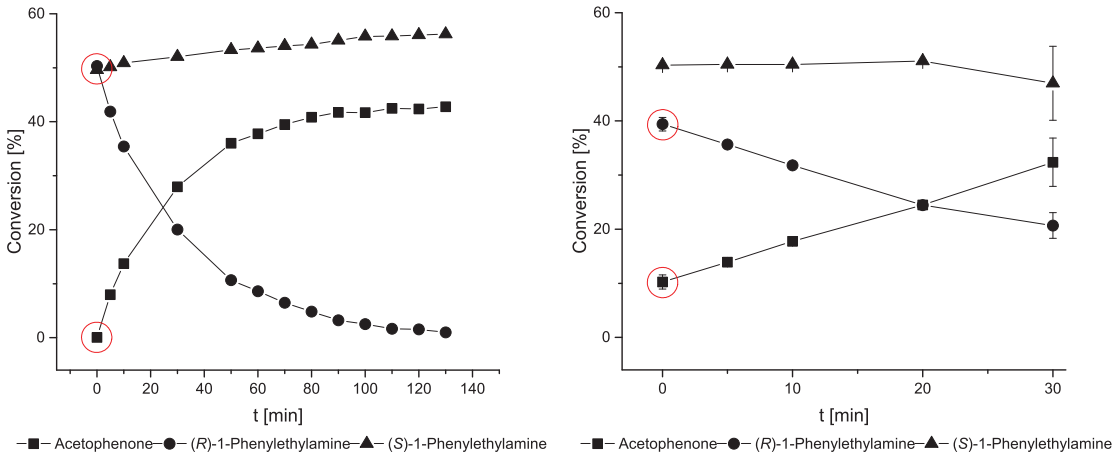

(a) Saturation plot **(b)** Linear plot

Fig. 4.14. *Optimization of GC assay. (a) Saturation plot. Adding NaOH first stopped the reaction immediately and no conversion was measured in time zero samples (red circles). (b) Linear plot of the optimized GC assay with 10 % conversion in time zero samples (red circles).*

The optimized GC assay was used for the determination and comparison of the amination activities of ω-transaminases with different ketones.

2.2. A fast Screening Assay in Microtiter Plates: D-Amino Acid Oxidase (D-AAO) Assay

In the D-AAO assay, the deamination reaction of an (*R*)-selective transaminase is coupled with a D-amino acid oxidase to regenerate puyruvate from D-alanine. By coupling a third enzyme, a horse radish peroxidase, and the addition of a colour reagent, the activity of the transaminase leads to a colour reaction (see Fig. 3.3). This colour reaction can be measured spectrophotometrically.

The D-AAO assay as described by Hopwood *et al.*[68] was used for the screening of ω-transaminase variants. Beforehand, the optimal composition of the coupled enzyme reactions for the deamination with ω-transaminases was investigated. A limitation of the transamination reaction by the coupled enzymes has to be avoided. Therefore, the activities determined with D-AAO assay and acetophenone assay should be comparable to each other.

In a first set up of the assay, D-AAO cell extract[98] was used. Because the activity of D-AAO from cell extract was too low, a commercial D-amino oxidase was used for the following tests.

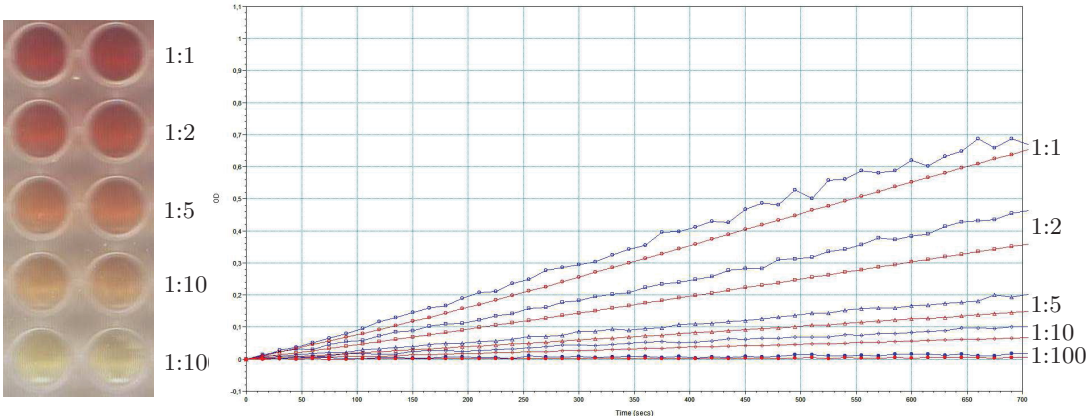

Fig. 4.15. *Picture of colour development in the D-AAO assay with different ω-transaminase concentrations (left). Depiction of SoftMax Pro of the corresponding slopes (red) compared to slopes of the acetophenone assay (blue).*

The enzymes HRP and the commercial D-AAO, together with the colour reagent *o*-dianisidine were tested in the coupled D-AAO assay in nine different concentrations and combinations. The enzyme combination which corresponded the best with the acetophenone assay was chosen for the screening assay. Additionally, the assay was tested with dilutions of R-TRTA from 1:1–1:100. Comparing the graphs of both assays, the slopes of the D-AAO assay were more smooth and the slopes of the acetophenone assay showed higher gradients (see Fig. 4.15). But, calculating the activity of R-TRTA, activities of both assays corresponded.

With R-TRTA dilutions from 1:1–1:5 slightly higher activities were measured with the D-AAO assay. In contrast to the more concentrated dilutions, the acetophenone assay gave higher activities for the dilutions 1:10 and 1:100. Probably, the influence of the D-amino acid oxidase on the reaction equilibrium leads to higher activities than measured with the acetophenone assay with the more concentrated dilutions. With higher dilutions, the acetophenone assay seems to be more sensitive.

The dilution 1:5 showed the best best correspondance of the acetophenone and D-AAO assay (see Fig. 4.16). With this dilution, the activity of D-AAO was ten times higher than the activity of the applied enzyme solution. Using the D-AAO assay for the determination of ω-transaminase activities, this proportion was maintained. With the commercial D-amino acid oxidase the assay conditions could be adapted to determine the activity

of R-TRTA without limiting the transaminase reaction. Also a correspondence to the acetophenone assay was given.

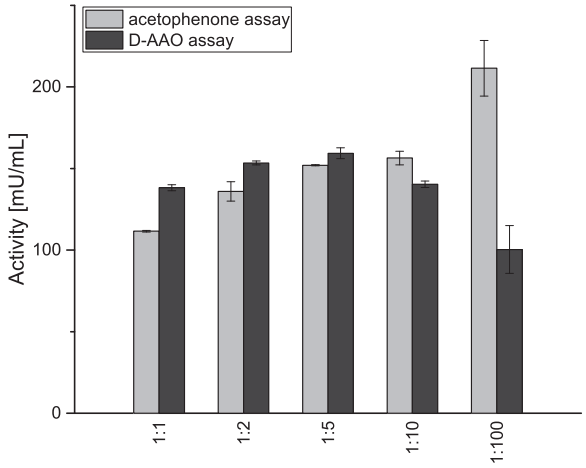

Fig. 4.16. *Comparison of activities of R-TRTA from different dilutions, measured with acetophenone assay and D-AAO assay. With a R-TRTA dilution of 1:5 both assays corresponded best.*

3. Mutagenesis of the ω-Transaminases R-TRTA and R-FPTA

The best candidates from the two *in silico* screenings (see section 1), R-TRTA and R-FPTA were further optimized and then characterized.

The active site of ω-transaminases is build of a large and a small binding pocket. Typical substrates matching the active site consist of a bulky group and a smaller group harbouring the amino or the keto function, respectively. Improving the ω-transaminases in activity or for substrate specificity therefore means altering the active site.

3.1. Site-Directed Mutagenesis

Since the target position for improving the ω-transaminases R-TRTA and R-FPTA lies in the binding pockets, a rational method for altering the active site of the enzymes was chosen. By using site-directed mutagenesis, specific DNA changes can be inserted and the screening effort can be calculated. Depending on the number of alterations and the choice of the used degenerated codon, the number of clones to be screened can be kept low.

3.1.1. Selection of the Target Position

Comparing the sequences of R-TRTA, R-FPTA and the ω-transaminases described in literature with regard to the sequence motif described by Höhne *et al.*,[1] it appeared that the ω-transaminases wearing Phe (like R-FPTA) at the position 113 (=position 95 in the sequence motif) are more active than ω-transaminases with Tyr (like R-TRTA) at position 113. Furthermore, R-TRTA and R-FPTA showed differences in their substrate spectra. Regarding the arrangement of the amino acid at position 113 within the active site, it lies at the border of the large and the small binding pocket. Thus, the entrance of the substrate to the large binding pocket could be limited by a larger amino acid (like Tyr) and the activity of the enzyme could be decreased.

Taken into account that the enlargement of the small binding pocket by exchanging large amino acids for small amino acids worked for the optimization of the sitagliptin transaminase,[29] the position 113 was chosen as target position for site-directed mutagenesis of the ω-transaminases R-TRTA and R-FPTA. Focusing on small amino acids, the NNK codon was chosen to mutate the DNA, coding for the amino acid at position 113. Additionally, the variants R-TRTA_C-His_Y113F and R-FPTA_C-His_F113Y were created.

3.1.2. Screening

The site-directed mutagenesis of the transaminase genes was done via PCR with primer oligonucleotides containing the desired mutation (see chapter I, 4.4.2). The transaminase genes with the C-terminal His-tag fusion were used as templates. After transforming *E. coli* BL21(DE3) cells with the mutated transaminase plasmids, the cells were spread on LB agar plates and incubated overnight. For the screening of the transaminase variants, selected clones were cultivated in microtiter plates in TB medium (see chapter I, 3.2) and then, cell extracts were prepared (see chapter I, 5.1). The cell extracts were diluted in a proportion of 1:10 and 1:20, respectively and the ω-transaminase activity was determined. First, as a control, the ω-transaminase activity was measured with the acetophenone assay (see chapter I, 6.3). Afterwards, the deamination activity of the ω-transaminases with the substrates **1a**–**1h** was screened with the D-AAO assay (see chapter I, 6.4).

From every microtiter plate, 20 candidates were chosen for sequencing. These candidates showed either high activities, changes in their substrate spectrum or very low activities. Despite different activities, almost half of the mutants turned out to be wild-types. Promising candidates with higher activities than the His-tagged wild-types

R-TRTA_C-His and R-FPTA_C-His were R-TRTA_C-His Y113F and R-FPTA_C-His F113M E115K. A first proof of the idea of increasing the activity of R-TRTA by changing Tyr113 to Phe113 (like in the wild-type R-FPTA) was found. Vice versa, the variant R-FPTA_C-His F113Y showed still as high activities as its wild-type (referred to **1a**).

Interestingly, a double mutant, the variant R-FPTA_C-His F113M E115K, stood out with a three times higher activity than R-FPTA_C-His (referred to **1a**) and was found twice in the investigated microtiter deepwell plate. As a negative example, the variant R-TRTA_C-His Y113R was chosen. The single amino acid exchange decreased the transaminase activity, but also influenced the substrate spectrum. Thereby, it has to be pointed out that also the other variants chosen show differences in their substrate spectra compared to their wild-types.

The results from the screening of the four chosen variants R-TRTA_C-His Y113F, R-TRTA_C-His Y113R, R-FPTA_C-His F113M E115K and R-FPTA_C-His F113Y are shown in Fig. 4.17.

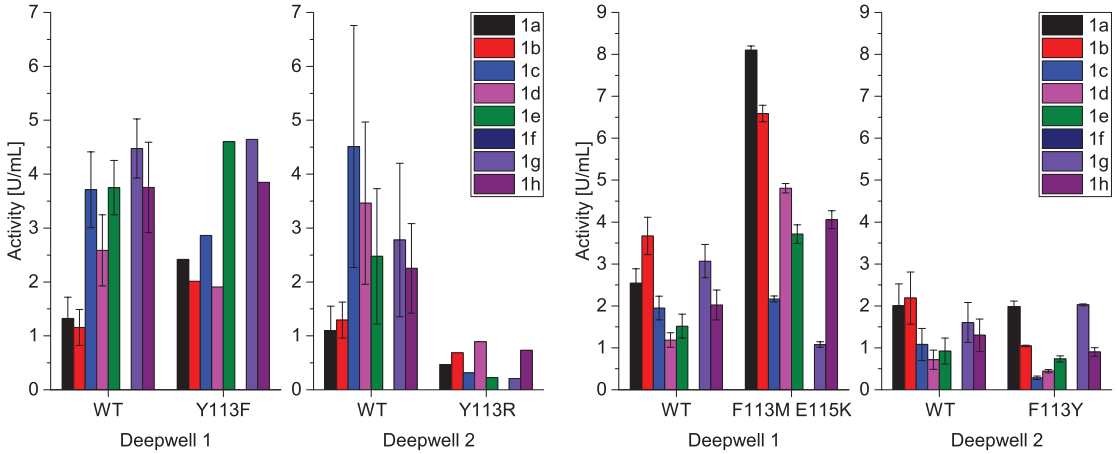

(a) R-TRTA **(b)** R-FPTA

Fig. 4.17. *Variants from screening of R-TRTA_C-His and R-FPTA_C-His were tested with different amine substrates. The deamination activity of the variants with the substrates* ***1a***–***1h*** *was screened with the* D*-AAO assay. Compared to their wild-types the variants R-TRTA_C-His Y113F, R-TRTA_C-His Y113R, R-FPTA_C-His F113M E113K and R-FPTA_C-His F113Y showed the most promising activities or substrate spectra, respectively. These variants were chosen for further investigation.*

3.2. R-TRTA, R-FPTA and Their New Variants: Biochemical Characterization

Since ω-transaminase activities from the deepwell microtiter plates showed a high variation throughout the wild-type enzymes, a validation of the results was necessary. To guarantee the comparability of the results and constant enzyme activity, lyophilisates from expression cultures (see chapter III, section 3.2 and section 5.1) of the chosen candidates and the wild-types with His-tag were produced. For the characterization, lyophilisates were resuspended in bidistilled water resulting in a concentration of 50 mg/mL. To give a first overview of the activities, the deamination activities of R-TRTA and R-FPTA and their variants were determined with the acetophenone assay (see Fig. 4.18).

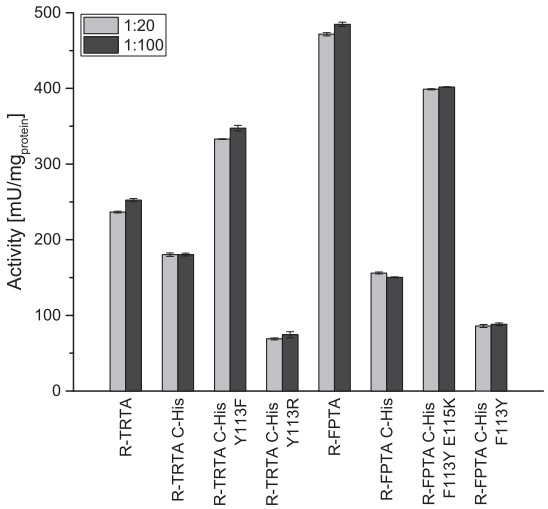

Fig. 4.18. *Activities of lyophilisates of the ω-transaminases R-TRTA and R-FPTA and their variants determined with acetophenone assay.*

As can be seen in Fig. 4.18, the C-terminal His-tag influences the activity of R-TRTA to a minor level (R-TRTA 236.44±1.14 mU/mg$_{protein}$, R-TRTA_C-His 180.36±2.24 mU/mg$_{protein}$). But, the activity of R-FPTA_C-His (155.98±1.26 mU/mg$_{protein}$) is only one third of the wild-type activity (471.58±2.05 mU/mg$_{protein}$). Therefore, it is supposed that the activity of both variants is also decreased by the His-tag. According to the analysis of the lyophylisates on SDS-PAGE (see Fig. 4.19), the concentration of the His-tagged variants is lower than the concentration of R-FPTA. Thus, minor expression of the His-tagged variants with the used expression conditions is more probable.

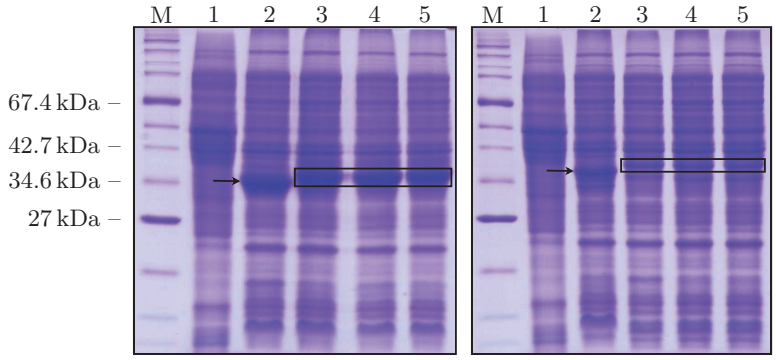

(a) R-TRTA **(b)** R-FPTA

Fig. 4.19. *SDS-PAGE from samples of lyophilisates of R-TRTA and R-FPTA (arrows) and their variants (frame). (a) R-TRTA. Lane 1: Empty vector. Lane 2: R-TRTA. Lane 3: R-TRTA_C-His. Lane 4: R-TRTA_C-His Y113F. Lane 5: R-TRTA_C-His Y113R. (b) R-FPTA. Lane 1: Empty vector. Lane 2: R-FPTA. Lane 3: R-FPTA_C-His. Lane 4: R-FPTA_C-His F113Y. Lane 5: R-FPTA_C-His F113M E115K. M: Protein Marker (New England Biolabs)*

3.2.1. pH Optima

The pH optima of the ω-transaminases and their variants were determined as mentioned in chapter III, section 6.3. As seen in Fig. 4.20, the pH optimum of R-FPTA is at pH 7.5. R-TRTA shows maximal activity in the alkaline environment at pH 9.

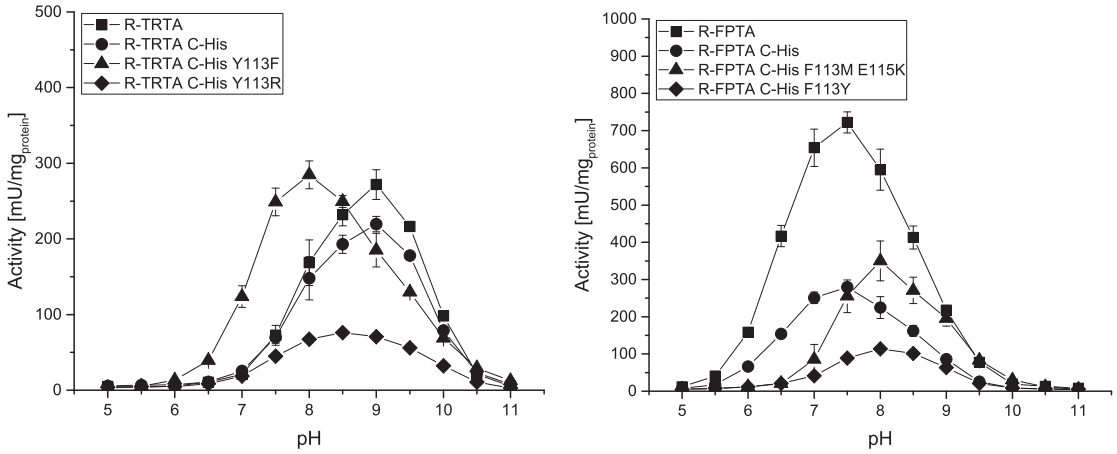

(a) R-TRTA **(b)** R-FPTA

Fig. 4.20. *Determination of the pH optima of the ω-transaminases R-TRTA (pH 9) and R-FPTA (pH 7.5) and their variants.*

The pH optima did not change by adding a C-terminal His-tag to neither R-TRTA nor R-FPTA (see Fig. 4.20). But both variants of R-TRTA have different pH optima. The optimum of R-TRTA_C-His Y113R is shifted to pH 8.5 and the pH optimum of R-TRTA_C-His Y113F is even shifted to pH 8 (see Fig. 4.20(a)). Since the acetophenone assay is carried out at pH 8, the variant R-TRTA_C-His Y113F is in advantage over the wild-type R-TRTA with its pH optimum at pH 9.

In case of R-FPTA (see Fig. 4.20(b)), the pH optima of both variants R-FPTA_C-His F113M E115K and R-FPTA_C-His F113Y are shifted to pH 8.

To conclude, the mutations of the ω-transaminases R-TRTA and R-FPTA at the position 113 cause shifts of the pH optima to lower pH values for R-TRTA and higher pH values for R-FPTA. It is presumed, that the change of the amino acid at this position alters the interaction of the amino acids which are responsible for the substrate binding.

3.2.2. Temperature Stability

The temperature stability of the ω-transaminases was determined as described in chapter III, section 6.3.

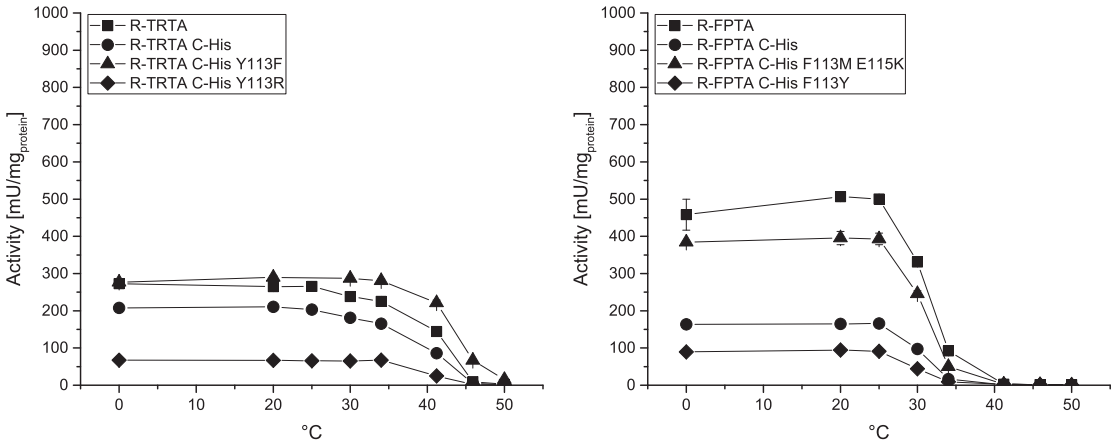

(a) R-TRTA **(b)** R-FPTA

Fig. 4.21. *Temperature stabilities of the ω-transaminases R-TRTA and R-FPTA and their variants.*

The activity of R-FPTA after the incubation at 20 °C and 25 °C did not change compared to the reference incubated on ice. Incubation at 30 °C lead to a loss of almost 30 % of the activity of R-FPTA. After incubation at 34 °C, the activity of R-FPTA was just 20 % of the reference activity. A nearly complete loss of activity was observed after the

incubation of R-FPTA at temperatures of 41.2 °C and higher. On the contrary, R-TRTA was more stable. After the incubation at 41.2 °C, the activity of R-TRTA was still 50 % of the reference activity. The activity was completely lost after incubation at 45.9 °C and 50 °C (see Fig. 4.21).

As for the wild-type enzymes, the temperature stability was also determined for R-TRTA_C-His, R-TRTA_C-His Y113F, R-TRTA_C-His Y113R, R-FPTA_C-His, R-FPTA_C-His F113M E115K and R-FPTA_C-His F113Y. As expected, the mutations caused no change in temperature stability of the ω-transaminases (see Fig. 4.21).

3.2.3. Enzyme Kinetics

The kinetic parameters of the ω-transaminases were determined as described in chapter III, section 6.3.1. For R-TRTA the value of V_{max} is 241.80±4.70 mU/mg and the value of K_m is 4.43±0.12 mM. The values for R-FPTA are V_{max}=797.92±8.13 mU/mg and K_m=0.28±0.05 mM. The parameters from the fit with the bi-substrate Hill-Equation are listed in Tab. 4.1 and Tab. 4.2. The maximal velocity P_{max} and the half-maximal activating substrate concentration K_a correspond to V_{max} and the Michaelis-Menten constant K_m, respectively.- These parameters are in the same range as the parameters determined with the Michaelis-Menten fit.

Tab. 4.1. *Catalytic parameters of ω-transaminase R-TRTA.*

		R-TRTA	C-His	C-His Y113F	C-His Y113R
$\mathbf{V_{max}}$	**[mU/mg]**	241.80 ± 4.70	202.28 ± 13.74	362.17 ± 20.84	78.74 ± 5.16
$\mathbf{K_m}$	**[mM]**	4.43 ± 0.12	6.49 ± 0.63	0.61 ± 0.49	1.71 ± 0.37
$\mathbf{P_{max}}$	**[mU/mg]**	198.43 ± 54.48	155.17 ± 36.90	368.90 ± 109.46	72.23 ± 21.30
$\mathbf{K_a}$	**[mM]**	3.02 ± 2.02	3.82 ± 1.02	0.72 ± 0.28	1.46 ± 0.35
$\mathbf{K_i}$	**[mM]**	15.53 ± 2.77	19.97 ± 0.95	16.79 ± 2.48	18.35 ± 2.29
$\mathbf{H_a}$		1.14 ± 0.61	1.19 ± 0.22	1.24 ± 0.16	1.16 ± 0.26
$\mathbf{H_i}$		6.53 ± 2.36	10.98 ± 1.19	4.23 ± 1.11	7.08 ± 1.25

Michaelis-Menten equation: V_{max} = maximal velocity, K_m = Michaelis-Menten constant.
Bi-substrate Hill equation: P_{max} = maximal velocity, K_a = half-maximal activating [S],
K_i = half-maximal inhibitory [S], H_a = activation Hill coefficient, H_i = inhibitory Hill coefficient.

Comparing the K_m values of R-TRTA and R-FPTA, R-FPTA has a fifteen times higher affinity for the substrate **1a**. This is also reflected in the initial gradient of the kinetics plots (see Fig. 4.22).

The catalytic parameters which were already determined for the wild-type enzymes R-TRTA and R-FPTA were also determined for their variants. The kinetic parameters of the tagged variant R-TRTA_C-His (see Tab. 4.1) are slightly higher than the parameters of the wild-type enzyme. Here, an influence of the His-Tag on the catalytic characteristics of the enzyme seems likely. With 0.61±0.49 mM and 1.71±0.37 mM the K_m values of the R-TRTA variants Y113F and Y113R are significantly lower than the K_m value of the wild-type.

Tab. 4.2. *Catalytic parameters of ω-transaminase R-FPTA.*

		R-FPTA	**C-His**	**C-His F113M E115K**	**C-His F113Y**
$\mathbf{V_{max}}$	**[mU/mg]**	797.92 ± 8.13	274.06 ± 20.75	411.83 ± 41.95	115.27 ± 3.35
$\mathbf{K_m}$	**[mM]**	0.28 ± 0.05	0.24 ± 0.11	1.66 ± 0.48	1.38 ± 0.27
$\mathbf{P_{max}}$	**[mU/mg]**	887.90 ± 83.21	258.66 ± 91.15	357.20 ± 86.52	99.66 ± 21.14
$\mathbf{K_a}$	**[mM]**	0.36 ± 0.08	0.23 ± 0.06	1.19 ± 0.28	1.18 ± 0.31
$\mathbf{K_i}$	**[mM]**	16.50 ± 1.24	17.72 ± 2.61	17.38 ± 1.87	20.14 ± 0.91
$\mathbf{H_a}$		0.72 ± 0.27	1.38 ± 1.57	1.17 ± 0.19	1.51 ± 0.34
$\mathbf{H_i}$		3.92 ± 0.46	4.91 ± 1.52	5.04 ± 0.98	11.43 ± 1.21

Michaelis-Menten equation: V_{max} = maximal velocity, K_m = Michaelis-Menten constant.
Bi-substrate Hill equation: P_{max} = maximal velocity, K_a = half-maximal activating [S],
K_i = half-maximal inhibitory [S], H_a = activation Hill coefficient, H_i = inhibitory Hill coefficient.

Although the His-tag variant of R-FPTA showed only one third of the wild-type activity, the Michaelis-Menten constant K_m=0.24±0.11 mM is similar to the value of the wild-type (see Tab. 4.2). As already mentioned, the lower activity of R-FPTA_C-His is explained by its minor expression (see Fig. 4.19 (b)). Even if the double mutant F113M E115K was more active than the His-tagged wild-type in the measurements done before, the initial gradient and the K_m value show a decrease in substrate affinity for **1a**. Compared to R-FPTA_C-His, a higher substrate concentration is necessary to reach V_{max}, which is represented in the kinetic plots.

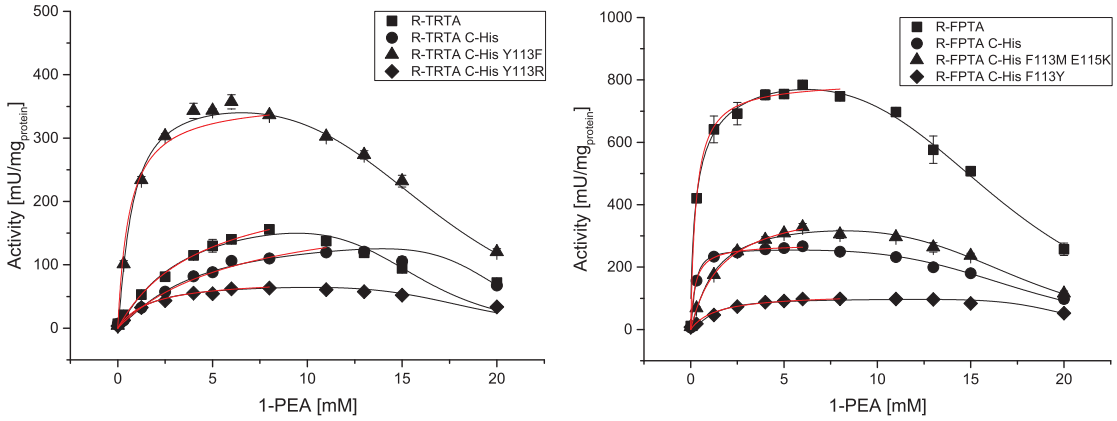

Fig. 4.22. *Enzyme kinetics of the ω-transaminases R-TRTA and R-FPTA. Red: Fit with Michaelis-Menten equation. Black: Fit with the bi-substrate Hill-Equation.*

3.2.4. Substrate Spectrum

Eight different ketones were applied for the biotransformation (see chapter III, section 7) with R-TRTA and R-FPTA and their variants to investigate the favoured substrates these ω-transaminases. Beforehand, the optimal amino donor was determined with the wild-types of R-TRTA and R-FPTA. Biotransformation with R-TRTA was performed under standard conditions. Because of its temperature instability, the biotransformation with R-FPTA was done at 15 °C. The conversion of the ketones to the corresponding amines was measured by gas chromatography (see chapter III, section 6.5).

3.2.5. Amino Donors

The amino donors D/L-alanine **1j**, *sec*-butylamine **1k** and isopropylamine **1l** were analysed in the amination reaction of **2a** at pH 7 and pH 8 with R-TRTA and R-FPTA. The racemates of **1j** and **1k** were applied in a concentration of 250 mM. Since amine **1l** is achiral, only 125 mM were applied.

As seen in Fig. 4.23, R-TRTA utilized **1k** as good as **1l**. The amination of **2a** with **1j** gave lower conversions. The differences between the amino donors were more significant with R-FPTA. The best conversion of **2a** was achieved with **1k**. Comparing the conversions at the different pH values, pH 8 was in advantage of pH 7.

Therefore, the biotransformation of ketones was performed with **1k** as amino donor at pH 8.

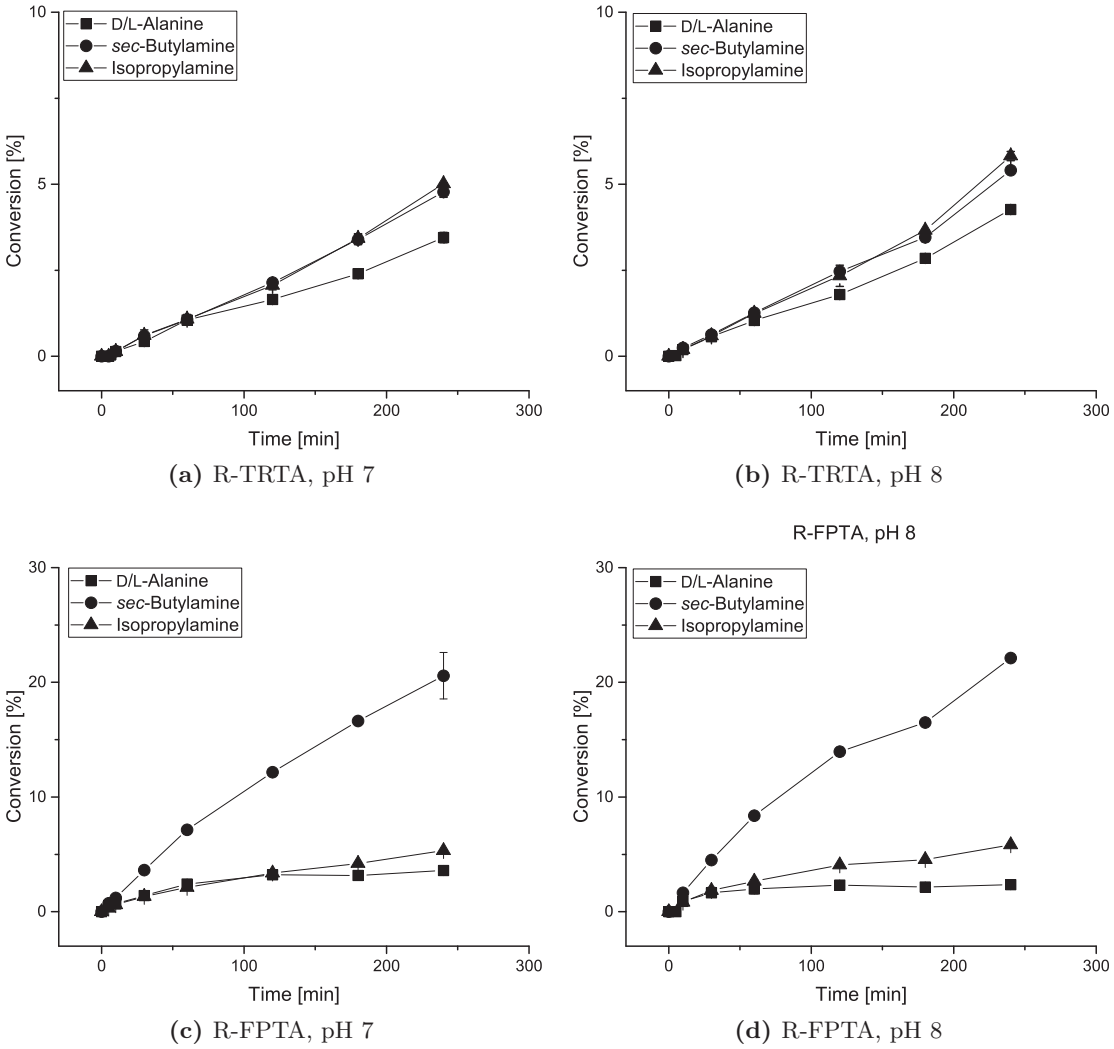

(a) R-TRTA, pH 7

(b) R-TRTA, pH 8

(c) R-FPTA, pH 7

(d) R-FPTA, pH 8

Fig. 4.23. *Testing of the amino donors* D/L-alanine ***1j****, sec-butylamine* ***1k*** *and isopropylamine* ***1l*** *for the amination of* ***2a*** *with the ω-transaminases R-TRTA and R-FPTA at pH 7 and pH 8.*

3.2.6. Amination of Ketones

The ketones **2a**–**2h** were aminated using R-TRTA and R-FPTA with **1k** as amino donor at pH 8. The conversions of the biotransformations were plotted against the time and the specific activities were calculated from the linear regression lines (see chapter Appendix, Fig. A.25 and Tab. A.1).

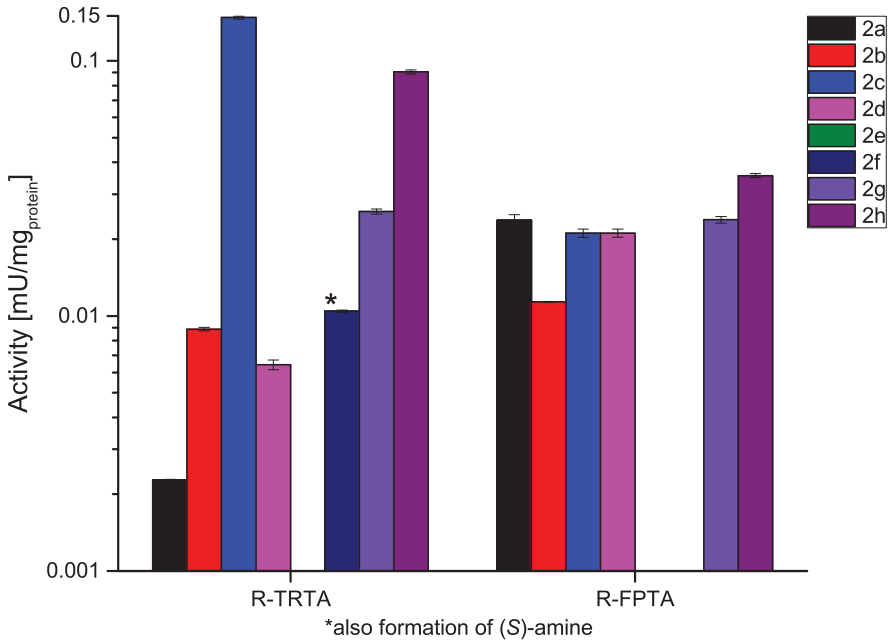

Fig. 4.24. *Amination activites of the ω-transaminases R-TRTA and R-FPTA from lyophilisates.The conversion of the ketones was determined by gas chromatography.*

The specific activities of R-TRTA vary from 0.002 mU/mg$_{protein}$ to 0.148 mU/mg$_{protein}$. No significant conversion was measured for the amination of substrate **2e**. The substrate **2f** was also converted to the corresponding (*S*)-amine. Compared to the ω-transaminase standard substrate **2a**, the specific activity of R-TRTA with **2c** (0.148 mU/mg$_{protein}$) was increased by 7400 %.

R-FPTA shows variations of its specific activities from 0.011 mU/mg$_{protein}$ to 0.035 mU/mg$_{protein}$. The substrates **2e** and **2f** were not converted by R-FPTA. The substrate converted best was ketone **2h** with 0.035 mU/mg$_{protein}$.

Compared to R-TRTA the measured activities for R-FPTA show no extreme increase for one substrate. Even if the specific activity of R-FPTA for **2a** is ten times higher than the specific activity of R-TRTA, specific activities of R-TRTA for the substrates **2g** and **2h** are higher than the specific activities of R-FPTA. R-TRTA shows therefore

more variation in its substrate spectrum. Moreover, the substrate specificities allow predictions about differences in the active sites of R-TRTA and R-FPTA.

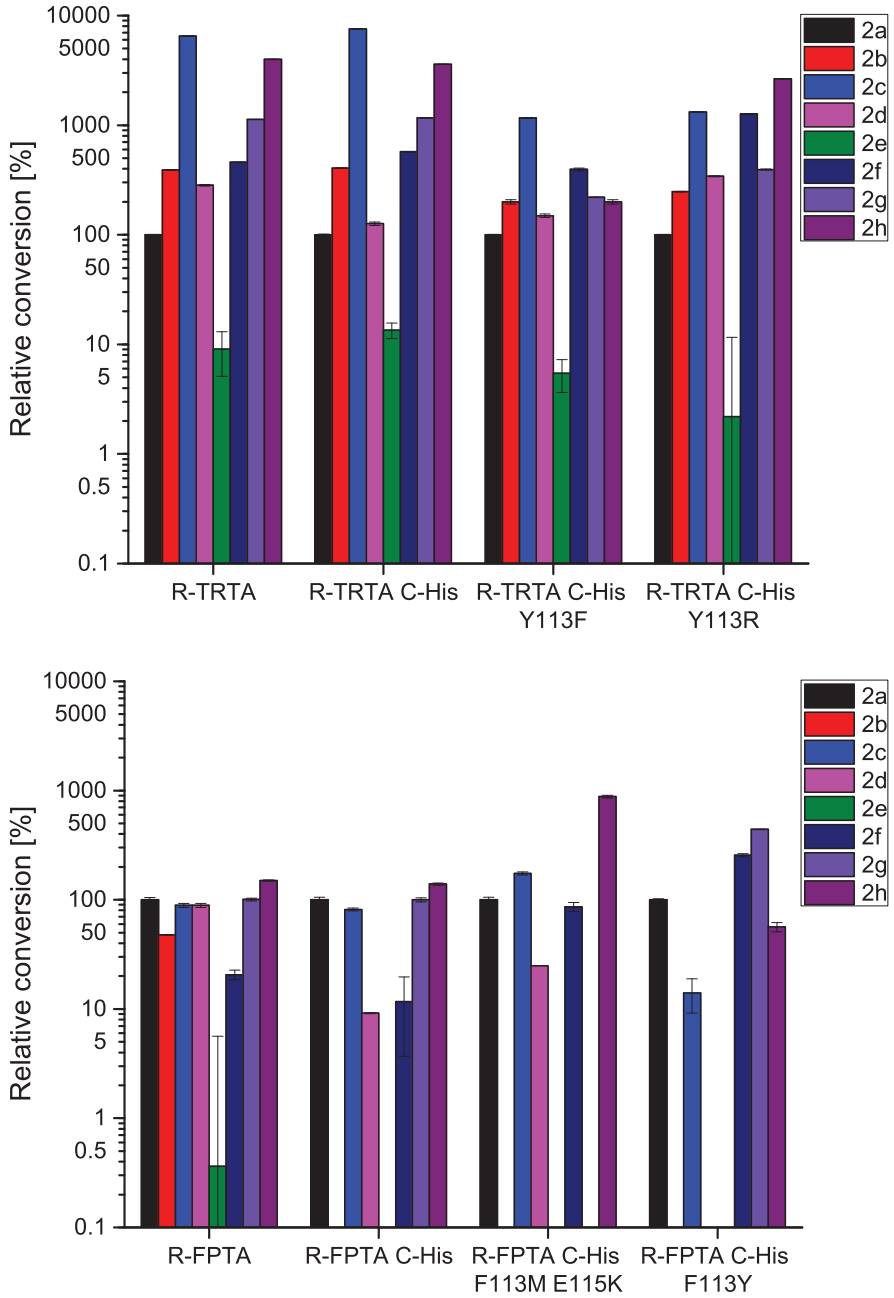

Fig. 4.25. *Substrate spectra of the ω-transaminases R-TRTA and R-FPTA. The activities are given as relative conversion in relation to the standard substrate acetophenone* ***2a****.*

In Fig. 4.25, the relative amination activities of the ω-transaminase variants are shown. The amination activities of R-TRTA_C-His compare to the wild-type activities of R-TRTA. Comparison of the substrate spectrum of the variant R-TRTA_C-His Y113F to the wild-type substrate spectrum, R-TRTA_C-His Y113F shows a decreased preference for especially **2g** and **2h**. Also the preference for **2c** was decreased. The variant R-TRTA_C-His Y113R was chosen from the screening because of changes in its substrate spectrum. In the amination assay these changes were less significant than in the screening assay. Comparing to the wild-type, the preference for **2f** was increased. The substrate **2c** which was converted by the wild-type R-TRTA with a highly increased activity was converted by R-TRTA_C-His Y113R with more moderate activity.

Whereas the substrate spectra of R-TRTA and its variants showed a good congruence between the screening assay and the biotransformation assay, there was hardly an an analogy between the deamination screening assay and the biotransformation assay for amination with R-FPTA and its variants. Due to the inhibition of the R-FPTA variants by the C-terminal His-tag and the resulting low conversion rates, the activity for the substrates **2b**, **2d**, **2e** and **2f** could not be determined. R-FPTA showed no outstanding high activity or preference for one special substrate like R-TRTA, but in contrast to R-TRTA, the substrates **2f** and **2e** were converted in smaller amounts than the standard substrate **2a**. The preference for mostly smaller substrates was shifted to the larger substrates with the variants R-FPTA_C-His F113M E115K and R-FPTA_C-His F113Y. R-FPTA_C-His F113M E115K showed a higher preference for the substrates **2c** and **2h**. In contrast to the assumption, that the preference of R-FPTA_C-His F113Y for larger substrates is decreased, this variant converted **2f** better than the wild-type and the second variant. The substrate which was converted best by R-FPTA_C-His F113Y was **2g**. A more detailed explanation of the ω-transaminases' specificity in correlation with the protein structure is given in chapter V, section 3.

3.3. Recent Developments

At the end of the labwork, a characterization of six new (R)-selective transaminases was published by Jiang *et al.*[99] Amongst others, the transaminases R-CMTA, R-TRTA, R-TATA and R-TVTA were described. While Jiang *et al.* could not overexpress R-CMTA, this was achieved in the present work and R-CMTA could be identified as an (R)-selective transaminase. Jiang *et al.* studied the transaminases in detail, regarding their optimal temperature, thermal stability, optimal pH and substrate spectrum. A comparison of the results for the transaminase R-TRTA, which was also characterized in this work, shows different outcomes.

Herein, the optimal pH for R-TRTA is pH 9.0 and the enzyme has 50 % of its activity after an incubation at 41.5 °C for 5 min. In contrast, Jiang *et al.* reported a pH optimum at pH 8.0 and still 90 % transaminase activity of R-TRTA even after incubating the enzyme at 50 °C for 20 min. It has to be pointed out that the comparison of these results has to be done with care, since the experimental set-ups differ. The main difference is the use of purified enzyme by Jiang *et al.*, whereas lyophilisate of crude cell extract was used in this work. Furthermore, the utilized instrumental analytics, as well as the incubation conditions differ. Due to the different assay conditions, like substrate concentrations and amino donor, also the comparison of the substrate spectra determined in this work and in the publication of Jiang *et al.* is limited. Nevertheless, Jiang *et al.* observed the same trend of R-TRTA to prefer rather large substrates.

4. The Three Dimensional Structure of R-TRTA

At the beginning of the laboratory work, only the key motifs of (*R*)-selective ω-transaminases were known from a rational approach by analysing the structural information of related enzymes (D-amino acid aminotransferases, L-branched-chain amino acid aminotransferases and 4-amino-4-deoxychorismate lyases).[1] To elucidate the arrangement of the key motif amino acids within the active site, the three dimensional structure of the (*R*)-selective ω-transaminase R-TRTA was determined.

4.1. Enzyme Preparation for Crystallization Experiments

R-TRTA was already provided with a C-terminal His-tag (see section 1.3). The His-tagged variant of R-TRTA was produced in a 7.5 L scale to gain enough protein product for further experiments.

4.1.1. Production of R-TRTA_C-His

E. coli BL21(DE3) pET-21a(+) R-TRTA_C-His was cultivated in a 7.5 L fed-batch fermentation (see section 3.3). After 22 h, the gene expression was induced with 1 mM IPTG at an optical density of OD_{580}=65.9. Another 24 h later, the biomass with an amount of 502.4 g was harvested and stored at –20 °C. The downstream processing of the biomass was tried first with a small amount. 5 g of cells from the fermentation were processed as described in chapter 5.1. As more than 40 % of the activity were lost during the first trial, the procession was repeated. The addition of 500 mM NaCl stabilized the

enzyme during the downstream procession. The remaining biomass (251 g) was then further processed with the optimized protocol (see Fig. 4.26).

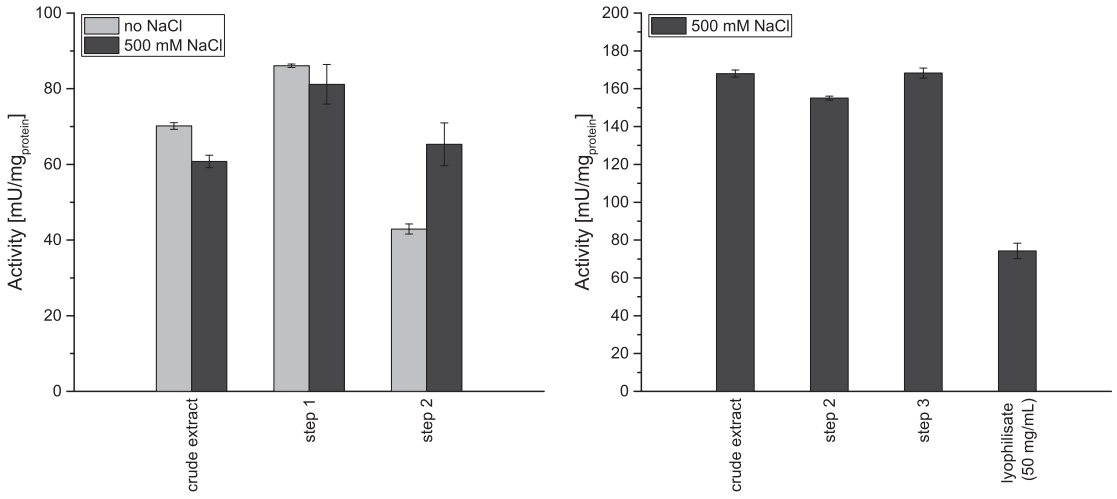

(a) Trial procession. **(b)** Optimized procession.

Fig. 4.26. *Downstream processing of R-TRTA_C-His biomass. Step 1: Incubation with DNase, step 2: Precipitation, step 3: Filtration. (a) In a trial, small amounts of biomass were processed. By adding 500 mM NaCl, R-TRTA_C-His was stabilized. (b) Complete processing of R-TRTA_C-His biomass. The specific activity of R-TRTA_C-His is ≈185.60±10.15 mU/mg$_{R\text{-}TRTA_C\text{-}His}$.*

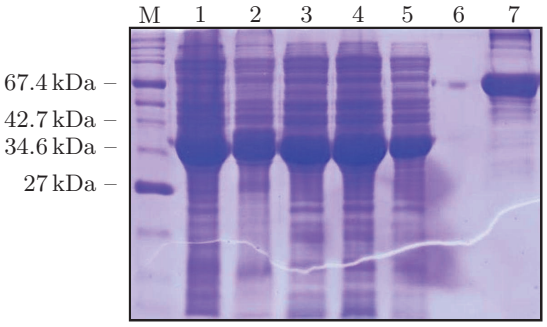

Fig. 4.27. *SDS-PAGE from biomass processing for lyophilisation. Lane 1: Sample from cell extracts. Lane 2: Sample from insoluble fractions after cell disruption . Lane 3: Sample after step 2. Lane 4: Sample after step3. Lane 5: Lyophilisate. Lane 6: Empty. Lane 7: 8 µg BSA. M: Protein Marker (New England Biolabs).*

On the basis of SDS-PAGE analysis of the R-TRTA_C-His lyophilisate (see Fig. 4.27), the concentration of R-TRTA_C-His could be estimated by comparing the R-TRTA_C-His band with the BSA band (8 µg). The activity of R-TRTA_C-His was determined with the acetophenone assay from the resuspended lyophilisate.

The ω-transaminase concentration in the lyophilisate was approximately 40 % of the total protein concentration (50 $mg_{lyophilisate}/mL \approx$ 9.92 $mg_{R\text{-}TRTA\_C\text{-}His}$). An activity of 74.24±4.06 $mU/mg_{protein}$ therefore results in a specific activity of R-TRTA_C-His of ≈185.60±10.15 $mU/mg_{R\text{-}TRTA\_C\text{-}His}$ within the lyophilisate.

4.1.2. Purification of R-TRTA_C-His

R-TRTA_C-His was purified from the lyophilisate with Ni-NTA Superflow resin (Qiagen GmbH, Hilden, Germany). For the protein crystallisation, the target concentration of the enzyme was about 10 mg/mL. 4 mL Ni-NTA Superflow resin with a binding capacity of up to 50 $mg_{His\text{-}tagged\ protein}/mL_{resin}$ were used. R-TRTA_C-His was purified from 500 mg lyophilisate, resuspended in 8 mL lysis buffer. In a first approach, the bound enzyme was washed three times with washing buffer and was finally eluted in three fractions. For the first and second elution of bound R-TRTA_C-His, the elution buffer was used. The third elution was done with the second elution buffer, containing a higher imidazole concentration (see chapter III, section 5.2). The activities in the particular fractions were monitored and the fractions were analyzed by SDS-PAGE. As still some by-protein was found in the third washing fraction, in a second approach, two more washings steps were done. The activities of the fractions and the SDS-PAGE of the second approach are shown in Fig. 4.28 and Fig. 4.29.

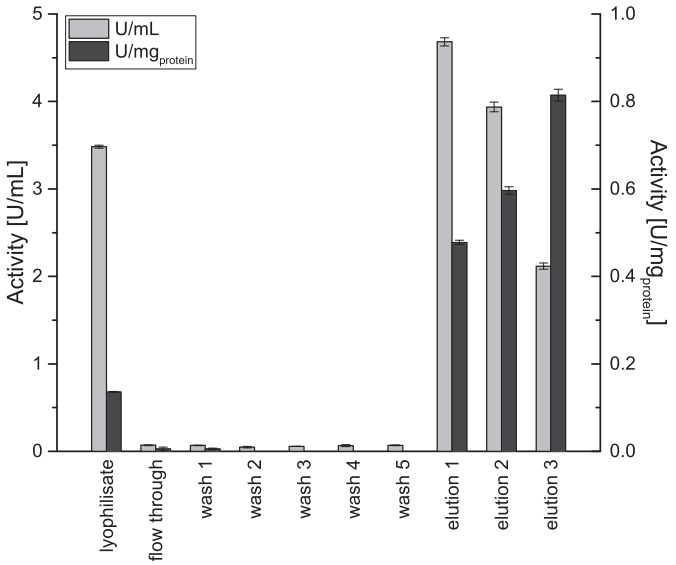

Fig. 4.28. *Activites of R-TRTA_C-His in eluates from protein purification via Ni-NTA resin. The elution steps 1–2 were done with 250 mM imididazole. The elution step 3 was done with 350 mM imidazole.*

By binding the ω-transaminase, the resin became yellow. Also the elution fractions showed a yellow colour which is caused by the yellow colour of the cofactor pyridoxal 5'-phosphate. The volume activity decreased from elution steps 1–3 (see Fig. 4.28), according to the concentration of R-TRTA_C-His as seen on the SDS-PAGE (see Fig. 4.29).

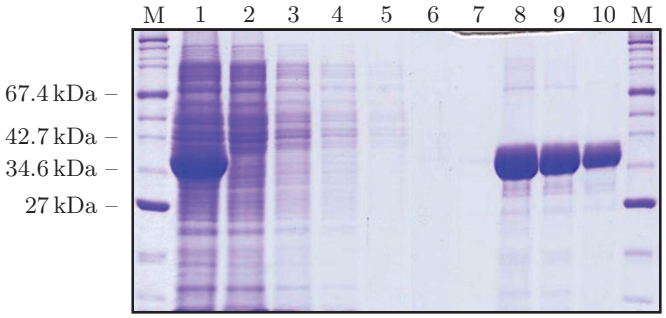

Fig. 4.29. *SDS-PAGE from of R-TRTA_C-His purification via Ni-NTA resin. Lane 1: Resuspended lyophilisate. Lane 2: Flow through. Lane 3: Washing 1. Lane 4: Washing 2. Lane 5: Washing 3. Lane 6: Washing 4. Lane 7: Washing 5. Lane 8: Elution 1. Lane 9: Elution 2. Lane 10: Elution 3. M: Protein Marker (New England Biolabs).*

A constant specific activity in the elution fractions was expected, but instead an increase of the specific activity was observed. Possible explanations could be the higher content of eluted by-protein in the elution fractions 1 and 2 or inactive enzyme due to improper folding, which was eluted at first at lower imidazole concentrations.

For protein crystallization, the elution fractions were pooled and first rebuffered over lysis buffer to Tris HCl buffer, pH 7.2. Finally, a sample with a concentration of 10.4 $mg_{R\text{-}TRTA\_C\text{-}His}$/mL with 0.64±0.03 U/$mg_{R\text{-}TRTA\_C\text{-}His}$ and a second sample with a concentration of 13.5 $mg_{R\text{-}TRTA\_C\text{-}His}$/mL with 0.51±0.01 U/$mg_{R\text{-}TRTA\_C\text{-}His}$ were provided to the collaboration partners.

4.2. Determination of Protein Structure

The determination of the three dimensional protein structure of R-TRTA was done in collaboration with Dr. Renu Batra-Safferling and Dr. Joachim Granzin from the Institute of Complex Systems (ICS-6: Structural Biochemistry) at the Forschungszentrum Jülich. For protein crystallography, crystals of R-TRTA_C-His were used (see Fig. 4.30).

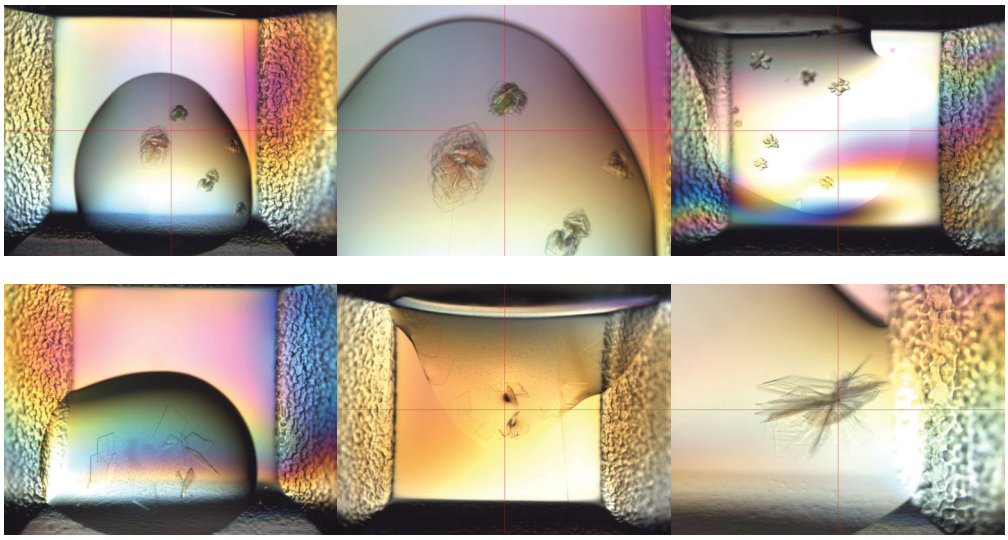

Fig. 4.30. *Crystals of ω-transaminase R-TRTA_C-His.*

The X-ray diffraction was done at the synchrotron beamline ID23-1 (European Synchrotron Radiation Facility, Grenoble, France). The data were collected at a wavelength of λ=0.97902 Å with a DECTRIS PILATUS 6M detector. The resolution of the highest-resolution shell was 1.78–1.75 Å. R-TRTA_C-His unit cells could be described with a primitive orthorhombic lattice system with α=β=γ=90° and the dimensions of a=73.45 Å, b=119.80 Å and c=129.35 Å. The space group was P 2_1 2_1 2_1.

The collected dataset consisted of 421774 (18829)[x1] reflections whereof 114909 (5590)[x1] were unique. The dataset reached a completeness of 99.6 % (99.2 %)[x1].

From an overall number of 321 (329 with his tag) protein residues, residues 2–319 were visible in the electron density map. For the cofactor pyridoxal 5'-phosphate (PLP), electron densities were found next to Lys178, indicating that PLP is covalently bound to the enzyme. Analyses of the stereochemistry of the structure model showed 99 % of the angles inside the Ramachandran plot and no angles outside the plot (complete data see Tab. 4.1).

[x1] Statistics for the highest-resolution shell are shown in parentheses

Tab. 4.1. *Data collection and refinement of X-ray diffraction data from R-TRTA_C-His crystals.*

Xray Data	
Beamline	ID23-1
Detector	DECTRIS PILATUS 6M
Wavelength [Å]	λ=0.97902
Resolution range [Å]	46.42 – 1.75 (1.78 – 1.75)^{x1}
Space group	P 2_1 2_1 2_1
Unit cell [Å]	
(α=β=γ=90°)	a=73.45 b=119.80 c=129.35
Total reflections	421774 (18829)^{x1}
Unique reflections	114909 (5590)^{x1}
Multiplicity	3.7 (3.4)^{x1}
Completeness [%]	99.6 (99.2)^{x1}
Mean I/σ(I)	9.9 (2.0)^{x1}
Wilson B-factor [Å^2]	13.40
R_{merge}	0.084 (0.547)^{x1}
R_{meas}	0.099 (0.648)^{x1}
Refinement	
R_{work}	0.1512 (0.2426)^{x2}
	^{x2}(resolution range 1.813 – 1.75)
R_{free}	0.1714 (0.2591)^{x2}
Coordinate error	
(max.-likelihood based)	0.16
Number of atoms	
Total	5976
Macromolecules	5071
Ligands	180
Protein residues	636
Water	725
RMS(bonds) [Å]	0.007
RMS(angles) [°]	1.13
Ramachandran plot [%]	
Favoured	99
Outliers	0
Clashscore	4.26
B-factor [Å^2]	
Average	22.56
Macromolecules	20.51
Ligands	42.20
Solvent	32.05

^{x1,x2} Statistics for the highest-resolution shell are shown in parentheses

4.3. Structure-Function Relation

R-TRTA is build as a homodimer. The monomer consists of two domains, the PLP-binding domain and the N-terminal domain, beginning with an α-helix (Met4–Ala20). The N-terminal domain is characterized by an α/β-structure with an anti-parallel β-sheet, having a large intra-domain loop (Arg120–Asn135). The PLP-binding domain has a wavy and slightly twisted β-sheet which appears almost like a barrel. This β-sheet is surrounded by loops and α-helices. Both domains are connected by a loop (Tyr144–Pro150) (see Fig. 4.31).

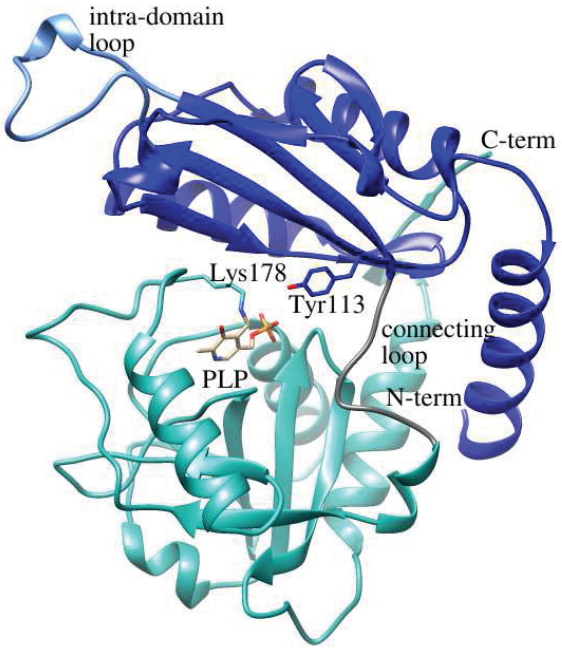

Fig. 4.31. *R-TRTA monomer. The N-terminal domain with the intra-domain loop (in light blue) is coloured in blue and the PLP-binding domain is coloured in cyan. The connecting loop is coloured in gray.*

The bowl-like monomers of R-TRTA form a dimer with the large intra-domain group extending into the hole of the second monomer. The β-strands Arg43–Pro45 of both monomers are thereby crossing each other. The overall three dimensional structure of the homo-dimer of R-TRTA has a butterfly wings-like shape (see Fig. 4.32).

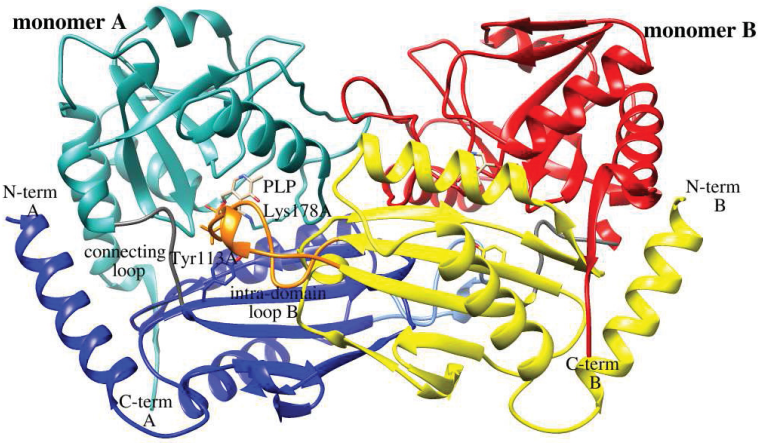

Fig. 4.32. *R-TRTA dimer. The monomer A is coloured in blue and cyan and monomer B is coloured in yellow and red. The orange intra-domain loop extends into the other monomer.*

4.3.1. Active Site of R-TRTA

The active sites are formed between the domains by the cavity of the first monomer and the intra-domain loop of the second monomer. Their entrances are located on either side of the homodimer. The cofactor PLP is covalently bound by the Lys178 in the large binding pocket (see Fig. 4.33). The phosphate group of PLP is coordinated through a salt bridge to the side chain of Arg77 and by H-bonds with the main chain nitrogens of Ile236, Thr237 and Thr273 and the side chain oxygens of Thr237 and Thr273 in the small binding pocket. The Glu211 in the large binding pocket coordinates the pyridine nitrogen of PLP with its carboxyl group.

R-TRTA was crystallized without any substrates. However, within the active site electron densities for Tris, L-Leucine and sulfate (originating from buffer) were found (see Fig. 4.34). The amino acid residues which are involved in binding Tris and L-Leucine correspond to the residues described for substrate binding in ω-transaminases.[46,75,76] Tris coordinates a water molecule which is coordinated by Glu115. Glu115 was crystallized as two rotamers and therefore offers flexibility in substrate binding. Tris was crystallized in different orientations in the active sites of R-TRTA. L-Leucine is completely located in the large binding pocket. The amino group is coordinated by Tyr113 and a water molecule which forms H-bonds to Tyr58 and His53*. The L-leucine oxygen interacts with the guanidinium group of Arg126* and the nitrogen of Tris.

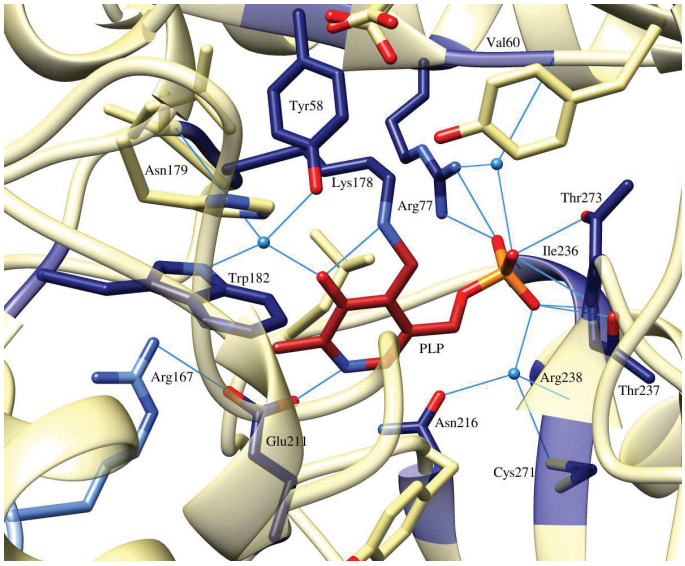

Fig. 4.33. *Binding of the cofactor PLP by R-TRTA. PLP (dark red) is covalently bound to Lys178. The amino acids which are involved in the binding of PLP are coloured in blue.*

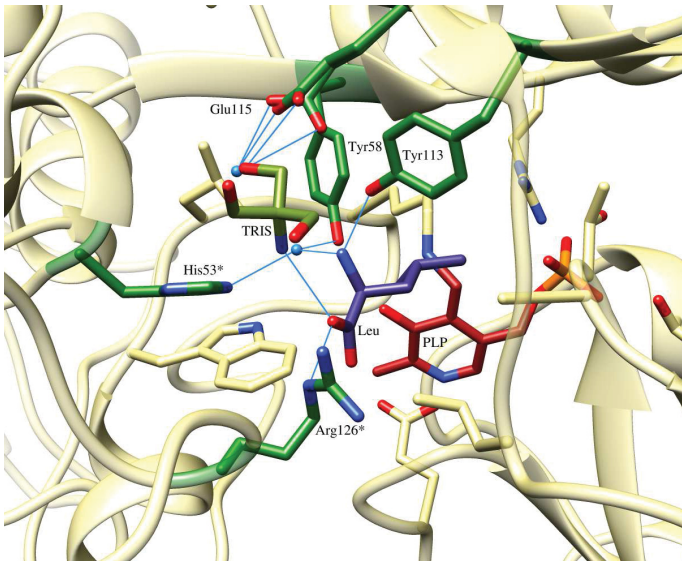

Fig. 4.34. *Active site of R-TRTA with Tris (olive green) and* L*-leucine (violet). The amino acids which are involved in the binding of Tris and* L*-leucine are coloured in dark green.*

An overlay with the structures of the ω-transaminases from *Aspergillus fumigatus*,[76] *Aspergillus terreus*[75] and *Nectria haematococca*[46] shows highly matching structures (see Fig. 4.36). In the corresponding alignment (Fig. 4.35), the amino acids which contribute to the binding of the cofactor and the substrate are labelled. The PLP binding amino acids are conserved in the class IV of the PLP binding enzymes.[100] The substrate binding amino acids correspond to the sequence motifs derived by Höhne *et al.*[1]

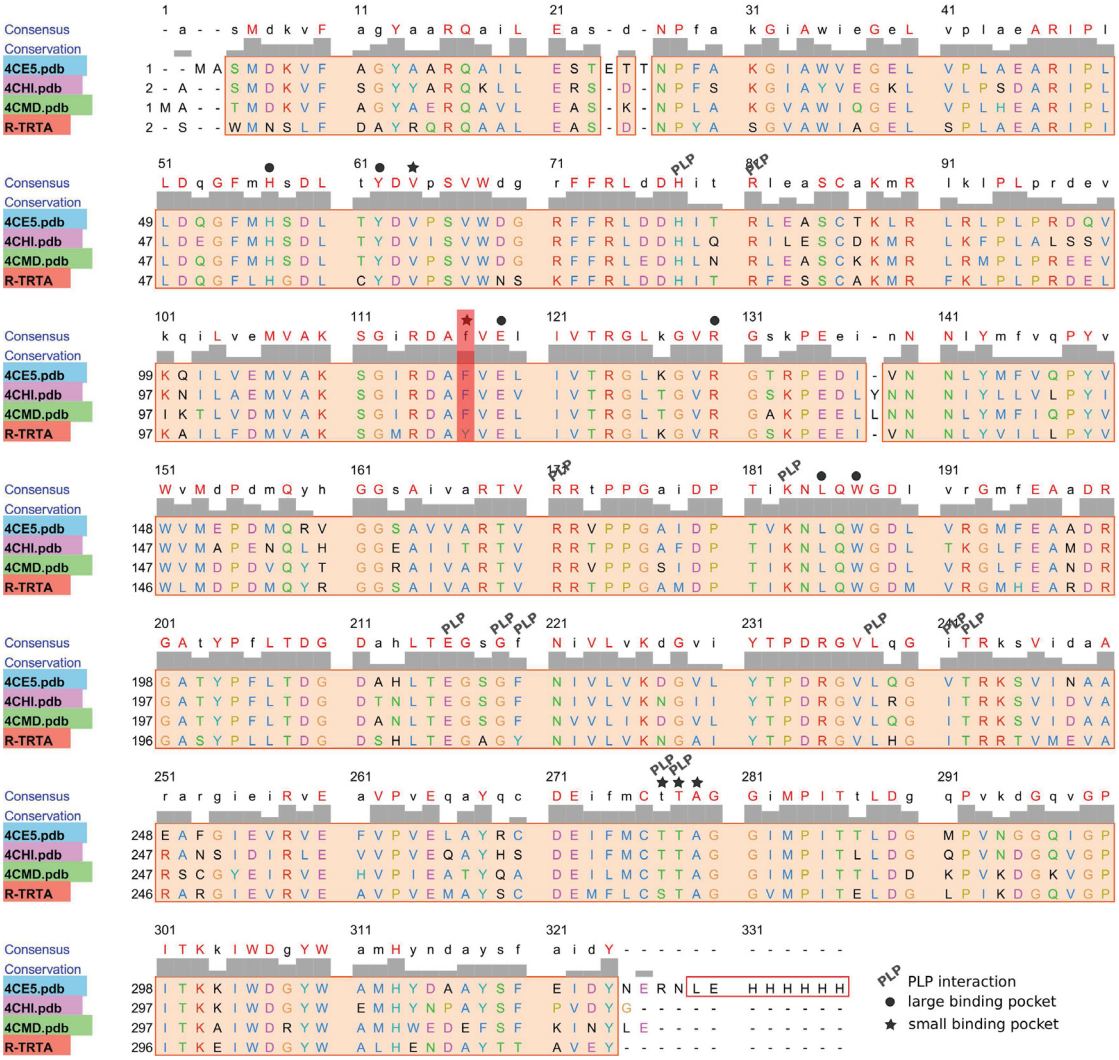

Fig. 4.35. *Alignment of the structure overlay of the ω-transaminases from A. fumigatus (4CHI), A. terreus (4CE5) and N. haematococca (4CMD) with R-TRTA. Amino acids contibuting to the binding of the cofactor and the substrate are labelled.The position 113 is highlighted in red. Completely conserved residues in the consensus sequence are shown in red. The grey bar high indicates the grade of conservation. The amino acid residues are coloured depending on their chemical characteristics.*

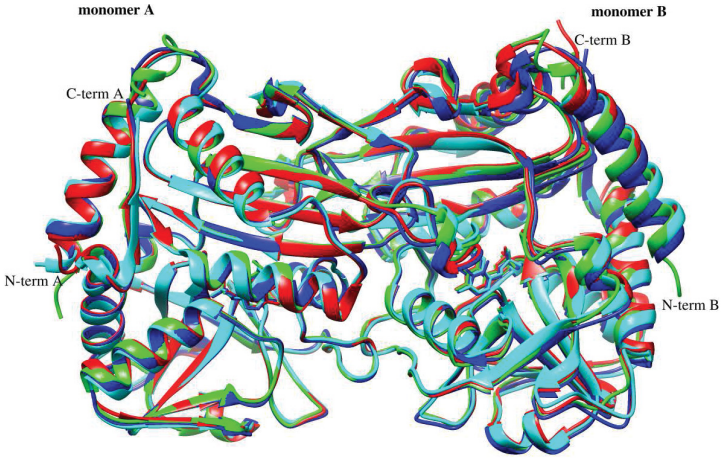

(a) Overlay of (R)-selective ω-transaminases.

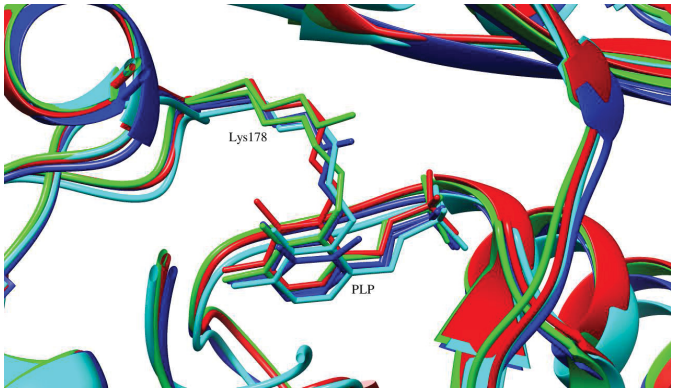

(b) Insight into the active site of (R)-selective ω-transaminases.

Fig. 4.36. *(a) Overlay of the ω-transaminases from A. fumigatus (blue), A. terreus (green) and N. haematococca (red) with R-TRTA (cyan). (b) Insight into the active site of the ω-transaminases: PLP bound to Lys178. The Lys180 of the ω-transaminase from A. terreus (green) was also crystallized in the unbound state.*

V. Discussion

1. Identification of Novel (*R*)-Selective ω-Transaminases

In 2003, the first (*R*)-selective ω-transaminase from *Arthrobacter* sp. KNK168 was found in soil isolates.[34,69,70] For seven years it was the sole known ω-transaminase with (*R*)-selectivity, until Höhne *et al.* published their *in silico* screening method to find new (*R*)-selective ω-transaminases in 2010.[1] Until then, besides the one (*R*)-selective ω-transaminase, ten synthetically relevant (*S*)-selective ω-transaminases and ten wild-type microorganisms showing (*S*)-selective ω-transaminase activity were known.[34] The necessity of an alternative approach to find new ω-transaminases with (*R*)-selectivity was pointed out by Clay *et al.*: By screening more than one hundred whole cell preparations of various species, only (*S*)-selective ω-transaminases were found.[71] This indicates that the (*R*)-selectivity of these enzymes is more rare than the (*S*)-selective counterpart.[34] Other possible explanations could be that (*R*)-selective ω-transaminases are mainly produced in microorganisms which are not included in the strain collections screened so far[71] or do not grow in media used typically for enrichment cultures e.g. from soil isolates. Also, too low expression of (*R*)-selective ω-transaminases in screening cultures below the detection level is possible.

1.1. *In Silico* Screening for new (*R*)-selective ω-Transaminases

In this work, the basic approach of a sequence alignment with known (*R*)-selective transaminases against the NCBI database was successful. The alignments were done in two stages. The enzymes from the first screening round R-CMTA and R-TRTA were identified as (*R*)-selective ω-transaminases. Their sequences were used as templates in the second screening round. Based on the annotation of the chosen sequences, (*R*)-selective ω-transaminase activity was not assured (see Tab. 5.1). The enzymes identified as (*R*)-selective ω-transaminases were annotated as (putative) class IV aminotransferase, D-alanine aminotransferase or hypothetical protein.

Considering the sequence motifs,[1] only the annotations of R-MKTA and R-TOTA were correct. Even though these enzymes were well overexpressed in *E. coli*, they showed no

activity with the ω-transaminase substrate **1a** (see chapter IV, section 1.1.1). A possible explanation for the lack of activity could be a too low reaction temperature, since the origins of both enzymes are thermophilic organisms. However, initial experiments for the amination of **2a** with glutamate as amino donor showed transaminase activity. These results and the sequence motifs of both enzymes show that R-MKTA and R-TOTA are branched-chain amino acid aminotransferases, like annotated.

Tab. 5.1. *Overview of new aminotransferases used in this work and their activities.*

Round	ω-TA	Annotation	Active
I	R-CMTA	class IV aminotransferase	yes
	R-CPTA	found in metagenome sequences	yes[x1]
	R-MKTA	branched-chain amino acid aminotransferase	no
	R-TOTA	branched-chain amino acid aminotransferase	no
	R-TRTA	D-alanine aminotransferase	yes
II	R-AFTA	branched-chain amino acid aminotransferase	no
	R-CGTA1	putative class IV aminotransferase	yes[101]
	R-CGTA2	putative class IV aminotransferase	yes[101]
	R-FPTA	hypothetical protein	yes
	R-GCTA	branched-chain amino acid aminotransferase	no
	R-PMTA	branched-chain amino acid aminotransferase	no
	R-TATA	hypothetical protein	yes[101]
	R-TVTA	hypothetical protein	yes

[x1] after refolding from inclusion bodies

R-TRTA, R-CMTA, R-FPTA and R-TVTA were identified as (*R*)-selective ω-transaminases. In initial expression studies, neither activity nor soluble protein could be determined for R-CPTA. But after refolding R-CPTA from inclusion bodies, transaminase activity could be proven for this enzyme from metagenome sequences (see chapter IV, section 1.1.4). In further studies, the expression of R-CGTA1, R-CGTA2 and R-TATA could be achieved in soluble form and the enzymes were proven to be (*R*)-selective ω-transaminases.[101] For R-AFTA, R-GCTA and R-PMTA neither transaminase activity could be determined nor an expression in soluble form was achieved. Therefore, the cause for the inactivity is most likely the absence of soluble and active enzyme. In case of R-AFTA and R-GCTA, the sequences seem to be incomplete and in consequence an expression is impossible. Nevertheless, these three transaminases were identified as (*R*)-selective ω-transaminases by their sequence motifs and were erroneously annotated as branched-chain amino acid aminotransferases.

The results in this work, as well as recent reports, show that a classification of a transaminase is possible with the help of the sequence motif. But this motif is no dogma, as changes within the motif are possible to optimize the enzyme for bulky-bulky substrates. For example the transaminase ATA-117-110 was optimized to replace the chemical amination of the antidiabetic drug sitagliptin by a biocatalytic process.[29] By optimizing ATA-117-110 for this relatively large substrate, the new sequence diverged from the sequence motif and its original ability to convert the standard substrate **1a** for (*R*)-selective ω-transaminases got lost. With equal overexpression compared to ATA-117, no activity could be measured in the acetophenone assay for ATA-117-110 (see chapter IV, section 1.2.1).

1.2. Heterologous Expression of Putative Transaminase Genes

For the production of enzymes for biotechnological purposes, high expression rates of the desired enzyme in soluble and active form are necessary. *E. coli* as a preferred host for heterologous protein expression offers the requirements such as the possibility of high-cell density fermentation and easy process scale up for this purpose.[102] Also, many tools for the production of active enzyme in *E. coli* are available.[102,103] However, despite their high similarity, the transaminases were not equally well expressed in *E. coli*. Differences in the protein concentration even occurred between transaminases of the same genus,[1,104] as shown here for the (*R*)-selective ω-transaminases R-TRTA, R-TVTA and R-TATA.

Several factors can influence the varying expression rates of the ω-transaminases and the formation of inclusion bodies, for example the inducer concentration, expression temperature, media composition, and availability of cofactor.[97,102] Additional difficulties during the heterologous expression of the ω-transaminases as active enzyme could arise from the homodimeric nature of the enzymes and, due to the (fungal) origin of the ω-transaminases, also from lacking post-translational modifications.[105] The formation of inclusion bodies is caused by insoluble protein due to too much expression and misfolding. Decreasing the inducer concentration and temperature slows down the expression and promotes proper folding of the recombinant protein due to reduction of temperature dependend hydrophobic interactions that contribute to protein misfolding.[102,105,106] As the formation of inclusion bodies depends on the final cell density, the composition of the culture medium also plays an important role.[102] The growth parameters such as pH and cofactor concentration are defined by the culture medium. The latter has a significant effect on protein folding and increases the formation of soluble and active enzyme.[97,102]

Under standard conditions, the transaminases in this work were produced in a large part in insoluble form in *E. coli*. By adjusting the inducer concentration, lowering the

temperature and adding pyridoxine, the expression in soluble form and the enzyme activity were increased. For example, neither in this work nor in a recent publication[104] active R-CMTA was produced in LB medium. A significant activity of R-CMTA was achieved by changing the cultivation medium to M9 with supplemented pyridoxine. Although buffers and solutions for enzyme preparation and activity assays are always supplemented with the cofactor PLP,[1,46,107–110] only in one case the PLP precursor pyridoxine was already added during gene expression.[29] The increased activity by adding pyridoxine during gene expression indicates an insufficient production of PLP by *E. coli* during the production of the recombinant transaminase. By adding the PLP precursor, the ω-transaminase activity is presumably increased by more proper folding by cofactor assistance and not by a higher production of the enzyme, since no differences in enzyme production were seen on SDS-PAGE gels (see chapter A, Fig. A.24).

In case of R-FPTA, lowering the temperature during gene expression lead to higher and reproducible activity of the enzyme. This might also be the reason why Höhne *et al.* chose 20 °C for the expression of their unknown ω-transaminases.[1] The determination of the thermal stability of R-FPTA showed a degradation of the transaminase activity at 30 °C (see chapter IV, section 3.2.2). Therefore, the expression of R-FPTA at 30 °C was probably hindered by its thermal instability. In contrast to R-FPTA, the expression of R-TRTA could be done at 30 °C without loosing activity. This is also reflected by the thermal stability of R-TRTA which is more stable than R-FPTA at temperatures above 25 °C. Since the habitats of the source organisms of R-FPTA and R-TRTA have average temperatures of 17 °C and above 26 °C, respectively, the assimilation of their ω-transaminases to their habitat's climate is a possible explanation for the different thermal stabilities of R-FPTA and R-TRTA.[111–113]

The temperature may also have an influence of the expression of R-CPTA which was found in metagenome sequences and is assigned to the marine bacterium *Candidatus pelagibacter ubique*. The bacteria itself grows at 20 °C[114] and therefore higher expression temperatures might lead to a coagulation and inclusion body formation of R-CPTA. Moreover, the conditions for protein folding in the marine ecosystem differ from the conditions in *E. coli*. But the more likely reason for the expression of R-CPTA as insoluble protein is another. Compared to the protein sequences of the active (*R*)-selective ω-transaminases, the sequence of R-CPTA is rather short and seems to miss part of the N-terminal sequence. The structure homology model of R-CPTA in comparison with the structure of R-TRTA clarifies the position of the missing sequence part (see Fig. 5.1). The missing part is an N-terminal α-helix which was described to be a feature of fungal (*R*)-selective ω-transaminases,[46,76] but is also existent in the bacterial trans-

aminase from *Arthrobacter* sp. Thomsen *et al.* identified this N-terminal α-helix to be important for the soluble expression of (R)-selective ω-transaminases in *E. coli*.[76] Since R-CPTA from metagenome sequences is assigned to a marine bacterium, the existence of this N-terminal α-helix seems to be an adaption for solubility improvement in terrestrial ecosystems. By refolding R-CPTA from inclusion bodies, transaminase activity was already proven in this work. Hence, the addition of an N-terminal α-helix from another (R)-selective ω-transaminase is also promising to gain soluble R-CPTA in *E. coli*.

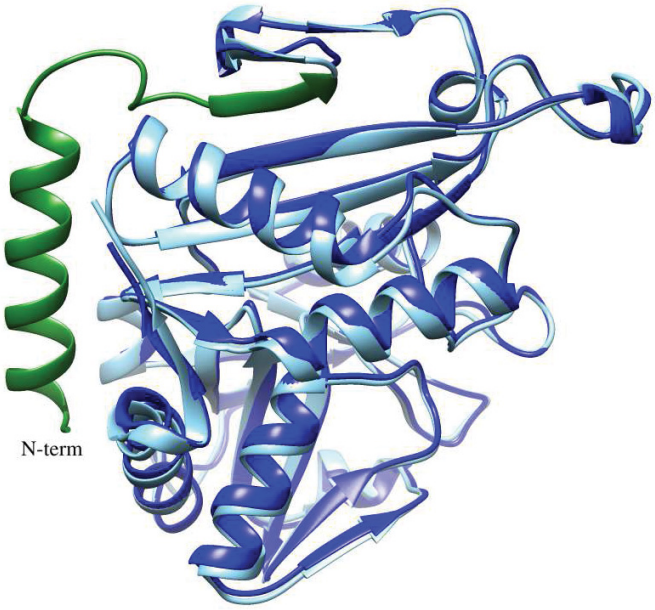

Fig. 5.1. *Overlay of the monomers of R-TRTA (light blue) and R-CPTA (blue). The N-terminal α-helix of R-TRTA is highlighted in green. R-CPTA has no N-terminal α-helix. The structure of the ω-transaminase from Aspergillus terreus served as template for modelling the structure of R-CPTA.*

Most of the known (R)-selective ω-transaminases are from fungal origin (for relation of class IV transaminases see phylogenetic tree in Fig. 5.2). Therefore, the formation of inclusion bodies is probably due to missing post-translational modifications of the eukaryotic enzymes in *E. coli*. Post-translational modifications like glycosylation support the proper folding of proteins.[115,116] Similar problems are known from the heterologous expression of laccases in *E. coli*. Like ω-transaminases, most laccases are of fungal origin and most of these enzymes are glycosylated.[117] The parallel overexpression of the (R)-selective ω-transaminases in this work showed that compared to the (R)-selective ω-transaminases from fungal origin, ATA-117 and its sitagliptin variant ATA-117-110 were overexpressed to a higher extend in soluble form (see chapter IV, Fig. 4.7) Espe-

cially the fungal ω-transaminases R-CMTA, R-PMTA were hardly or not at all expressed in soluble form in *E. coli*.

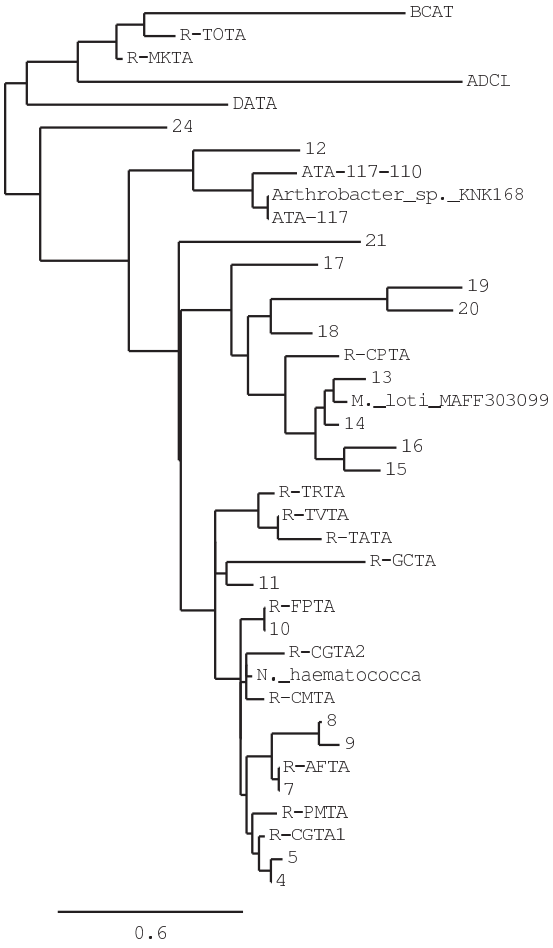

Fig. 5.2. *Phylogenetic tree of class IV transaminases. The tree was generated with Phylogeny.fr.*[118–124] *Included in the phylogenetic analysis were the transaminases found in this work, the ω-transaminase from Nectria haematococca*[46] *and the (R)-selective transaminases identified by Höhne et al.*[1] *The (R)-selective transaminases from Höhne et al. and their gene IDs are as follows: ADCL (4-amino-4-deoxychorismate lyase, E. coli, PDB 1ET0), BCAT (branched-chain amino acid aminotransferase, E. coli, PDB 1IYD), DATA (*D*-amino acid aminotransferase, Bacillus sp., PDB 3DAA), 4 (Aspergillus terreus, 115385557), 5 (Penicillium chrysogenum, 211597081), 6 (A. niger, 145258936), 7 (A. oryzae, 169768191), 8 (A. fumigatus, 70986662), 9 (Neosartorya fischeri, 119483224), 10 (Giberella zeae, 46109768), 11 (Hyphomonas neptunium, 114797240), 12 (Mycobacterim vanbaalenii, 120405468), 13 (Mesorhizobium loti, 13471580), 14 (M. loti, 20804076), 15 (Roseobacter sp., 86137542), 16 (Marinomonas sp., 87122653), 17 (Rhizobium etli, 190895112), 18 (Rhodoferax ferrireducens, 89899273), 19 (Jannaschia sp., 89053613), 20 (Labrenzia alexandrii, EEE43073), 21 (Burkholderia sp., 78059900), 24 (Gamma proteobacterium, 219677744).*

Considering the high potential of the *E. coli* toolbox for the overexpression of recombinant enzymes, further optimization of fungal transaminase expression seems possible. A possible approach could be the coexpression of the ω-transaminases with chaperones in *E. coli* to increase the solubility, but the performance of chaperones is hard to predict.[103,125] Another procedure would be the production in an eukaryotic host. Eukaryotic expression systems, especially yeasts, offer the advantages of fast growth and easy gene manipulation thereby performing post-translational modifications.[117]

2. Customization of Transaminase Analytics

The analysis of transaminase activity with substrates different from the standard substrates **1a** and **2a** is still a challenge. In contrast to spectrophotometric measurements of e.g. the cosubstrates NAD^+ and NADH, the transaminase assays depend on the determination of product or educt. Artificial substrates with the chromophoric *p*-nitrophenyl group which are used in various hydrolase assays cannot be used.

Since the assay can become the limiting step in transaminase analysis,[67] faster methods for screening transaminases were in demand. In 2004, Hwang *et al.* developed a staining method for the α-amino acid product of the ω-transaminase reaction.[65] Several drawbacks of this method motivated Schätzle *et al.* five years later to develop another assay for the measurement of ω-transaminase activity.[67] With this so called acetophenone assay, a rapid and kinetic characterization of ω-transaminases is possible, but limited to the substrate 1-phenylethylamine **1a**.[67]

In contrast to these high-throughput (HTP) methods, chromatographic methods are relatively independent from the applied reactants but also often low-throughput (LTP). Spectrophotometric methods are normally well-established and require less technical equipment. The chromatographic methods can also be adjusted to HTP but need higher investment due to more expensive technical equipement and knowledge of the used instruments. Nevertheless, this investigation is worthwhile, since the HTP chromatographic methods like HTP-GC and HTP-HPLC are appropriate to determine transaminase conversion and enantiomeric excess of the reaction simultaneously, employing chiral stationary phases.

Recent publications document the demand of new fast and simple screening assays and show promising approaches.[68,126–133]

2.1. Determination of Conversion and Enantiomeric Excess: Gas Chromatographic Screening Assay

In this work, chiral GC was used to determine the conversion and enantiomeric excess of different ω-transaminase substrates. Gas chromatographic analysis of the ω-transaminase products offers the possibility of a fast and good separation of the analytes with narrow peaks. By the extraction of the aqueous assay samples with an organic solvent, the analytes are concentrated in the organic phase and separated from proteins in a single step. In the organic phase also the derivatization of the amines can simply be done. GC and especially HPLC are often used in transaminase analytics, but due to the higher effort compared to spectrophotometric assays, measure-

ments are often done at a defined time point and not during the course of the reaction.

Since the equilibrium of the transamination favours the deamination reaction, a single endpoint measurement to determine the amination activity of a ω-transaminase might not be sufficient. As observed during this work, the amination reaction returns to the favoured deamination at a certain point. In consequence it is possible that measurements at defined time points result in low ω-transaminase activities, but in fact the enzyme is as reactive as to reach the reversal point of the reaction. Therefore, the set up of the GC screening assay used in this work was adjusted so as to measure the initial velocity of the (R)-selective ω-transaminases. By measuring the initial velocity, the effect of the back reaction is eliminated. This results in improved comparability of substrates and enzymes.

Despite the higher effort compared to a spectrophotometric assay, comparable results with low deviations were gained. Though, the analysis of minor conversions was difficult due to small product peaks within the baseline noise. This was the case for the measurements with the His-tagged variants of R-FPTA. Here, a pre-test to align the enzyme concentration and evaluable product peaks would have been helpful. Due to time constraints and the high number of samples a pre-test was omitted.

2.2. A fast Screening Assay in Microtiter Plates: D-Amino Acid Oxidase (D-AAO) Assay

The GC screening assay is tedious and time consuming; thus, the D-AAO assay[68] was used for a HTP screening of the generated ω-transaminase variants in microtiter plates. The advantage of this assay is, in contrast to the acetophenone assay, the independence from the ω-transaminase substrates. However, a sufficient activity of the coupled enzymes D-AAO and HRP is required to measure the ω-transaminase activity. Since activity by ApDAAO from cell extracts was insufficient, a commercial D-AAO with higher activity was used. To prevent a limitation of the assay by the ω-transaminases, the concentrations of the coupled enzymes and the colour reagent were adjusted to the transaminase activity. Thereby, a correspondence to the acetophenone assay was given.

Different dilutions of the ω-transaminase were measured with both, acetophenone and D-AAO assay. For the dilutions 1:1, 1:2 and 1:5 the D-AAO assay showed higher activities and for the dilutions 1:10 and 1:100 higher activities were measured with the acetophenone assay. This indicates an influence of the coupled enzymes on the equilibrium of the transaminase reaction. By coupling the D-AAO to the deamination reaction,

the product D-alanine is regenerated to pyruvate, drawing the reaction equilibrium more forward in product direction (Chatelier's principle). This results in a higher activity of the ω-transaminase compared to the acetophenone assay, where pyruvate is consumed and is not available as amino acceptor anymore.

Although the D-AAO assay shows a decreased activity with the 1:100 dilution, the acetophenone assay shows an increased activity with this dilution. The difference between the two assays with the 1:100 dilution is most likely caused by a low signal-to-noise ratio and results in a higher deviation due to the low transaminase activity at this dilution. With the D-AAO assay, it is to assume that the product development is too low for the coupled enzymes to show an adequate colour reaction at low transaminase activities. This could result in undetected ω-transaminase variants with minor activity. Further adjustment of the coupled reactions or use of a more sensitive colour reagent could prevent this.

2.2.1. Considerations on Transaminase Mutagenesis and Screening

During the screening, half of the variants turned out to be wild-types. A longer digestion of the parental DNA after PCR would have reduced this wild-type background (see chapter III, section 4.4.2). Even between variants which were identified as wild-types by sequence analysis, a high variation of the activities occurred in the screening. These variances can be led back to differences during inoculation of the wells. In contrast to shake flask cultures where inoculation and cell growth is controlled by optical density, the wells were directly inoculated from single cell colonies. By picking the colonies from agar plates, the amount of the adherent cells and therefore the amount of the cells for inoculation cannot be controlled. As a consequence of this, the cell densities within the wells are not constant which affects the ω-transaminase activites. A synchronisation of the cell densities within the wells could be possible if the inoculation of the microtiter plates is done in two steps, using a pre-culture. Also an auto-induction medium could be helpful for an even expression of ω-transaminase in microtiter plates. Moreover, devices for monitoring and controlling cell growth in high-throughput cultivation exist, which allow biomass-specific induction in microtiter plates.[134]

However, two ω-transaminase variants with higher activities than their wild-types could be identified in this screening. One possibility to exclude inactive ω-transaminase variants beforehand would be a colony solid phase screening.[127,130,132] This solid phase screening can be done based on the D-AAO assay by co-expressing an (*R*)-selective ω-transaminase and a D-AAO.[127] Weiss *et al.* developed a screening assay with glyoxylate as amino acceptor and glycine oxidase as coupled enzyme which is applicable for

both, (*R*)- and (*S*)-selective ω-transaminases.[130] Although high-throughput screenings are possible with the described assays, chromatographic methods seem to be necessary to analyse the amination activity of ω-transaminases, since only the deamination reaction is covered with these spectrophotometric assays. Since ω-transaminases are a helpful tool for the production of chiral amines, screening the amination reaction instead of the deamination reaction would be more adequate. In this work, the amination activities of ω-transaminase variants chosen from the deamination pre-screening were determined with chiral GC. For this screening, the chosen methods were sufficient but in an ideal screening set-up, low-throughput methods should be reduced to a minimum. A screening assay for the determination of the amination activity therefore could replace the kinetic GC measurements, so GC is only used to determine the enantiomeric excess of the produced amine.

The first method to determine the amination activity was an pH based colourimetric assay with coupled lactate and glucose dehydrogenase.[135] Recently, two one-enzyme ω-transaminase assays where the amino donor products undergo spontaneous polymerization and form coloured precipitates were described.[131,132] The advantages of these two assays are the independence of additional enzymes, the use of inexpensive achiral amino donors and the irreversibility of the product polymerization (which blocks the back reaction). Furthermore, both assays can be used as high-throughput screening as well as solid-phase screening. Otherwise, it is questionable if the amino donors are broadly accepted ω-transaminase substrates. Since the enzyme-coupled assays like the D-AAO assay offer high sensitivities,[132] the costs for the expensive coupling enzymes can be neglected in favour of higher sensitivity for small screenings projects as in this work.

3. Substrate Specificity: Differences between R-TRTA and R-FPTA

Despite the high similarity of the ω-transaminase sequences and structures, differences in their substrate spectra occur. R-TRTA and R-FPTA have a sequence identity of 64 %. Even though, these two (*R*)-selective ω-transaminases vary in their substrate spectra and show different performances. Schätzle *et al.* described strongly related ω-transaminases (72–96 % sequence identity) with different performances and substrate spectra. On the other hand, an outsider enzyme with similarity scores not exceeding 40 % showed as good perfomances as the ω-transaminases with a high relationship.[136]

Besides the biochemical characterization of R-TRTA and R-FPTA and their variants,

the three dimensional structure of R-TRTA was solved to give an insight into the arrangement of the key motif amino acids. At the beginning of the lab work for the crystallization process, no crystal structure of an (*R*)-selective ω-transaminase was published. Still, the structure of R-TRTA is the first and sole (*R*)-selective ω-transaminase with Tyr at position 113.[46,75,76] To compare the binding pockets of R-TRTA and R-FPTA, a structural model of R-FPTA was generated (see Fig. 5.3). Because of its high sequence identity of 77.2 %, the structure of the ω-transaminase from *N. haematococca* was used as a template for the structure modelling of R-FPTA.

3.1. Influence of the Amino Acid at Position 113

Like R-TRTA and R-FPTA the new ω-transaminases identified by Höhne *et al.* had Phe as well as Tyr at position 113, where enzymes with Tyr113 showed lower activities. As explained in chapter IV, section 3.1.1, this position 113 was chosen for mutagenesis because of its arrangement within the active site and hence its probable influence on activity and substrate specificity, respectively. Also Willies *et al.* identified this position for altering the binding pocket of an (*R*)-selective ω-transaminase.[127]

R-TRTA showed a highly increased activity towards the bulky substrate **2c**, whereas the activity of R-FPTA towards this substrate is decreased. For the ω-transaminase from *N. haematococca*, a fourfold decrease of activity against the corresponding amine of this substrate was described. By docking studies, the lower activity could be explained with a sterical hindrance of the substrate in the small binding pocket due to its longer carbon chain.[76] Like R-TRTA, the ω-transaminases from *A. oryzae* and *Hyphomonas neptunium* showed an increased activity for **1c**.[1] When comparing the sequences, especially the substrate binding amino acids, it stands out, that R-TRTA and the ω-transaminase from *H. neptunium* differ at the positions 113 (Tyr instead Phe) and 272 (Ser instead of Thr).

It can only be speculated how these amino acids influence activity. Tyr113 with its hydroxy group could support the positioning of the substrate to a larger extend, because of its ability to form hydrogen bonds. Ser instead of Thr at positions 272 enlarges the space for the long side chain of the substrate. This additional space could be necessary for the substrate to get into the binding pocket or to have enough freedom of movement for a fast transamination reaction. Since the ω-transaminase from *A. oryzae* does not show these differences, also amino acids which are not directly involved in substrate binding seem to have an effect on the substrate binding or orientation (see chapter IV, Fig. 4.35).

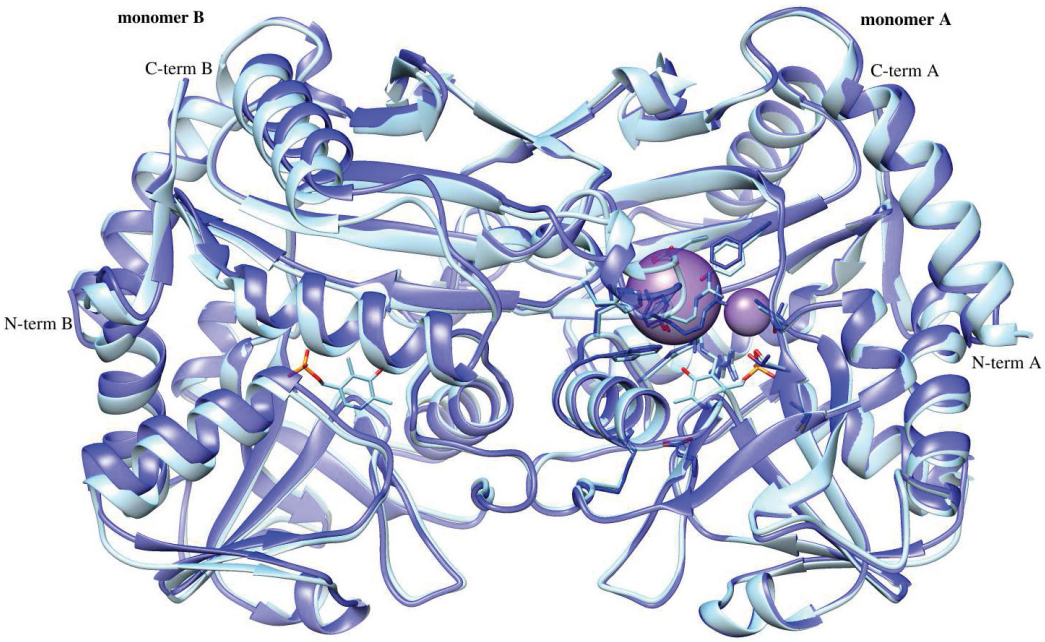

(a)

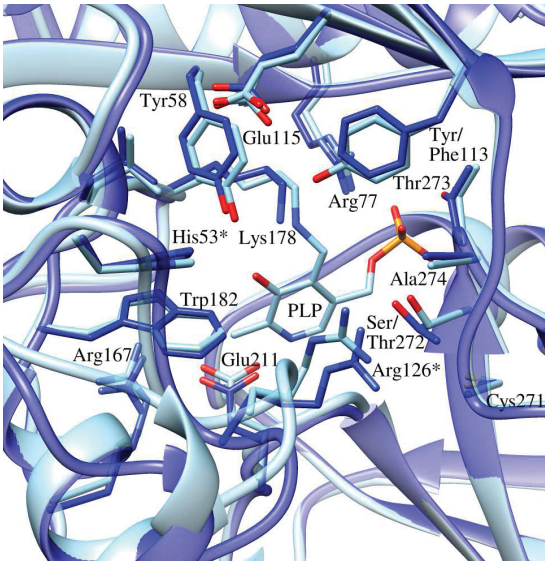

(b)

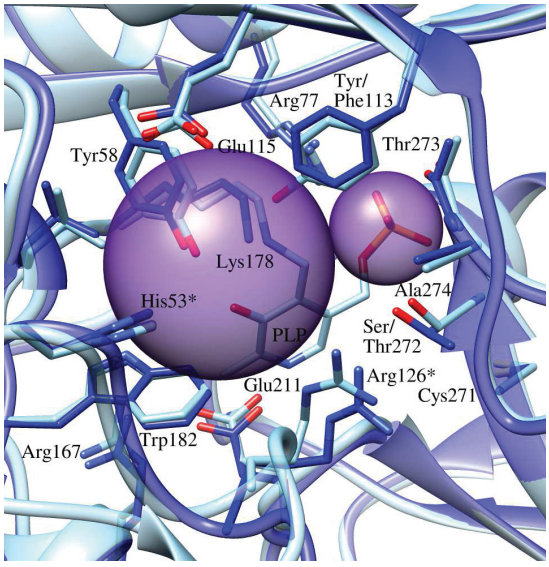

(c)

Fig. 5.3. *Overlay of the structures of R-TRTA (light blue) and R-FPTA (blue). The structure of the ω-transaminase from Nectria haematococca served as template for modelling the structure of R-FPTA.* ***(a)*** *Complete structure.* ***(b)*** *Active site of the ω-transaminases with the cofactor PLP bound to Lys178 of R-TRTA.* ***(c)*** *The large and the small binding pockets within the active sites of R-TRTA and R-FPTA are highlighted as violet spheres.*

4. Mutagenesis of the ω-Transaminases R-TRTA and R-FPTA

The mutagenesis of R-TRTA and R-FPTA lead to an improvement of these (*R*)-selective ω-transaminases. The improvement of R-TRTA was achieved by a point mutation at position 113, whereas the double mutant R-FPTA_C-His F113M E115K showed higher activities. The study of less active variants gave an additional insight into the role of the amino acid at position 113.

The specific activity of purified R-TRTA_C-His was about 0.6 $U/mg_{protein}$ (see chapter IV, section 4.1.2). Comparable activities show the (*R*)-selective ω-transaminases from *Gamma proteobacterium*, *Penicillium chrysogenum* and *Aspergillus oryzae* with activities between 0.6–1.4 $U/mg_{protein}$.[1] Because of different assay conditions in publications and this work, an exact comparison cannot be made and therefore only tendencies are compared. In this work, the acetophenone assay was typically done with 5 mM *rac*-**1a** and 5 mM **2i** as amino acceptor. This results in an effective concentration of 2.5 mM *R*-**1a**. As an excess of amino acceptor could inhibit the transaminase reaction, differences of activities measured under conditions with equal amounts of amino donor enantiomer and amino acceptor are likely.

The characteriziation of the ω-transaminases R-TRTA, R-FPTA and their variants was done with lyophilisates from crude extracts. Since purified enzyme is often too expensive for bioprocesses, enzymes are applied as less purified lyophilisates.[137] For this reason, it is also important to analyse the enzyme within this matrix.

Based on the specific activity of R-TRTA further conclusion about the activity of its variants and the second ω-transaminase R-FPTA can be drawn. The replacement of Tyr at position 113 by Phe in R-TRTA led to a variant with nearly two times higher deamination activity (acetophenone assay, see Tab. 5.1) than the wild-type. Relating the activity difference to the specific activity of purified R-TRTA_C-His (0.51±0.01 $U/mg_{R\text{-}TRTA\_C\text{-}His}$, see chapter IV, section 4.1.2), activities of 1 $U/mg_{protein}$ can be reached. In the amination reaction even an activity ten times higher than the wild-type was determined. In this case, the assumption that ω-transaminases with Phe at position 113 are more active than ω-transaminases with Tyr at this position, was confirmed. The point mutation therefore made R-TRTA as active as the ω-transaminases from *P. chrysogenum* or *A. oryzae*.

The second investigated (*R*)-selective ω-transaminase R-FPTA was ten times more active with **2a** than R-TRTA with a significant lower concentration in the lyophilisate (see chapter IV,Fig. 4.19). This indicates a much higher activity of R-FPTA than R-TRTA and an activity of about 20 $U/mg_{protein}$ seems possible.

The activity of the double mutant R-FPTA_C-His F113M E115K was 4.5 times higher with the standard substrate **1a** than with the His-tagged wild-type enzyme. A further increase in activity of this variant without His-tag is likely.

The substrate spectra of the variants of R-TRTA and R-FPTA show significant differences with mutations at the position 113 (and 115). The direct involvement of Tyr113 and Glu115 in the substrate binding of R-TRTA is shown in Fig. 4.34. The overlay of the structures (the structural model, respectively) of R-TRTA and R-FPTA indicates differences at the active sites (see Fig. 5.3). The binding pockets (highlighted with violet spheres) within the active site in Fig. 5.3 (c) show the smaller space requirement of Phe113 and how close Glu115 is positioned to the large binding pocket.

Tab. 5.1. *Deamination activites of the ω-transaminases R-TRTA and R-FPTA from lyophilisates. The activities were determined with the acetophenone assay.*

Enzyme	**Activity** [$\mathbf{mU/mg_{lyophilisate}}$]	**spec. Activity** [$\mathbf{mU/mg_{protein}}$]
R-TRTA	75.66 ±0.36	236.44 ±1.14
R-TRTA_C-His	69.26 ±0.86	180.36 ±2.24
R-TRTA_C-His Y113F	138.49 ±0.04	332.91 ±0.10
R-TRTA_C-His Y113R	28.11 ±0.48	68.91 ±1.18
R-FPTA	154.68 ±0.67	471.58 ±2.05
R-FPTA_C-His	66.14 ±0.53	155.98 ±1.26
R-FPTA_C-His F113M E115K	134.02 ±0.25	398.86 ±0.76
R-FPTA_C-His F113Y	30.29 ±0.73	86.06 ±2.08

Altering Tyr113 to Phe113 in R-TRTA shifted the substrate acceptance to a higher conversion of the bulky substrates **2f** and **2d**. With R-TRTA C-His Y113R, the conversion of the bulky substrates in relation to **2a** is even higher than for R-TRTA C-His Y113F. The acceptance of larger substrates indicates an enlargement of the small binding pocket by the mutations.

Taken the overall activity into account, which was increased for R-TRTA C-His Y113F and decreased for R-TRTA C-His Y113R, different mechanisms are implied. As shown in Fig. 5.3, the small binding pocket is enlarged by the substitution of Tyr113 with the smaller Phe. Compared to Phe, the Arg residue is larger and hence the better conversion of bulkier substrates compared to **2a** and the decreased overall activity could be explained by the high flexibility of the long Arg side chain. Its possibility to move, either could give more space for large substrates, but, on the other hand, could block the entrance to the binding pocket for all substrates and therefore decrease the overall

activity. The high flexibility of the Arg side chain seems to offer a good adaption to the substrate. This assumption is supported by a decreased Michaelis-Menten constant K_m of R-TRTA_C-His Y113R, which indicates a higher affinity for the substrate (see chapter IV, section 3.2.3).

A unique feature of R-TRTA is the strongly increased activity with **2c** and **1c**, respectively. The (*R*)-selective ω-transaminases from *H. neptunium* and *A. oryzae* showed increased activities for this reaction pair,[1,136] but for **2c** R-TRTA is 74 times more active. Increased activities were also measured for the substrates **2f**–**2h**. Probably, these molecules, together with **2c**, adopt a similar conformation. Although the activity of R-TRTA_C-His Y113F was generally increased compared to the wild-type enzyme, the activity with **2c** and **2f**–**2h** was increased less significantly. The hydroxyl group of Tyr seems to be important for these substrates. Since the increased activity of R-TRTA_C-His Y113R with the mentioned substrates is similar to the wild-type spectrum, the possibility to build hydrogen bonds at position 113 could be more important than the overall size of the amino acid.

As sole substrate, **2f** was aminated to (*R*)-**1f** and (*S*)-**1f** by R-TRTA and R-FPTA. Other amines were exclusively produced as (*R*)-enantiomer. The wild-type R-TRTA aminated **2f** with an enantiomeric excess of 65 % *ee*. R-TRTA C-His Y113F and R-TRTA C-His Y113R catalysed this amination with 94 % *ee* and 91 % *ee*, respectively. The activity of R-FPTA with **2f** was only 20 % of the activity with the standard substrate with **2a** with an enantioselectivity of 84 % *ee*. As a publication of Pressnitz *et al.* shows, 2-tetralone **2f** is indeed an exceptional substrate. Even though ω-transaminases are highly enantioselective,[18] the amination of **2f** was performed only by one (*S*)-selective ω-transaminase with more than 99 % *ee*. Of four tested (*R*)-selective ω-transaminases, only the ω-transaminase from *Arthrobacter* sp. and its variant did the amination with 54 % *ee* and 76 % *ee*, respectively. The ω-transaminases from *A. terreus* and *H. neptunium* did no amination of **2f** at all.[138]

In contrast to R-TRTA, the influences of the mutations on substrate binding are less clear in R-FPTA. Even though the space within the active site is more restricted by changing Phe113 to Tyr, **2f** and **2g** were better converted than **2a** and **2c**. The kinetic parameters of R-FPTA_C-His F113Y also indicate a decreased affinity for **2a**. As diametral observations were made with R-TRTA_C-His Y113F, the hydroxyl group of Tyr has a significant effect on the ω-transaminase activity and acceptance of large substrates.

The mutation at position 113 in the double mutant R-FPTA_C-His F113M E115K lead to an enlargement of the small binding pocket. Besides the deamination activity

towards **1a**, the amination activity with the large substrates **2c**, **2f** and **2h** in relation to **2a** was increased. **2g** was not converted at all by the double mutant. The amino donor **1k** and the substrate are most likely too small to serve as a substrate for this R-FPTA variant. The specificity of the double mutant F113M E115K could have been lost for small substrates because of a too large binding pocket. A good reason for this argument is the high deamination activity compared to rather low amination activities with the small amino donor **1k**. Moreover, for the optimization of the reported (*R*)-selective ω-transaminase from *Arthrobacter sp.* for bulky substrates, the amino acid at position 113 was also exchanged against Met.[29] With this amino acid at position 113, the sequence motif for (*R*)-selective ω-transaminases[1] is complemented or even disproved.

The mutations in the R-FPTA variants apparently seem to have an effect on substrates with different chain length besides their overall size. Therefore, the orientation of the keto function seems to be affected by the mutations. In R-FPTA C-His F113Y the restriction of the small pocket by the larger and polar Tyr might force the keto funtion of the short chain substrates in a favoured position for reaction. With a larger active site, as in R-FPTA_C-His F113M E115K, the specificity of the enzyme could be lost for small substrates like 2-pentanone **2g**. The high K_m value of the the double mutant for **1a** of 1.66±0.48 mM (0.28±0.05 mM for wild-type R-FPTA) points out the lower affinity for the transaminase substrate. Probably also the position of the substrate is influenced by the increased size at position 115 through the replacement of Glu by Lys. Additionally, the change of a hydrogen bond acceptor to a hydrogen bond donor is likely to change the interaction between the amino acids of the binding site and the substrate. Even though R-FPTA_C-His F113M E115K showed minor activity in the acetophenone assay, it was more active than the His-tagged wild-type enzyme.

The activity of both, R-TRTA and R-FPTA was increased by mutagenesis. As already mentioned, identical conditions of activity assays are necessary for the comparability of results. This can be clearly seen from the determination of the ω-transaminases' pH optima. By means of the standard activity assay at pH 8, the activities of R-TRTA_C-His Y113F and R-FPTA_C-His F113M E115K were increased by the mutations. But the determination of the pH optima revealed a change of the pH optima to pH 8, indeed. Therefore, the pH optimum of the ω-transaminases was optimized rather than the activity.

4.1. Shifting the pH Optima by Point Mutations

Besides the substrate spectrum, also the pH optima of the variants were shifted compared to the wild-type enzymes. By changing the amino acids at the positions 113 and 115,

the network of hydrogen bonds within the active site was changed. Phe, in contrast to Tyr and Arg, cannot form hydrogen bonds. The replacement of Glu115 by Lys115 even changed an amino acid with an acidic side chain to an amino acid with a basic side chain. Even though the pH optima of the ω-transaminases were shifted by the mutations, they still lie within the normal range of (R)-selective ω-transaminases. The (R)-selective ω-transaminases described by Schätzle *et al*. have their optima between pH 7.5 and 8.[136]

4.2. Conclusion

Even though mild reaction conditions, such as moderate temperatures, are an advantage of biocatalytic processes, many processes demand solvent and temperature stable catalysts. For example organic solvents and an increased temperature are necessary to dissolve organic enzyme substrates in an aqueous reaction mixture.[29] Despite its lower activity, R-TRTA has a higher temperature stability than R-FPTA (see chapter IV, section 3.2.2). For the amination process with R-FPTA, the temperature had to be decreased so as to find an equilibrium between high conversion and enzyme stability (see chapter IV, section 3.2.4). With higher thermal stability, R-TRTA therefore seems to be more sustainable for a biocatalytic process than R-FPTA. Eventually, it has to be determined whether a more active or a more stable enzyme is a more economic catalyst for a certain process.

Besides finding new enzymes and optimizing them, also their production in the right formulation and the optimization of the reaction system are important.[136] The concentration of R-FPTA in the lyophilisates is lower than the concentration of R-TRTA (see chapter IV, Fig. 4.19), even though the R-FPTA lyophilisate has higher ω-transaminase activity. Furthermore, the His-tag led to lower expression of the enzyme. With an optimized formulation, which also means optimized expression and no His-tag, R-FPTA is an efficient biocatalyst. Additives to enhance the enzyme stability could also be discussed.

Altogether, the new (R)-selective ω-transaminases R-TRTA and R-FPTA are potent and tunable biocatalysts. Where R-FPTA is more active, R-TRTA is more stable. The mutagenesis of both ω-transaminases on a small scale showed that the pH optima and the substrate spectrum of these enzymes can be influenced by little intervention in their binding pockets. Since ω-transaminases are affected by substrate and product inhibition, changing the substrate spectrum could reduce this inhibition.[110] Therefore, they seem suitable for a number of different reactions and my thus contribute to fulfill the increasing demand of amination catalysts.

VI. Bibliography

[1] M. Höhne, S. Schätzle, H. Jochens, K. Robins, U. T. Bornscheuer, *Nat. Chem. Biol.* **2010**, *6*, 807–813.

[2] E. B. Banning, *Near East. Archaeol.* **1998**, *61*, 188–237.

[3] P. E. McGovern, J. Zhang, J. Tang, Z. Zhang, G. R. Hall, R. A. Moreau, A. Nuñez, E. D. Butrym, M. P. Richards, C.-S. Wang, G. Cheng, Z. Zhao, C. Wang, *Proc. Natl. Acad. Sci.* **2004**, *101*, 17593–17598.

[4] F. G. Meussdoerffer in *Handb. Brew.*, Wiley-VCH Verlag GmbH & Co. KGaA, Weinheim, Germany, **2009**, pp. 1–42.

[5] J. R. Porter, *Bacteriol. Rev.* **1976**, *40*, 260–269.

[6] L. Pasteur, *Comtes rendus des séances l'Academie des Sci.* **1857**, *45*, 913–916.

[7] E. Buchner, R. Rapp, *Ber. Dtsch. Chem. Ges.* **1897**, *30*, 2668–2678.

[8] K. Buchholz, J. Collins, *Appl. Microbiol. Biotechnol.* **2013**, *97*, 3747–3762.

[9] F. Crick, J. Watson, *Nature* **1953**, *171*, 737–738.

[10] R. E. Franklin, R. G. Gosling, *Nature* **1953**, *171*, 740–741.

[11] M. H. F. Wilkins, A. R. Stokes, H. R. Wilson, *Nature* **1953**, *171*, 738–740.

[12] G. Gwehenberger, M. Narodoslawsky, *Process Saf. Environ. Prot.* **2008**, *86*, 321–327.

[13] J. M. Woodley, M. Breuer, D. Mink, *Chem. Eng. Res. Des.* **2013**, *91*, 2029–2036.

[14] S. M. Thomas, R. DiCosimo, V. Nagarajan, *Trends Biotechnol.* **2002**, *20*, 238–242.

[15] G. A. Strohmeier, H. Pichler, O. May, M. Gruber-Khadjawi, *Chem. Rev.* **2011**, *111*, 4141–4164.

[16] M. T. Reetz, *Angew. Chemie Int. Ed.* **2013**, *52*, 2658–2666.

[17] A. Schmid, J. S. Dordick, B. Hauer, A. Kiener, M. Wubbolts, B. Witholt, *Nature* **2001**, *409*, 258–268.

[18] S. Mathew, H. Yun, *ACS Catal.* **2012**, *2*, 993–1001.

[19] F. H. Arnold, *Chemical Engineering Science* **1996**, *51*, 5091–5102.

[20] T. S. Wong, K. L. Tee, B. Hauer, U. Schwaneberg, *Nucleic Acids Research* **2004**, *32*, e26–e26.

[21] W. P. Stemmer *et al.*, *Nature* **1994**, *370*, 389–391.

[22] U. T. Bornscheuer, M. Pohl, *Curr. Opin. Chem. Biol.* **2001**, *5*, 137–143.

[23] K. Steiner, H. Schwab, *Comput. Struct. Biotechnol. J.* **2012**, *2*, 1–12.

[24] G. Yang, Y. Ding, *Bioorg. Med. Chem.* **2014**, *22*, 5604–5612.

[25] D. J. Pollard, J. M. Woodley, *Trends Biotechnol.* **2007**, *25*, 66–73.

[26] E. J. Ariens, *Eur. J. Clin. Pharmacol.* **1984**, *26*, 663–668.

[27] H. Caner, E. Groner, L. Levy, I. Agranat, *Drug Discov. Today* **2004**, *9*, 105–110.

[28] S. S. Dewan, *Global Markets for Chiral Technology – Focus on the U.S., BCC Research LLC*, **2012**.

[29] C. K. Savile, J. M. Janey, E. C. Mundorff, J. C. Moore, S. Tam, W. R. Jarvis, J. C. Colbeck, A. Krebber, F. J. Fleitz, J. Brands, P. N. Devine, G. W. Huisman, G. J. Hughes, *Science* **2010**, *329*, 305–309.

[30] Codexis Press Release, *FDA Approves Use of Codexis Enzymes in Merck Manufacturing Process*, **2012**.

[31] Codexis Press Release, *Codexis Signs Multi-year Extension of Contract with Merck to Supply Enzyme Used in Manufacture of Sitagliptin*, **2015**.

[32] A. J. L. Cooper, A. Meister, *Biochimie* **1989**, *71*, 387–404.

[33] D. I. Stirling, A. L. Zeitlin, G. W. Matcham, *Enantiomeric enrichment and stereoselective synthesis of chiral amines. U.S. Patent No. 4.950.606*, **1990**.

[34] D. Koszelewski, K. Tauber, K. Faber, W. Kroutil, *Trends Biotechnol.* **2010**, *28*, 324–332.

[35] M. Fuchs, J. E. Farnberger, W. Kroutil, *Eur. J. Org. Chem.* **2015**, *2015*, 6965–6982.

[36] M. Höhne, U. T. T. Bornscheuer, *ChemCatChem* **2009**, *1*, 42–51.

[37] D. Ghislieri, N. J. Turner, *Top. Catal.* **2014**, *57*, 284–300.

[38] D. Zhu, L. Hua, *Biotechnol. J.* **2009**, *4*, 1420–1431.

[39] J. E. Clifton, I. Collins, P. Hallet, D. Hartley, L. H. C. Lunts, P. D. Wicks, *Am. Chem. Soc.* **1982**, *886*, 670–679.

[40] D. Koszelewski, M. Göritzer, D. Clay, B. Seisser, W. Kroutil, M. Göritzer, D. Clay, B. Seisser, W. Kroutil, *ChemCatChem* **2010**, *2*, 73–77.

[41] S. Lecht, S. Haroutiunian, A. Hoffman, P. Lazarovici, *Ther. Clin. Risk Manag.* **2007**, *3*, 467–474.

[42] K. T. Reddy, K. S. Kumar, G. Omprakash, P. K. Dubey, *Der Pharma Chem.* **2011**, *3*, 110–115.

[43] G. Ma, Z. Xu, P. Zhang, J. Liu, X. Hao, J. Ouyang, P. Liang, S. You, X. Jia, *Org. Process Res. Dev.* **2014**, *18*, 1169–1174.

[44] R. A. Jensen, D. H. Calhoun, *Crit. Rev. Microbiol.* **1981**, *8*, 229–66.

[45] G. Schneider, H. Käck, Y. Lindqvist, *Structure* **2000**, *8*, R1–6.

[46] C. Sayer, R. J. Martinez-Torres, N. Richter, M. N. Isupov, H. C. Hailes, J. A. Littlechild, J. M. Ward, *FEBS J.* **2014**, *281*, 2240–2253.

[47] E.-S. Park, M. Kim, J.-S. Shin, *Appl. Microbiol. Biotechnol.* **2012**, *93*, 2425–2435.

[48] K. E. Cassimjee, B. Manta, F. Himo, *J. Phys. Chem. B* **1999**, *103*, 1193–1202.

[49] P. K. Mehta, T. I. Hale, P. Christen, *Eur. J. Biochem.* **1993**, *214*, 549–561.

[50] J. N. Jansonius, *Curr. Opin. Struct. Biol.* **1998**, *8*, 759–769.

[51] R. D. Finn, P. Coggill, R. Y. Eberhardt, S. R. Eddy, J. Mistry, A. L. Mitchell, S. C. Potter, M. Punta, M. Qureshi, A. Sangrador-Vegas, G. A. Salazar, J. Tate, A. Bateman, *Nucleic Acids Res.* **2016**, *44*, D279–D285.

[52] B.-Y. Hwang, B.-K. K. Cho, H. Yun, K. Koteshwar, B.-G. G. Kim, *J. Mol. Catal. B: Enzym.* **2005**, *37*, 47–55.

[53] M. S. Malik, E.-S. Park, J.-S. Shin, *Appl. Microbiol. Biotechnol.* **2012**, 1163–1171.

[54] M. Höhne, U. T. Bornscheuer in *Enzym. Catal. Org. Synth.* (Eds.: K. Drauz, H. Gröger, O. May), Wiley-VCH Verlag GmbH & Co. KGaA, Weinheim, Germany, 3rd ed., **2012**, Chapter 19, pp. 779–818.

[55] J.-S. Shin, B.-G. Kim, *J. Org. Chem.* **2002**, *67*, 2848–2853.

[56] J.-S. Shin, H. Yun, J.-W. Jang, I. Park, B.-G. Kim, *Appl. Microbiol. Biotechnol.* **2003**, *61*, 463–471.

[57] J.-S. Shin, B.-G. Kim, *Biotechnol. Bioeng.* **1997**, *55*, 348–358.

[58] P. Tufvesson, J. Lima-Ramos, J. S. Jensen, N. Al-Haque, W. Neto, J. M. Woodley, *Biotechnol. Bioeng.* **2011**, *108*, 1479–1493.

[59] M. Höhne, S. Kühl, K. Robins, U. T. Bornscheuer, *ChemBioChem* **2008**, *9*, 363–365.

[60] D. Koszelewski, I. Lavandera, D. Clay, D. Rozzell, W. Kroutil, *Adv. Synth. Catal.* **2008**, *350*, 2761–2766.

[61] M. D. Truppo, J. D. Rozzell, N. J. Turner, *Org. Process Res. Dev.* **2010**, *14*, 234–237.

[62] M. D. Truppo, J. D. Rozzell, J. C. Moore, N. J. Turner, *Org. Biomol. Chem.* **2009**, *7*, 395–398.

[63] P. Tufvesson, J. S. Jensen, W. Kroutil, J. M. Woodley, *Biotechnol. Bioeng.* **2012**, *109*, 2159–2162.

[64] S. Mathew, G. Shin, M. Shon, H. Yun, *Biotechnol. Bioprocess Eng.* **2013**, *18*, 1–7.

[65] B.-Y. Hwang, B.-G. Kim, *Enzyme Microb. Technol.* **2004**, *34*, 429–436.

[66] S. Schätzle, M. Höhne, K. Robins, U. T. Bornscheuer, *Anal. Chem.* **2010**, *82*, 2082–2086.

[67] S. Schätzle, M. Höhne, E. Redestad, K. Robins, U. T. Bornscheuer, *Anal. Chem.* **2009**, *81*, 8244–8248.

[68] J. Hopwood, M. D. Truppo, N. J. Turner, R. C. Lloyd, *Chem. Commun.* **2011**, *47*, 773–775.

[69] A. Iwasaki, Y. Yamada, Y. Ikenaka, J. Hasegawa, *Biotechnol. Lett.* **2003**, *25*, 1843–1846.

[70] A. Iwasaki, Y. Yamada, N. Kizaki, Y. Ikenaka, J. Hasegawa, *Appl. Microbiol. Biotechnol.* **2006**, *69*, 499–505.

[71] D. Clay, D. Koszelewski, B. Grischek, J. Gross, I. Lavandera, W. Kroutil, *Tetrahedron: Asymmetry* **2010**, *21*, 2005–2009.

[72] J.-S. Shin, B.-G. Kim, *Biotechnol. Bioeng.* **2002**, *77*, 832–837.

[73] M. S. Humble, K. E. Cassimjee, M. Håkansson, Y. R. Kimbung, B. Walse, V. Abedi, H.-J. Federsel, P. Berglund, D. T. Logan, *FEBS J.* **2012**, *279*, 779–792.

[74] C. Rausch, A. Lerchner, A. Schiefner, A. Skerra, *Proteins Struct. Funct. Bioinforma.* **2013**, *81*, 774–787.

[75] A. Łyskowski, C. Gruber, G. Steinkellner, M. Schürmann, H. Schwab, K. Gruber, K. Steiner, *PLoS One* **2014**, *9*, e87350.

[76] M. Thomsen, L. Skalden, G. J. Palm, M. Höhne, U. T. Bornscheuer, W. Hinrichs, *Acta Crystallogr. Sect. D: Biol. Crystallogr.* **2014**, *70*, 1086–1093.

[77] L.-J. Guan, J. Ohtsuka, M. Okai, T. Miyakawa, T. Mase, Y. Zhi, F. Hou, N. Ito, A. Iwasaki, Y. Yasohara, M. Tanokura, *Sci. Rep.* **2015**, *5:10573*, 1–11.

[78] J. Bruinvels, *Br. J. Pharmacol.* **1971**, *42*, 281–286.

[79] G. Bertani, *J. Bacteriol.* **1951**, *62*, 293–300.

[80] G. Bertani, *J. Bacteriol.* **2004**, *186*, 595–600.

[81] R. W. Davis, D. Botstein, J. R. Roth, *Advanced bacterial genetics: A manual for genetic engineering*, Cold Spring Harbor Laboratory Press, New York, **1980**.

[82] L. G. Davis, M. D. Dibner, J. F. Battey, *Basic Methods in Molecular Biology*, Elsevier Science Publishing Co., Inc., New York, **1986**.

[83] D. Hanahan, *J. Mol. Biol.* **1983**, *166*, 557–580.

[84] F. W. Studier, B. A. Moffatt, *J. Mol. Biol.* **1986**, *189*, 113–130.

[85] J. Sambrook, E. F. Fritsch, T. Maniatis, *Molecular Cloning: A Laboratory Manual*, Cold Spring Harbor Laboratory Press, New York, 2nd ed., **1989**.

[86] R. K. Saiki, D. H. Gelfand, S. Stoffel, S. J. Scharf, R. Higuchi, G. T. Horn, K. B. Mullis, H. a. Erlich, *Science* **1988**, *239*, 487–491.

[87] J. Braman, C. Papworth, A. Greener, *Methods Mol. Biol.* **1996**, *57*, 31–44.

[88] F. Sanger, S. Nicklen, a. R. Coulson, *PNAS* **1977**, *74*, 5463–5467.

[89] M. M. Bradford, *Anal. Biochem.* **1976**, *72*, 248–254.

[90] U. K. Laemmli, *Nature* **1970**, *227*, 680–685.

[91] A. V. Hill, *Biochemical Journal* **1913**, *7*, 471.

[92] G. A. F. Seber, C. J. Wild, *Nonlinear Regression*, John Wiley and Sons, New York, **1989**.

[93] L. Michaelis, M. L. Menten, *Biochem. Z.* **1913**, *49*, 333–369.

[94] A. Claiborne, I. Fridovich, *Am. Chem. Soc.* **1979**, *18*, 2324–2329.

[95] T. Hall, *Nucleic Acids Symp. Ser.* **1999**, *41*, 95–98.

[96] E. F. Pettersen, T. D. Goddard, C. C. Huang, G. S. Couch, D. M. Greenblatt, E. C. Meng, T. E. Ferrin, *Journal of Computational Chemistry* **2004**, *25*, 1605–1612.

[97] P. Wittung-Stafshede, *Acc. Chem. Res.* **2002**, *35*, 201–208.

[98] M. Kuzu, PhD thesis, Heinrich-Heine-Universität Düsseldorf, **2005**.

[99] J. Jiang, X. Chen, D. Zhang, Q. Wu, D. Zhu, *Appl. Microbiol. Biotechnol.* **2015**, *99*, 2613–2621.

[100] R. Singh, F. Spyrakis, P. Cozzini, A. Paiardini, S. Pascarella, A. Mozzarelli, *J. Enzyme Inhib. Med. Chem.* **2013**, *28*, 183–194.

[101] *Internal communication, evocatal GmbH*, **2014**.

[102] S. Sahdev, S. K. Khattar, K. S. Saini, *Mol. Cell. Biochem.* **2008**, *307*, 249–264.

[103] H. P. Sørensen, K. K. Mortensen, *J. Biotechnol.* **2005**, *115*, 113–128.

[104] J. Jiang, X. Chen, J. Feng, Q. Wu, D. Zhu, *J. Mol. Catal. B: Enzym.* **2014**, *100*, 32–39.

[105] F. Baneyx, M. Mujacic, *Nat. Biotechnol.* **2004**, *22*, 1399–1408.

[106] K. Terpe, *Appl. Microbiol. Biotechnol.* **2006**, *72*, 211–222.

[107] E.-S. Park, J. Y. Dong, J.-S. Shin, *Appl. Microbiol. Biotechnol.* **2014**, *98*, 651–660.

[108] A. Iwasaki, K. Matsumoto, J. Hasegawa, *Appl. Microbiol.* **2012**, *168*, 1563–1573.

[109] M. Svedendahl, C. Branneby, L. Lindberg, P. Berglund, *ChemCatChem* **2010**, *2*, 976–980.

[110] H. Yun, B.-Y. Hwang, J.-H. Lee, B.-G. Kim, *Appl. Environ. Microbiol.* **2005**, *71*, 4220–4224.

[111] D. Backhouse, L. W. Burgess, *Australas. Plant Pathol.* **2002**, *31*, 321–327.

[112] V. Seidl, C. Seibel, C. P. Kubicek, M. Schmoll, *Proc. Natl. Acad. Sci. USA* **2009**, *106*, 13909–13914.

[113] Australian Bureau of Meteorology and CSIRO, *Climate Change in the Pacific: Scientific Assessment and New Research Volume 2: Country Reports*, **2011**.

[114] P. Carini, L. Steindler, S. Beszteri, S. J. Giovannoni, *ISME J.* **2012**, *7*, 592–602.

[115] A. A. Tokmakov, A. Kurotani, T. Takagi, M. Toyama, M. Shirouzu, Y. Fukami, S. Yokoyama, *J. Biol. Chem.* **2012**, *287*, 27106–27116.

[116] D. Shental-Bechor, Y. Levy, *Curr. Opin. Struct. Biol.* **2009**, *19*, 524–533.

[117] P. Alessandra, P. Cinzia, G. Paola, F. Vincenza, G. Sannia, *Bioeng. Bugs.* **2010**, *1*, 252–262.

[118] A. Dereeper, S. Audic, J.-M. Claverie, G. Blanc, *BMC Evol. Biol.* **2010**, *10*, 1–8.

[119] A. Dereeper, V. Guignon, G. Blanc, S. Audic, S. Buffet, F. Chevenet, J.-F. Dufayard, S. Guindon, V. Lefort, M. Lescot, J.-M. Claverie, O. Gascuel, *Nucleic Acids Res.* **2008**, *36*, W465–W469.

[120] R. C. Edgar, *Nucleic Acids Res.* **2004**, *32*, 1792–1797.

[121] J. Castresana, *Mol. Biol. Evol.* **2000**, *17*, 540–552.

[122] S. Guindon, O. Gascuel, *Syst. Biol.* **2003**, *52*, 696–704.

[123] M. Anisimova, O. Gascuel, *Syst. Biol.* **2006**, *55*, 539–552.

[124] F. Chevenet, C. Brun, A.-L. Bañuls, B. Jacq, R. Christen, *BMC Bioinformatics* **2006**, *7*, 1–9.

[125] A. Petříčková, A. B. Veselá, O. Kaplan, D. Kubáč, B. Uhnáková, A. Malandra, J. Felsberg, A. Rinágelová, P. Weyrauch, V. Křen, K. Bezouška, L. Martínková, *Appl. Microbiol. Biotechnol.* **2012**, *93*, 1553–1561.

[126] J. E. B. Barber, A. M. Damry, G. F. Calderini, C. J. W. Walton, R. A. Chica, *Anal. Biochem.* **2014**, *463*, 23–30.

[127] S. C. Willies, J. L. Galman, I. Slabu, N. J. Turner, *Philos. Trans. R. Soc. London Ser. A* **2016**, *374*, 1–6.

[128] T. Sehl, R. C. Simon, H. C. Hailes, J. M. Ward, U. Schell, M. Pohl, D. Rother, *J. Biotechnol.* **2012**, *159*, 188–194.

[129] K. Weinhandl, M. Winkler, A. Glieder, A. Camattari, *Tetrahedron* **2012**, *68*, 7586–7590.

[130] M. S. Weiß, I. V. Pavlidis, C. Vickers, M. Höhne, U. T. Bornscheuer, *Anal. Chem.* **2014**, *86*, 11847–11853.

[131] A. P. Green, N. J. Turner, E. O'Reilly, *Angew. Chem. Int. Ed.* **2014**, *53*, 10890–10893.

[132] D. Baud, N. Ladkau, T. S. Moody, J. M. Ward, H. C. Hailes, *Chem. Commun.* **2015**, *51*, 17225–17228.

[133] T. Scheidt, H. Land, M. Anderson, Y. Chen, P. Berglund, D. Yi, W. D. Fessner, *Adv. Synth. Catal.* **2015**, *357*, 1721–1731.

[134] R. Huber, D. Ritter, T. Hering, A.-K. Hillmer, F. Kensy, C. Müller, L. Wang, J. Büchs, *Microb. Cell Fact.* **2009**, *8*, 1–15.

[135] M. D. Truppo, N. J. Turner, *Org. Biomol. Chem.* **2010**, *8*, 1280–1283.

[136] S. Schätzle, F. Steffen-Munsberg, A. Thontowi, M. Höhne, K. Robins, U. T. Bornscheuer, *Adv. Synth. Catal.* **2011**, *353*, 2439–2445.

[137] H. Chmiel, *Bioprozesstechnik*, Spektrum Akademischer Verlag, Heidelberg, **2011**.

[138] D. Pressnitz, C. S. Fuchs, J. H. Sattler, T. Knaus, P. Macheroux, F. G. Mutti, W. Kroutil, *ACS Catal.* **2013**, *3*, 555–559.

A. Appendix

1. Plasmid Maps

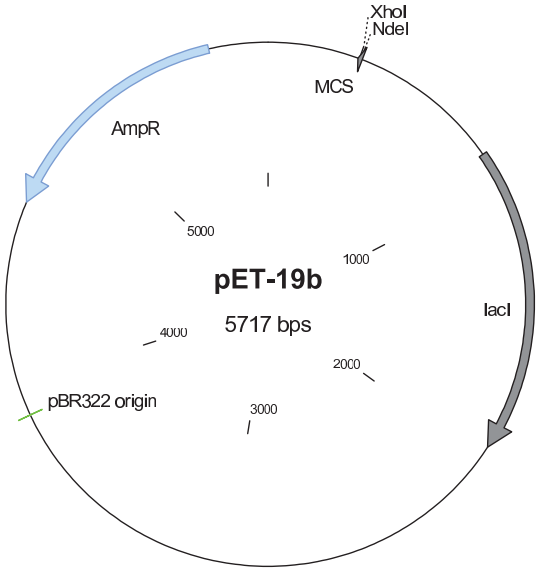

Fig. A.1. *Map of expression vector pET-19b.*

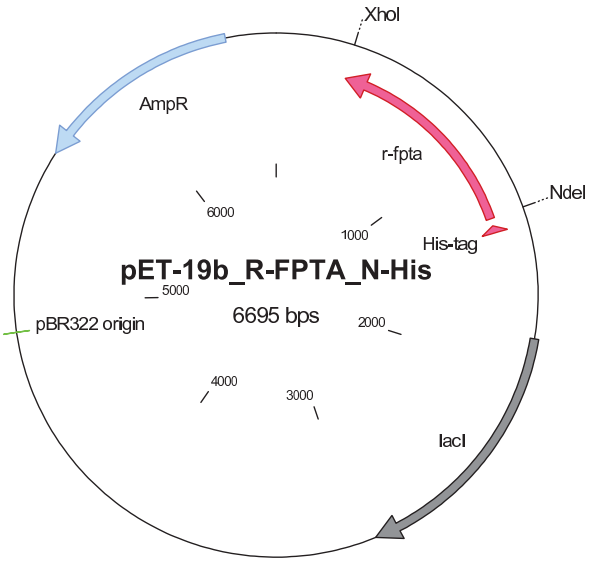

Fig. A.2. *Map of plasmid pET-19b_R-FPTA_N-His with* r-fpta *gene and N-terminal His-tag.*

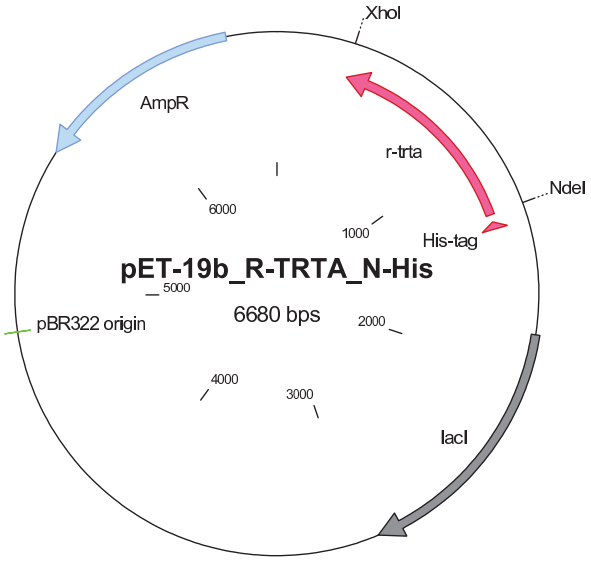

Fig. A.3. *Map of plasmid pET-19b_R-TRTA_N-His with* r-trta *gene and N-terminal His-tag.*

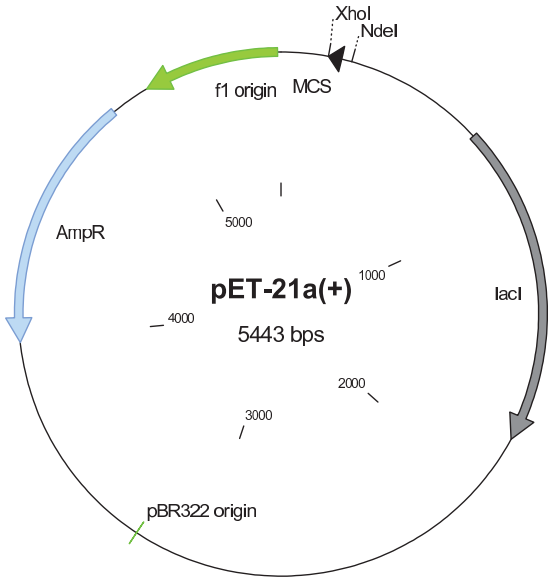

Fig. A.4. *Map of expression vector pET-21a(+).*

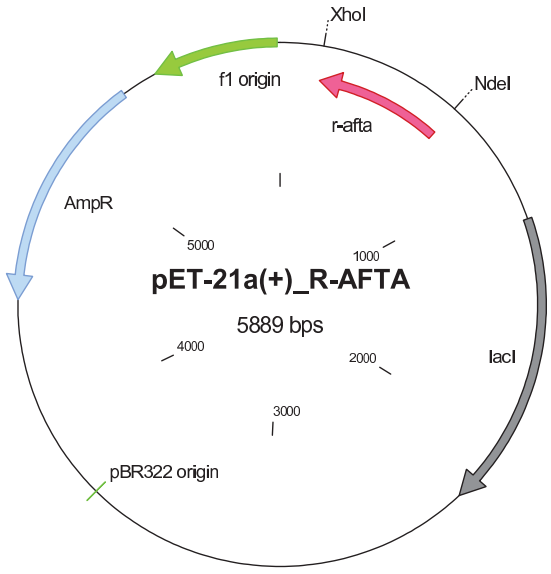

Fig. A.5. *Map of plasmid pET-21a(+)_R-AFTA with* r-afta *gene.*

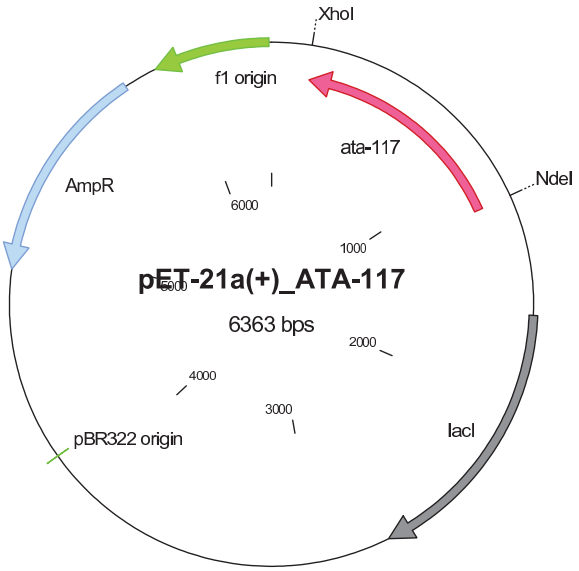

Fig. A.6. *Map of plasmid pET-21a(+)_ATA-117 with* ata-117 *gene.*

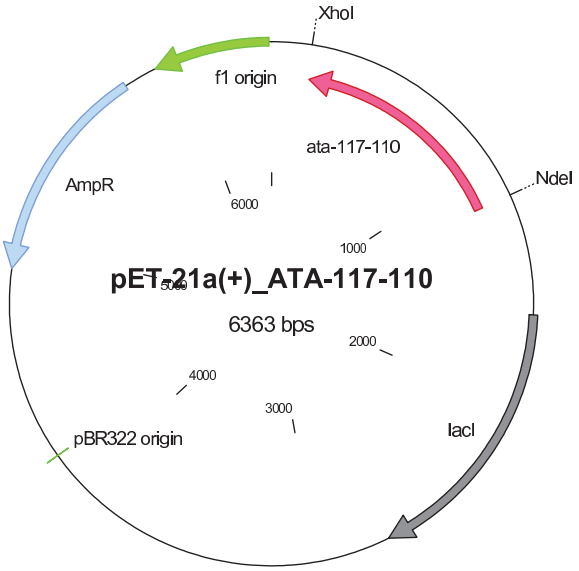

Fig. A.7. *Map of plasmid pET-21a(+)_ATA-117-110 with* ata-117-110 *gene.*

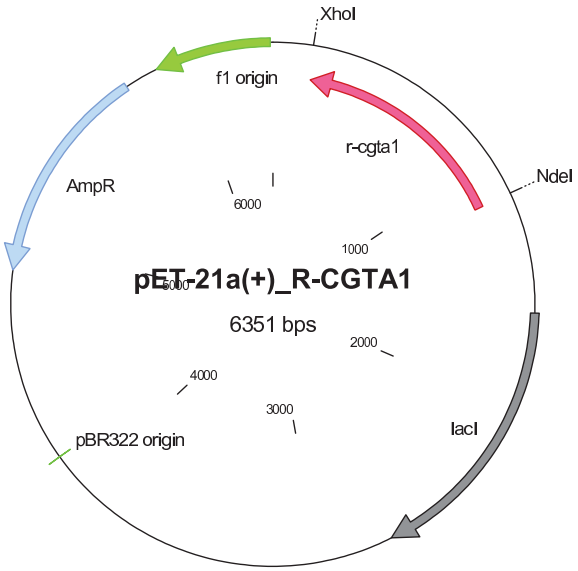

Fig. A.8. *Map of plasmid pET-21a(+)_R-CGTA1 with* r-cgta1 *gene.*

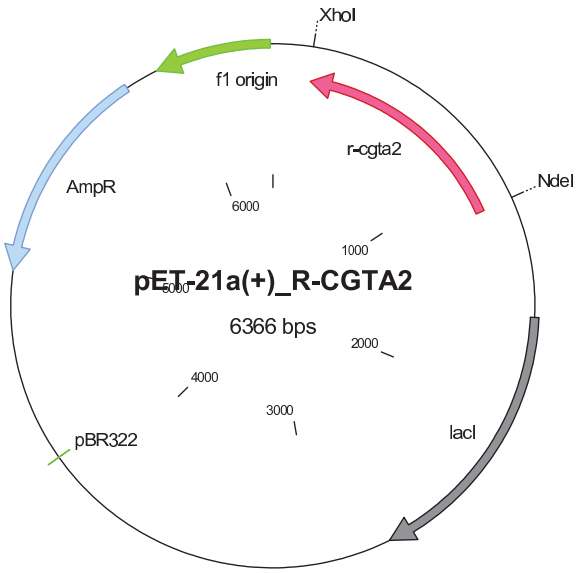

Fig. A.9. *Map of plasmid pET-21a(+)_R-CGTA2 with* r-cgta2 *gene.*

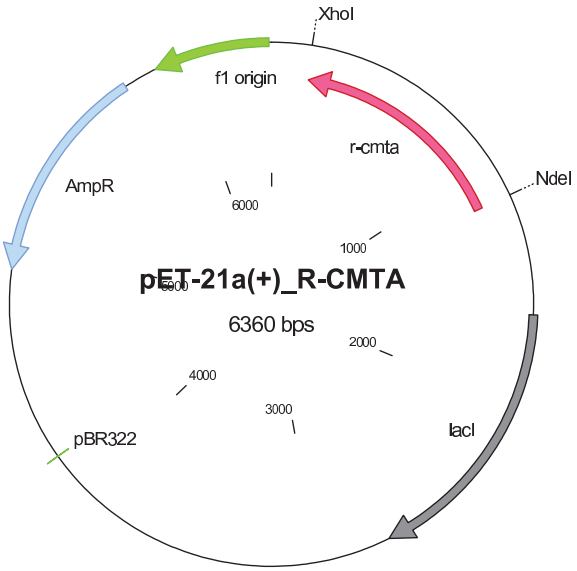

Fig. A.10. *Map of plasmid pET-21a(+)_R-CMTA with* r-cmta *gene.*

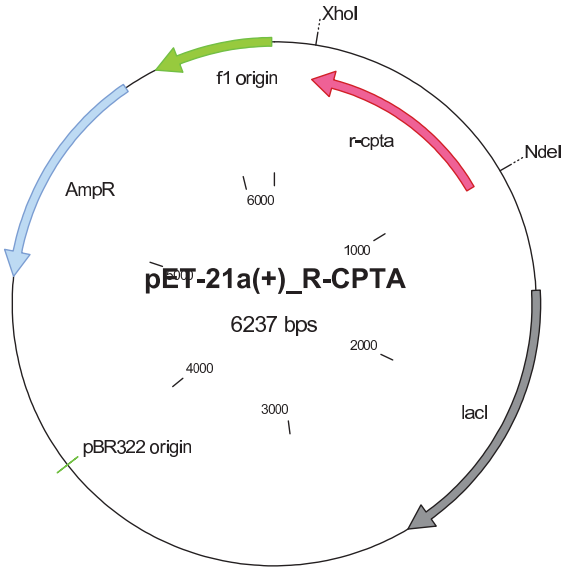

Fig. A.11. *Map of plasmid pET-21a(+)_R-CPTA with* r-cpta *gene.*

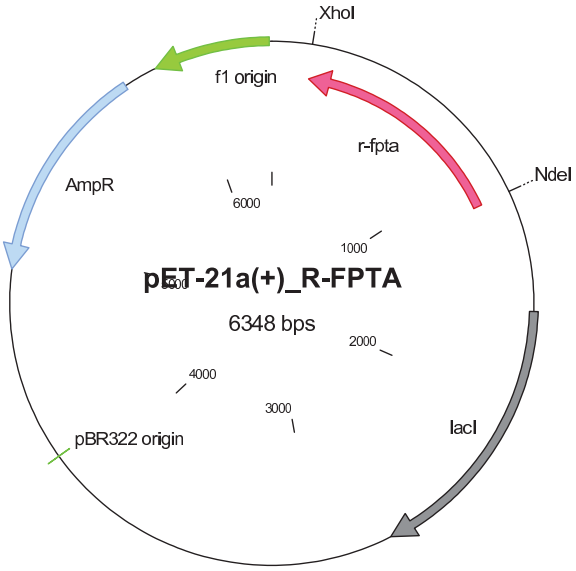

Fig. A.12. *Map of plasmid pET-21a(+)_R-FPTA with* r-fpta *gene.*

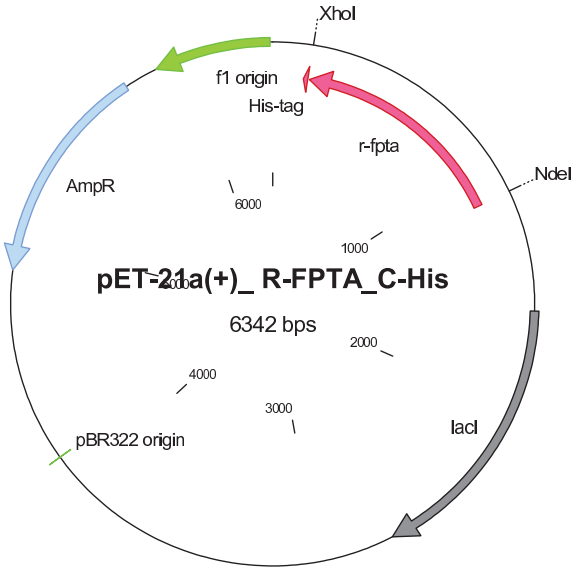

Fig. A.13. *Map of plasmid pET-21a(+)_R-FPTA_C-His with* r-fpta *gene and C-terminal His-tag.*

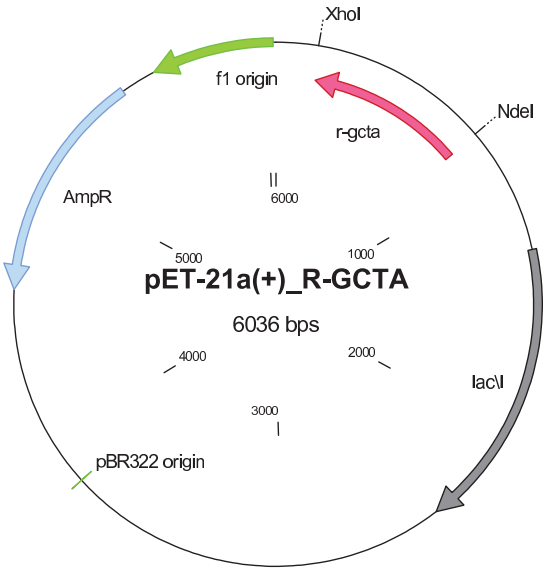

Fig. A.14. *Map of plasmid pET-21a(+)_R-GCTA with* r-gcta *gene.*

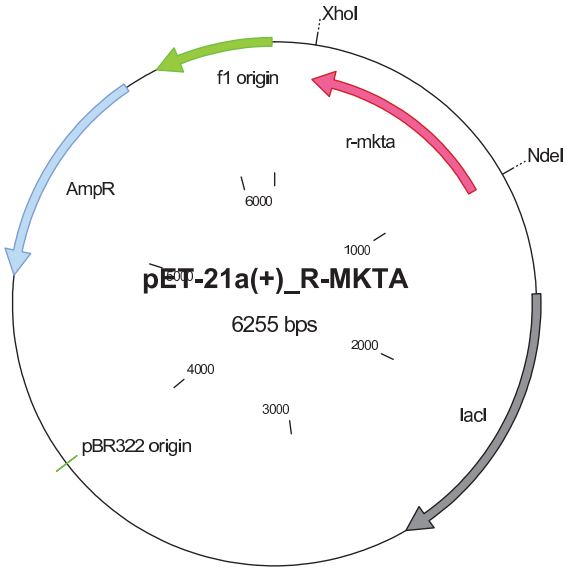

Fig. A.15. *Map of plasmid pET-21a(+)_R-MKTA with* r-mkta *gene.*

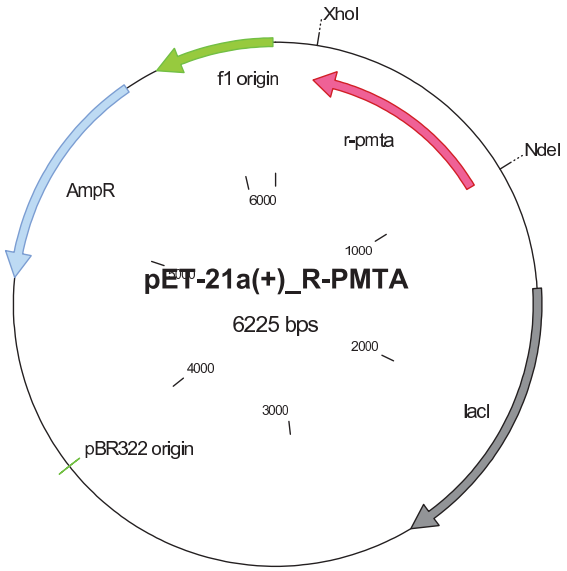

Fig. A.16. *Map of plasmid pET-21a(+)_R-PMTA with* r-pmta *gene.*

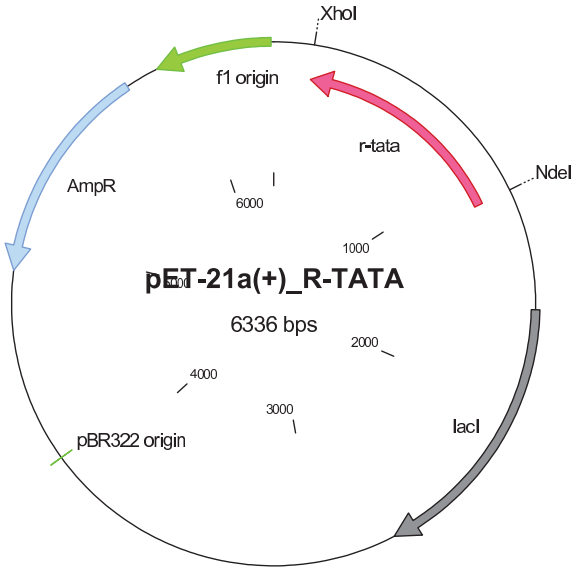

Fig. A.17. *Map of plasmid pET-21a(+)_R-TATA with* r-tata *gene.*

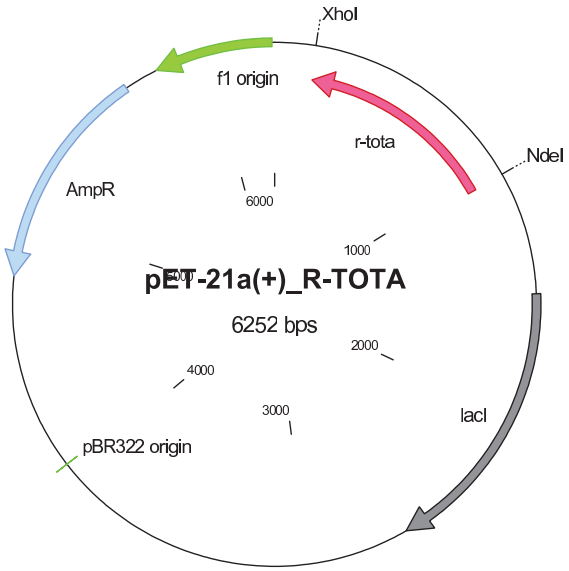

Fig. A.18. *Map of plasmid pET-21a(+)_R-TOTA with* r-tota *gene.*

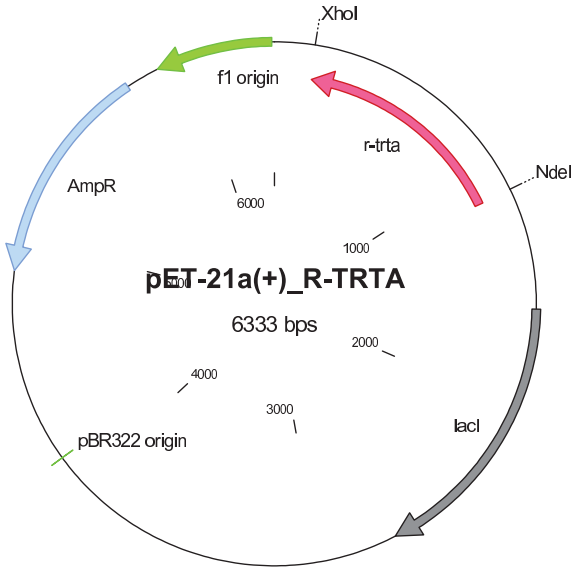

Fig. A.19. *Map of plasmid pET-21a(+)_R-TRTA with* r-trta *gene.*

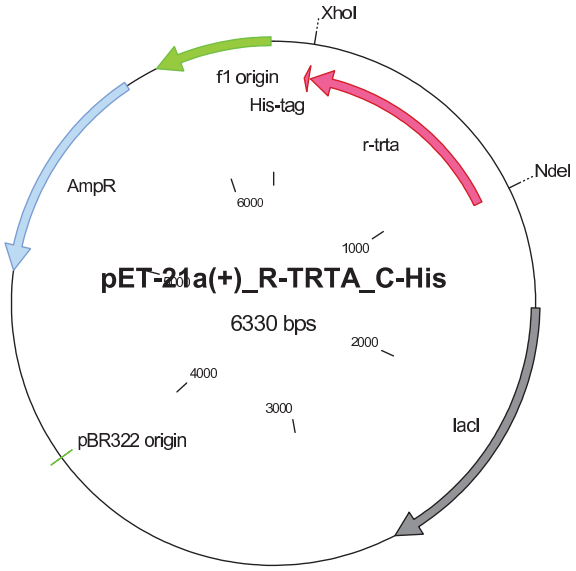

Fig. A.20. *Map of plasmid pET-21a(+)_R-TRTA_C-His with* r-trta *gene and C-terminal His-tag.*

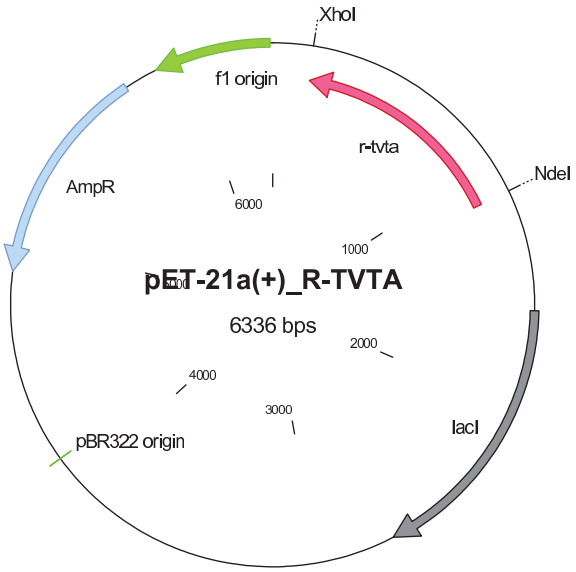

Fig. A.21. *Map of plasmid pET-21a(+)_R-TVTA with* r-tvta *gene.*

2. Additional Information

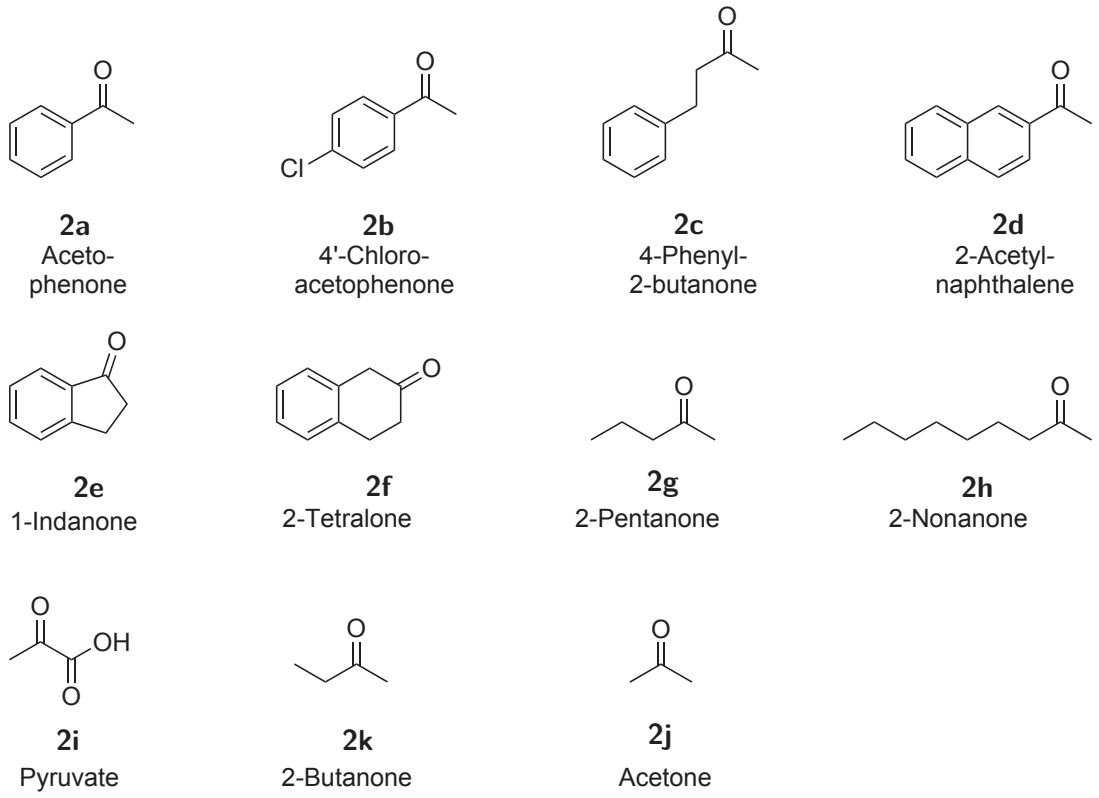

Fig. A.22. *Corresponding ketones for chosen amine substrates for the characterization of (R)-selective ω-transaminases.*

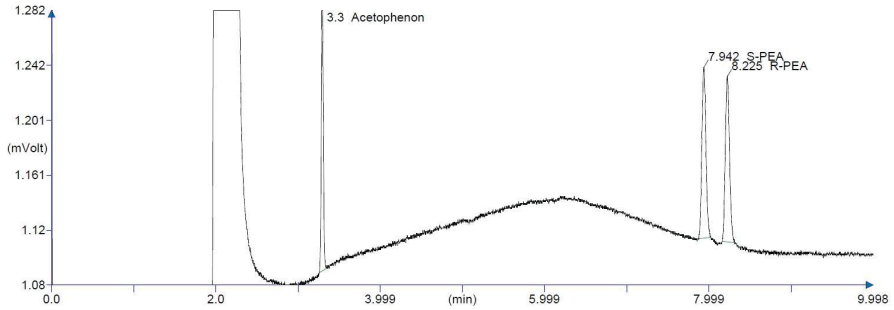

(a) Standards

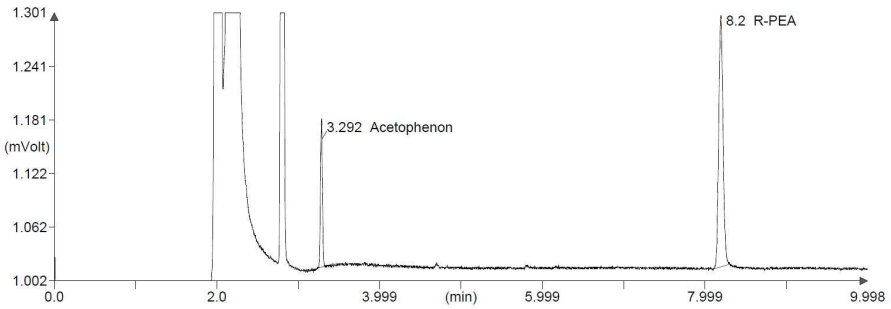

(b) Amination with R-TRTA

Fig. A.23. *Gas chromatograms of (a) standards acetophenone* ***2a*** *and the enantiomers of 1-phenylethylamine* ***1a*** *and (b) amination of* ***2a*** *with R-TRTA after 93 h.*

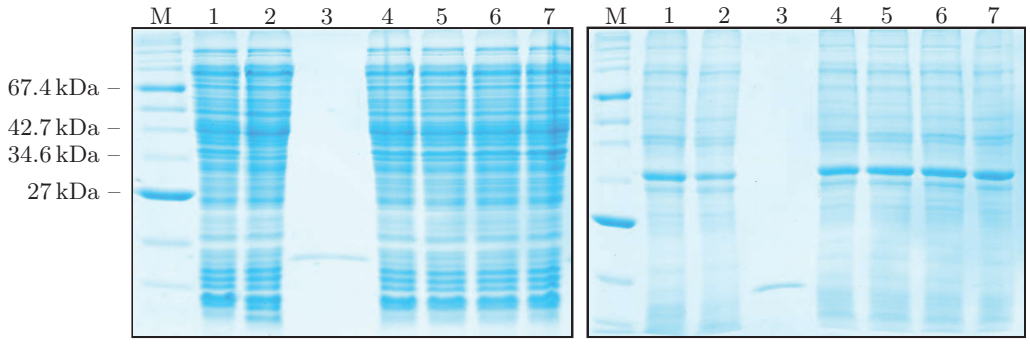

(a) soluble **(b)** insoluble

Fig. A.24. *SDS-PAGE from samples of the expression of the ω-transaminases R-TRTA and R-CMTA in* E. coli *BL21(DE) with and without 0.1 mM pyridoxine. The cultivation was done in M9 medium and the gene expression was induced with 0.05 mM IPTG. The incubation was continued at 25 °C. Lane 1:* E. coli *BL21(DE). Lane 2:* E. coli *SoluBL21(DE). Lane 3: 1 µg Interferon. Lane 4: R-CMTA (37 kDa). Lane 5: R-CMTA (37 kDa) with pyridoxine. Lane 6: R-TRTA (36 kDa). Lane 7: R-TRTA (36 kDa) with pyridoxine. Lane 8: 3 µg Interferon. M: Unstained Protein Marker, Broad Range (New England Biolabs).*

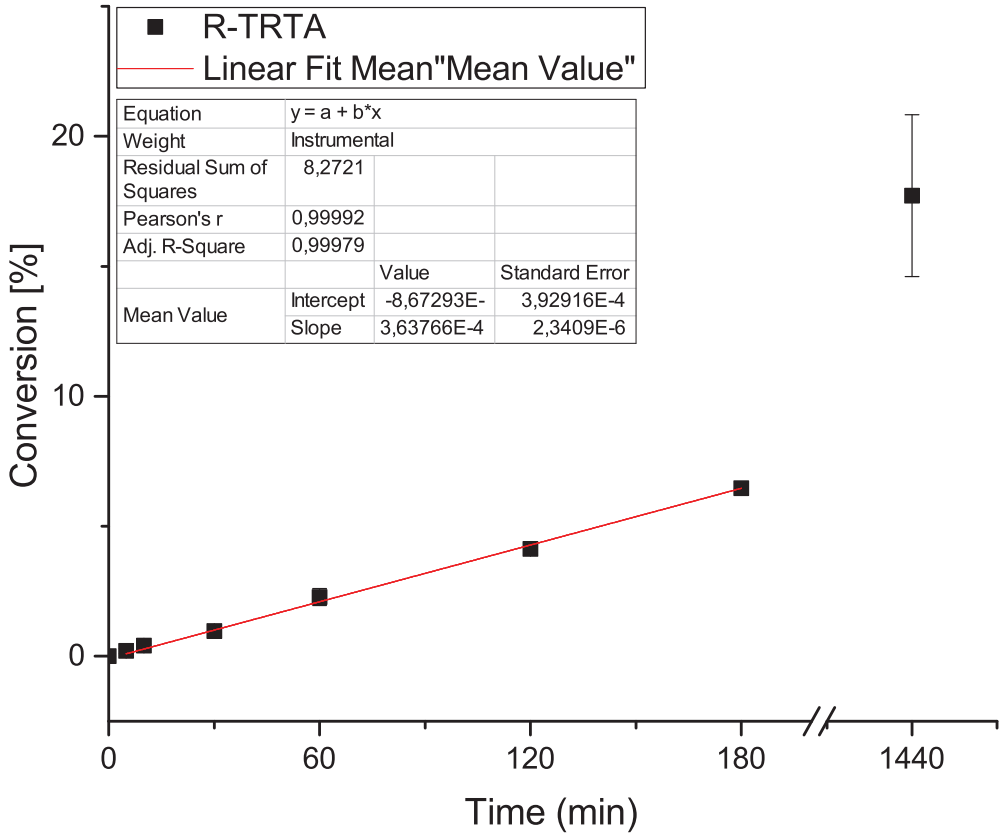

Fig. A.25. *Biotransformation of acetophenone* **2a** *to (R)-phenylethylamine (R)-***1a** *by R-TRTA.*

Tab. A.1. *Mean amination activites of the ω-transaminases R-TRTA and R-FPTA from lyophilisates.*

Substrate	**R-TRTA** [$\mathbf{mU/mg_{protein}}$]	**R-FPTA** [$\mathbf{mU/mg_{protein}}$]
2a	0.002	0.024
2b	0.009	0.011
2c	0.148	0.021
2d	0.006	0.021
2e	–	–
2f	0.010*	0.005
2g	0.026	0.024
2h	0.091	0.035

*also formation of (*S*)-amine